POLYMERIC BINDER DESIGN FRAMEWORKS FOR HIGH CAPACITY LI-ION BATTERY ANODES

A Dissertation
Presented to
The Academic Faculty

by

Krysten Minnici

In Partial Fulfillment
of the Requirements for the Degree
Doctor of Philosophy in the
School of Chemical & Biomolecular Engineering

Georgia Institute of Technology
August 2019

POLYMERIC BINDER DESIGN FRAMEWORKS FOR HIGH CAPACITY LI-ION BATTERY ANODES

Approved by:

Dr. Elsa Reichmanis, Advisor
School of Chemical & Biomolecular Engineering
Georgia Institute of Technology

Dr. Thomas Fuller
School of Chemical & Biomolecular Engineering
Georgia Institute of Technology

Dr. Nian Liu
School of Chemical & Biomolecular Engineering
Georgia Institute of Technology

Dr. Carson Meredith
School of Chemical & Biomolecular Engineering
Georgia Institute of Technology

Dr. Natalie Stingelin
School of Materials Science & Engineering
Georgia Institute of Technology

Date Approved: June 20, 2019

To my parents, who encouraged me to be anything I wanted to be.

ACKNOWLEDGEMENTS

First and foremost, I would like to thank my advisor, Dr. Elsa Reichmanis. I would have left Georgia Tech during my second year with a M.S. in chemical engineering without her constant guidance and support throughout the entire Ph.D. process. Her unique advising style shaped me into the scientist I am today. My career trajectory would not be the same without her allowing me to take complete ownership of my thesis.

I would like to thank my committee members: Dr. Thomas Fuller, Dr. Carson Meredith, Dr. Nian Liu, and Dr. Natalie Stingelin. They provided essential feedback on my thesis proposal, six-month review, and this dissertation. Dr. Fuller and Dr. Meredith also guided me through the M.S. thesis process and provided me with essential feedback to prepare me for the next steps in my Ph.D. I am particularly grateful for the Fuller and Liu labs for allowing me to use their facilities to fabricate countless coin cells, conduct impedance and CV testing.

I would also like to thank my collaborators at Stony Brook University: Dr. Esther Takeuchi and Dr. Amy Marschilok. They challenged me to think critically about my results and dive deeper to understand polymeric binders at a more fundamental level. I am also grateful to the M2M collaboration that provided my Ph.D. funding. Our annual meetings and biweekly teleconferences forced me stay on track with my research goals.

The Reichmanis group has been an essential component to my graduate school experience and their support has helped me survive the last four years. I would especially like to thank Yo Han Kwon for his expertise in lithium-ion batteries and extreme patience

when teaching me electrochemical techniques. I am also grateful for the support of Bailey Risteen, Michael McBride, Audrey Scholz, Brian Khau, Carolyn Buckley, Miguel Gonzalez, and Aaron Liu. I would also like to give a special shout-out to Nils Persson for encouraging me to join the Reichmanis group four years ago, despite my concern about such a vague thesis project title. Joining the Reichmanis group turned into one of the best decisions I have ever made. Ranging from intellectual conversation to lunch-time shenanigans, words cannot express my gratitude to my research group.

I am also appreciative of the help from my undergraduate students: Mark deSimon, Johnathan O'Neil, Aarti Mathur, and Luke Roeber. My thesis would not be complete without their hard work and dedication. Mark learned new techniques in lab with me and helped develop the ion exchange protocol used in Chapter 2. Johnathan spent a summer working for me and was essential to the completion of the ion exchange project. Aarti was brave enough to do the undergraduate thesis option with me and I'm so proud of the work she accomplished in two semesters, which is not included in this dissertation.

Last, but certainly not least, I must thank my family for their continuous and unwavering support in everything I have done. My parents have not always understood what exactly I am doing for my Ph.D. thesis at Georgia Tech, but they have continued to encourage me every step of the way. I have to think a small part of my completion of this degree is thanks to the religious candles my mom would light for me during every major milestone. I am especially grateful to my fiancé, Bobby, for his constant support and encouragement over the past 9 years of my education.

TABLE OF CONTENTS

LIST OF TABLES

LIST OF FIGURES

SUMMARY

Battery electrodes are complex mesoscale systems comprised of an active material, conductive agent, current collector, and polymeric binder. While the focus of research related to the design of robust, high-performance Li-ion batteries relates to the synthesis of active particles, the binder plays a crucial role in stability and ensures electrode integrity during volume changes that occur with cycling. Conventional polymeric binders such as poly(vinylidene difluoride) generally do not interact with active particle surfaces and fail to accommodate large changes in particle spacing during cycling. Recently, a poly[3-(potassium-4-butanoate)thiophene] (PPBT) binder component, coupled with a polyethylene glycol (PEG) surface coating for the active material was demonstrated to enhance both electron and ion transport in magnetite based anodes; and it was established that the PEG/PPBT approach aids in overall battery electrode performance.

In this thesis, the PEG/PPBT system is first used as a model polymeric binder system for understanding cation effects in anode systems. As such, the potassium ion was replaced with sodium, lithium, hydrogen and ammonium through ion exchange. Potassium showed the most stable electrochemical performance, which is attributed to cation size and proposed to be a result of higher ionic conductivity. Lithium demonstrated an initial increase in capacity, but was unable to maintain this performance over 100 cycles. Sodium increased in capacity as cycling progressed as a result of slow reaction kinetics. Whereas, hydrogen and ammonium demonstrated poor electrochemical performance. The results from the effect of ion exchange creates a framework for understanding how cations on the

polymer impact electrochemical performance and aids in the overall design of binders for composite Li-ion battery anodes.

Next, a series of water-soluble, carboxylated polymers with varying functional groups were investigated as alternative polymeric binders to aid in electron and ion transport in magnetite-based anodes. Conjugated polymers under investigation include PPBT, a poly(3,4-ethylenedioxythiophene) (PEDOT) derivative, and the potassium salt form of poly(acrylic acid) (PAA-K). The PEDOT derivative showed comparable cycling performance to PPBT over 100 cycles at 0.3 C, demonstrating enhanced capacity retention compared to the traditional PVDF. Rate capability testing revealed similarities between PPBT and PAA-K. The results of this investigation create a framework of desirable qualities necessary for polymeric binders by investigating how different functional groups aid or hinder overall electrochemical performance in the overall design of composite Li-ion battery anodes.

Finally, the overall role of the composite electrode is investigated. The model PPBT polymer was functionalized onto the magnetite surface using two covalent attachment strategies, specifically an (3-aminopropyl)triethoxysilane (APTES) and 1-ethyl-3-(3-dimethylaminopropyl) carbodiimide (EDC)/N-hydroxysuccinimide (NHS) chemistry and a Fischer esterification approach, are implemented for understanding how surface chemistry and functionalization strategy impacts overall electrochemical performance. Direct attachment of PPBT onto the magnetite surface via Fischer esterification led to enhanced performance. A closer look is given to electrodes consisting solely of the functionalized active material and carbon-polymer composites. Optimal carbon to polymer loading is between 60 wt% to 80 wt% carbon, leading to a balance in capacity and stability.

CHAPTER 1. INTRODUCTION

1.1 Overview of Li-ion Batteries

Rechargeable lithium-ion batteries have been the most utilized batteries in the portable electronic market for many years, but challenges exist to meet demands for high density energy storage.[1–3] Despite the impressive growth in sales of batteries worldwide, the science underlying battery technology is often criticized for its slow development.[4] New battery technologies are rare, and the energy density of lithium-ion batteries has only increased 8-9% per year since the 1990s.[5] However, lithium-ion batteries have replaced other energy storage device chemistries, particularly in the mobile electronics market.[6] Research has focused on improving both energy and power density of energy storage technology, particularly through new materials development.

A number of Li-ion battery configurations exist, including coin-, cylindrical-, prismatic-type, and pouch-type cells. Despite their different configurations, the battery consists of an anode, cathode, immersed in electrolyte and separated by a polymer membrane, which has essentially remained unchanged from the earliest development of batteries.[4,7] The working principle of a lithium-ion battery is based on the reversible intercalation and de-intercalation of the lithium ions, Li^+, into electrodes, as illustrated in **Figure 1**. The electrolyte enables ion transfer between the two electrodes.[8] During the first cycle, the organic electrolyte decomposes to form a solid electrolyte interface (SEI) layer on the surface of the electrodes.[6] The SEI film permits the diffusion of Li ions and can also prevent aggregation of active particles, while maintaining a uniform chemical composition

at the electrodes. However, the SEI layer also increases the internal resistance of the battery and consumes Li ions from the cathode, resulting in capacity loss.[7]

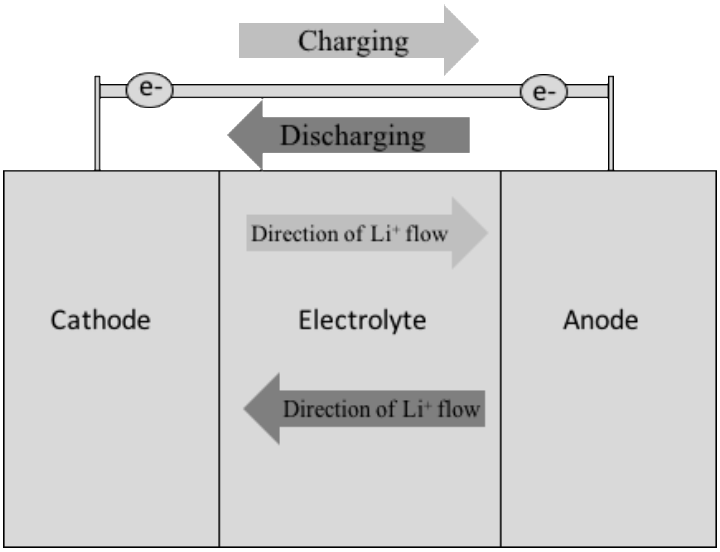

Figure 1: Schematic of a lithium-ion battery [Adapted from literature[6]]

In this thesis, the coin-type half-cell battery configuration was utilized to evaluate battery electrode performance. The specific components of this configuration are shown in **Figure 2**. Li metal was used as a counter/reference electrode, while the electrode of interest (*e.g.* anode or cathode) was the working electrode.

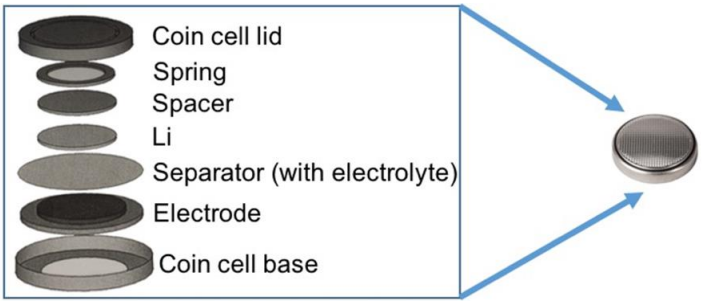

Figure 2: Half-cell battery configuration.

The electrode materials are crucial to determine the capacity and power density of the lithium-ion battery, whereas the capacity retention is governed by the quality and stability of the interfaces within the electrode system. A composite electrode is composed of an active material, conductive agent, current collector, and polymeric binder (**Figure 3**). A major challenge for electrode design is to provide high capacity and high coulombic efficiency.[9] This thesis specifically focuses on anode material development. Currently, graphite is widely used as a commercial anode active material due to its high coulombic efficiency and stable cycle performance, but has a very low specific capacity of 372 mAh g^{-1}.[4] To meet growing consumer energy demands, electrode materials with higher energy and power densities are a necessity. However, a number of requirements must be met to replace graphite as an active material, including high accommodation of Li ions, cycle ability, high operating voltage, and insolubility in the electrolyte. Furthermore, an ideal anode is cheap, environmentally friendly, safe and demonstrates good electrical and ion conductivity.[6]

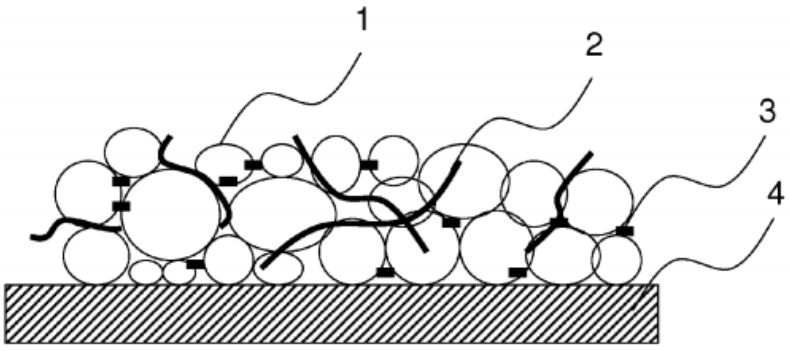

Figure 3: Schematic of electrode: (1) active material, (2) polymeric binder, (3) carbon additives, (4) current collector (Cu foil). [Reproduced with permission from the author[10]]

1.2 Alternative Active Materials

1.2.1 High-capacity active materials

Next generation Li-ion batteries require high specific capacities to meet the demands of the consumer. Promising alternatives to graphite include transition metal oxides (MO, where M is Co, Ni, Cu or Fe), silicon, tin, and their derivatives. However, the main obstacle impeding the use of these high-capacity active materials results from large volume changes during lithiation/delithiation processes that lead to poor cycling performance.[11–13] **Table 1** summarizes the theoretical capacity and associated volume changes for high-capacity anode materials, as compared to graphite.

Table 1: Comparison of Electroactive Anode Materials for Li-Ion Batteries[11,14–17]

Material	Theoretical Capacity (mAh g^{-1})	Volume Change (%)
Graphite	372	10
Silicon	4200	420
Tin	994	260
Metal Oxides (Fe_3O_4)	500-1000 (926)	- (200)

1.2.2 Magnetite as an active material

This thesis will focus on magnetite (Fe_3O_4), which is readily available. Its high theoretical specific capacity (~926 mA h g^{-1}) results from the eight electron conversion reaction during the lithiation process, which is based on the novel conversion:[18,19]

$$Fe_3O_4 + 8Li^+ + 8e^- \rightleftarrows 3Fe^0 + 4Li_2O$$

In particular, magnetite is a naturally occurring mineral found in the earth's crust, making it abundant, environmentally friendly, cheap, and non-toxic.[20] Furthermore, it is

easy to synthesize and can be prepared through a variety of methods, including sol-gel,[21] ultrasound irradiation,[22] reverse micelle method,[23] hydrothermal,[24–26] thermal decomposition,[25] and co-precipitation.[20,27] Co-precipitation and thermal decomposition are the most commonly employed synthesis techniques. Co-precipitation is a non-hazardous, facile approach, involving low temperatures and does not require elaborate synthetic equipment.[28] This technique typically involves mixtures of Fe^{2+} and Fe^{3+} dissolved in water with an added base to form Fe_3O_4 precipitate.[29] My previous work demonstrated the effects of surface chemistry on electrochemical performance, comparing co-precipitation using triethylamine and ammonium hydroxide as the base. Triethylamine-based systems demonstrated interactions between the active material and polymeric binder leading to enhanced capacity and capacity retention.[30] Therefore, in this thesis, co-precipitation was used as the synthesis method for magnetite, using the triethylamine base.

Magnetite has not been practically implemented as an anode material due its poor cycling stability, resulting from drastic volume changes during lithiation/delithiation processes.[31] A number of design strategies have been implemented to improve Fe_3O_4, including carbon coatings,[1,32] nanostructures,[33] and nanocomposites.[31,34,35]

The particle size of the active material plays a crucial role in enhancing electrochemical performance in the electrode. A reduction in particle size leads to a higher surface area.[36] Komaba *et al.*[37] conducted the first Fe_3O_4 crystallite size effect investigation, where they concluded that nanocrystalline (10 nm) magnetite had the highest initial capacity. Sizing down particles to the nanoscale has previously demonstrated a shorter Li ion diffusion pathway, increased reversible capacity, and improved rate capability performance.[18,20,38] However, nanoparticle-based electrodes exhibit a higher

propensity to aggregate, which can disrupt conductive pathways and lead to increased charge resistance in the electrode.[39] Another challenge at the nanoscale results from undesirable side reactions with the electrolyte, resulting from the larger surface area available.[20,40] Despite these complications, the large surface area/volume ratios provide more pathways for ion movement, leading to improvements in kinetics since the Li ion diffusion path occurs along smaller distances.[20] The magnetite utilized in this thesis is a 10 nm crystallite size, which previously demonstrated superior cycling stability, rate capability performance and reduced charge transfer resistance, when compared to a 20 nm counterpart.[30]

Carbon materials are often utilized to enhanced electrical conductivity, improve rate performance, and have been shown to improve the electrochemical properties of magnetite-based anodes.[1,20,32] Carbon coatings serve as a barrier to protect active materials and maintain higher capacities. The introduction of carbon coatings on iron oxide nanospindles preserved the integrity of particles, enhanced electronic conductivity, stabilized SEI layer formation, leading to a high specific capacity of ~749 mAh g^{-1} at C/5, enhanced cycling performance, and high rate capability as compared to commercial magnetite particles.[13] Xie et al.[41] used a two-step hydrothermal method followed by an annealing treatment to prepare Fe_3O_4/carbon core-shell nanotubes, which delivered improved cycling performance and rate capability, as compared to the Fe_2O_3 nanotube control electrode. The capacity of the carbon coating on magnetite nanoparticles has been demonstrated to enhance electrical conductivity and suppress cracking of the anode during cycling.[32]

The introduction of polymers or organic molecules on the magnetite surface have also been shown to stabilize the particles through both steric and electrostatic forces.[42,43] Magnetite nanoparticles are known to aggregate due to strong van der Waals and magnetite interactions.[44] Polyethylene glycol (PEG) is one of the most frequently used polymers for magnetite surface modification, as it has been shown to improve colloidal stability of the particles. PEG has shown a reduction in aggregate size, leading to improve particle dispersion in magnetite-based systems.[11,43,45] In **Chapters 2 and 3**, a PEG coating was introduced onto the Fe_3O_4 particle surface through a facile-probe type ultrasonication process.

1.3 Polymeric Binders

The majority of electrode material research for Li-ion batteries focuses on the synthesis of active particles, with less focus on polymeric binders. The binder plays a crucial role in a Li-ion battery, as it binds the active materials onto the current collector and keeps conductive carbon physically connected to the active materials.[46,47] The repeated expansion/contraction of active materials during cycling often results in severed contact between particles and the conductive network.[48] Choice in binder is critical for the cycling performance of silicon and magnetite based anodes. Poly(vinylidene fluoride) (PVDF) has been extensively used commercially and is arguably the prevalent polymeric binder in battery electrode applications; however, it is unable to accommodate large volume changes in spacing between particles that occurs during cycling, due to weak van der Waals interactions between the active material and polymer.[49,50] The key to a successful polymeric binder relies not only on high elasticity and mechanical resistance to stretching, but promotes adhesion onto the particle surface through chemical bonding.[51]

1.3.1 Water-soluble polymeric binders

While PVDF is robust and readily available, water-soluble alternatives are beginning to emerge as attractive, low cost, and more sustainable alternatives. Early work on binders focus on carboxymethyl cellulose (CMC) and polyacrylic acid (PAA), which enable aqueous processing, eliminating the need for toxic solvents, and it has been suggested that hydrogen bonding interactions between the carboxylic groups on the polymer and surface hydroxyl groups on the active material (i.e. Si, Fe_3O_4) may enhance electrode stability.[50,52–57] Strong mechanical strength of the composite electrode depends on numerous polymer bridges between particles and covalent bonding between polymeric binder and particles.[48] Weak van der Waals interactions, as observed with PVDF, or acid-base bonds are not preferential for enhanced performance.

Hochgatter *et al.* showed that CMC was able to chemically bond with the silicon surface through a condensation mechanism between carboxylic acid COOH groups of the CMC and the SiOH groups present on the surface of silicon.[58] Mazouzi *et al.* demonstrated that the mechanism is dependent on pH, where a pH 3 buffer solution is used for electrode preparation (i.e. a pH value lower than the isoelectric point of Si particles and pK_a of CMC).[48] By altering the pH, SiOH groups were able to react with the COOH groups present on the CMC surface, leading to enhanced cycling stability.

Previous research on silicon-based anodes demonstrated success with poly(acrylic acid) (PAA) as the binder.[50,56,57,59] PAA is low cost, exhibits excellent surface binding, improved stability, and is water-soluble, allowing for "green" electrode fabrication.[57] PAA is not only soluble in water, but in a variety of ecologically friendly organic solvents,

allowing for tunable properties. Furthermore, PAA is commercially available with a variety of molecular weights, which was shown to significantly impact performance in Si-anodes,[57,59] and allows for further property adjustments. The tunable properties of PAA allow freedom in the design for electrode preparation and process optimization. In comparison to CMC, PAA showed superiority due to its higher concentration of carboxylic functional groups.[50]

1.3.2 Conductive polymeric binders

Other alternatives to the traditional PVDF include semiconducting polymeric binders that can be doped during battery cycling and support electronic conductivity in the electrode.[60] Typically, polymeric binders serve to hold the active material and additives together. Electrically conductive additives, such as Super P or Carbon Black, are required to ensure electrical conductivity of the entire composite electrode. The polymeric binder combines with carbon additives to maintain electrical bridges within the electrode. The electronic integrity of electrodes relies on these electrical connections between the active material and conductive additives. Due to the nature of high-capacity active materials and subsequent volume changes during cycling, the electrical connection between active material and additives will often break after extended cycling.[61]

The use of a conductive polymeric binder reduces the need for excess conductive additives. Conductive additives increase the amount of non-active materials in the composite electrode, causing a decrease in the energy density. A higher content of active material is achieved when using a conductive polymeric binder that no longer requires the use of additive carbon.[62]

Liu *et al.* have prepared a number of conductive polymers for use as binders, including a functional conductive poly(9,9-dioctylfluorene-co-fluorenone-co-methylbenzoic ester) (PFM),[63,64] PFM with a triethyleneoxide monomethylether side chain (PEFM),[61,65] a polyfluorene-type polymer with carbonyl and methylbenzoic ester functional groups (PFFOMB),[66] and poly(1-pyrenemethyl methacrylate) (PPy),[62] leading to enhanced cycle stability and specific capacity for Si-based anodes, without the use of conductive additives. Conductive polymers with improved adhesion to the active material particles have shown improvement for the electrical connection in Si anodes.[61] The PFM conductive polymeric binder has polar ester functional groups, specifically designed for adhesion to the active material surface, while methylbenzoic ester groups also serve to form chemical bonding with the surface. The synergistic effects of the improved adhesion between the polymeric binder and active material surface, and the conductive nature of PFM, allows for an increase in active material loading that improves the energy density of the lithium-ion cell.[64]

1.3.3 Combining the effects of water-soluble and conductive polymers

Few initiatives have combined the effects of both water-soluble and conductive polymeric binders. Conventional, non-conductive, water-soluble binders display insulating characteristics, since they have non-conductive functional groups of polymers causing poor electrical connections. During the charge-discharge cycling process, the active materials suffer from large volume expansion, pushing conducting additives away from them and leading to loss of electrical contacts. As a result of this, it has been suggested that water-based binders should also possess electronic and ionic conductivity, in addition to strong binding capabilities. A water-soluble, conductive polymeric binder can ensure constant

adhesion and electrical connection, even when the electrode integrity is damaged during cycling.[46]

Demonstrated in silicon anode systems, a novel water-soluble, conductive binder consisting of carboxymethyl cellulose (CMC) and poly(3,4-ethylenedioxythiophene): poly(styrenesulfonate) (PEDOT:PSS) showed improved electrochemical performance, particularly enhancing conduction.[55] PEDOT:PSS is one of the most successful conducting polymers and has drawn interest in a variety of electronic applications, including OLEDs, flexible photovoltaic devices, and sensors, due to its high conductivity and excellent thermal/chemical stability.[67,68] The incorporation of PEDOT:PSS into a water-soluble binder eliminates the use of conductive carbons, which tend to aggregate, causing gaps in conductive bridges to the active material, leading to a decrease in electrochemical performance. PEDOT:PSS is able to form homogenous and continuous conductive bridges throughout the electrode and reduces the use of carbon conducting agents. The Si electrodes composed of the water-soluble composite binder demonstrated higher initial Coulombic efficiencies, better cycling, and rate performances.[55]

1.4 Motivation: PEG/PPBT System

Previous studies using a semiconducting polymer, poly(3-hexylthiophene) (P3HT), with magnetite-based electrodes demonstrated the importance of considering both electron and ion transport in the design of composite electrodes.[38] Following this investigation, a poly[3-potassium-4-butanoate) thiophene] (PPBT), a water-soluble, carboxylate-substituted polythiophene, was introduced as a polymeric binder in combination with a polyethylene glycol (PEG) surface coating for the magnetite active material.[11] A facile

approach was developed for coating the Fe_3O_4 particles with PEG 1500 in aqueous medium via probe-type ultrasonication and is demonstrated in **Figure 4a**. The PEG coating process limited the growth of aggregates (**Figure 4b**) and improved materials dispersion in the composite electrode.

Conjugated polythiophenes exhibit high electronic conductivity (10^{-2}-10^{-4} S cm^{-1}, i.e. P3HT) and undergo electrochemical doping, which enhances electron transport and builds electrical bridges between active particles and carbon additives.[38] Furthermore, chemical interactions between the carboxylate moieties and metal oxide favorably impacted electrochemical performance. Strong interactions between a binder and active material surface are one of the most critical factors in influencing electrode stability, and were previously limited to Si anodes.[48,69–71]

Overall, the PEG/PPBT system demonstrated improved cycling stability and rate capability in magnetite-based systems.[11] **Figure 4c** shows charging-discharging performance over 50 cycles at a current density of 240 mAh g^{-1} (~0.3 C) between 0.01 and 3 V. Notably, the PEG/PPBT system exhibited a 91.2% capacity retention at 50 cycles, as compared to the PVDF control demonstrating only 25.9% retention. Newly fabricated half coin cells were demonstrated in rate capability testing (**Figure 4d**), where cells were under a constant lithiation current density of 80 mA g^{-1} (~0.1 C) and over a wide range of delithiation current densities (80 – 1600 mA g^{-1}) in a voltage range of 0.01 – 3 V. The PEG/PPBT system showed a much higher delithiated capacity than the PVDF control.

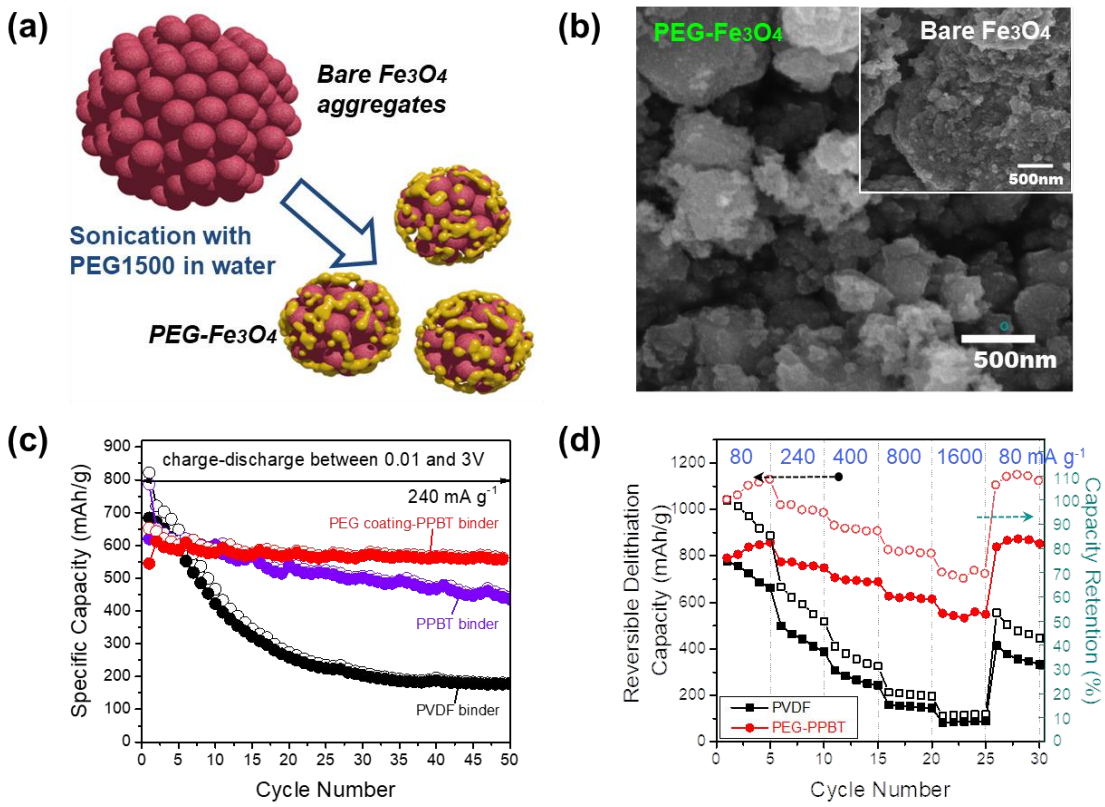

Figure 4: Overview of PEG/PPBT system. (a) PEG sonication procedure, (b) SEM images of PEG-Fe_3O_4 as compared to inset of bare Fe_3O_4, (c) Capacity retention (capacity as a function of cycle number) at 240 mA g^{-1} (~0.3 C) between 0.01 and 3 V comparing PPBT (with and without PEG coating) to PVDF control system, (d) Delithiation rate capability where cells were lithiated at a constant current density of 80 mA g^{-1} (~0.1 C) and delithiated at different current densities between 0.01 and 3 V (open circles: capacity retention, filled symbols: Li-extraction capacity). [Adapted with permission from Ref[11]]

A lithium exchanged form of the water-soluble polythiophene, poly(3-lithium-4-butanoate) thiophene 2,5-diyl) (P-Li-BT), was demonstrated in silicon and graphite anodes.[60] Here, electrically conductive polythiophenes, functionalized with an ionic alkyl carboxylate group, with various side chain lengths, were successfully implemented as binders in silicon and graphite electrodes systems. This work aimed to combine the advantages of using water-soluble and semiconducting binders, where the polythiophene

backbone provides electronic conductivity and the carboxylate groups allow for interaction with silicon particles. Interactions between active materials and polymeric binders allow for adhesion to the current collector, resulting in overall electrode stability. The polymeric binder with the shorter side chain gave the highest reversible capacity, which were higher than an electrically, but not ionically conductive PEDOT:PSS binder, and an ionically, but not electrically conductive sodium carboxymethyl cellulose binder.

The water-soluble, carboxylated polythiophene studies demonstrate the importance of having electrically and ionically conductive binders in magnetite and silicon based systems, which undergo large volume changes during cycling. Water-soluble binders allow for interaction with the active material surface during cycling, whereas the electrically conductive component enables high conductivity and electron transport by building electrical bridges between active materials and conductive carbon additives.

1.5 Thesis Overview

This thesis revisits the PEG/PPBT system and provides systematic approaches to improving Li-ion battery anodes by further understanding the polymeric binder. Each chapter provides a building block in the design of polymeric binders and the subsequent impact on electrochemical performance. **Chapter 2** investigates the role of the cation on the polymeric binder through the use a model water-soluble polythiophene (PPBT) and ion exchange. **Chapter 3** examines how functional groups on the polymeric binder impact overall performance. Finally, **Chapter 4** explores the model polythiophene binder as an active material coating using two surface functionalization techniques and how this influences performance. The effect of carbon additive and polymeric binder interactions

are also explored here to aid in composite electrode fabrication. **Chapter 5** summarizes the major findings of these chapters and provides suggestions for future work.

CHAPTER 2. CARBOXYLATED POLY(THIOPHENE) BINDERS FOR HIGH PERFORMANCE MAGNETITE ANODES: IMPACT OF CATION STRUCTURE

2.1 Introduction

Lithium-ion batteries are used for a wide range of applications and are considered to be the best option to meet electrical vehicle needs; however, to accommodate future demands for high density energy storage, performance enhancements are needed[2,72,73]. Transition metal oxides, such as Fe_3O_4 or alternatively magnetite, exhibit a high theoretical capacity (~500-1000 mAh g^{-1}) when fully reduced, and thus represent a class of promising alternative electrode material[13,74–76]. While magnetite has a high theoretical capacity (~925 mAh g^{-1}),[77] high electronic conductivity,[77–79] low cost and low environmental impact, as with most other transition metal oxides, capacity retention with cycling can be challenging due to large volume changes that take place during repeated charging-discharging[80–83]. Thus, if this high capacity active material is to become commercially viable, further research is needed to understand the electrochemistry of Fe_3O_4 anodes and how that chemistry is impacted by interfacial interactions and materials processing during composite electrode fabrication.

The performance of magnetite based anodes was recently demonstrated to benefit from the incorporation of a poly[3-(potassium-4-butanoate)thiophene] (PPBT) binder coupled with a polyethylene glycol (PEG) surface coating on the active material, which together enhance both electron and ion transport in the composite[11]. While carbon-based coatings are often utilized to enhance electron pathways[11,42,43,84,85], less attention has been

placed on ion transport. Both characteristics are important considerations for the selection of the binder component for electrodes. PPBT is a water soluble, carboxylate substituted polythiophene that supports ion and electron transport through pore formation and electrochemical doping. In conjunction with PPBT, PEG acts as a coating on the active material surface to reduce aggregate formation and improve material dispersion[45,86].

A preliminary investigation of the PEG/PPBT system demonstrated improved Fe_3O_4 capacity and rate capability, warranting further exploration into this model system for the design and development of robust Li-ion anode materials. Herein, the polythiophene binder is investigated further to evaluate the role of the carboxylate counterion. Previous work from Salem *et al*.[87] employed ion exchange to convert the PPBT potassium salt to its lithium counterpart, but no comparison between the resulting poly[3-(lithium-4-butanoate) thiophene-2,5-diyl] (P-Li-BT) and the PPBT precursor was presented. The focus of the investigation related to the use of P-Li-BT as a binding agent for silicon and graphite anodes, where they studied the side chain length impact on electrochemical performance. These results in conjunction with those on PPBT[21] suggest that the counterion may impact electrode performance and warrants further study.

Here, PEG/PPBT is used as a model system to examine how the carboxylate counterion impacts the performance of composite anodes. An ion exchange process was used to replace the potassium ion present in the commercial PPBT with the sodium, lithium, hydrogen and ammonium analogs. The resulting composite electrodes where characterized from the materials chemistry and electrochemical perspectives, whereby a framework for understanding how cation structure can impact overall electrode

performance. The results of this investigation is expected to aid in the future design and improved polymeric binders for Li-ion battery anodes.

2.2 Materials and Methods

2.2.1 Materials

Fe_3O_4 nanoparticles (~10 nm) were synthesized by a previously reported co-precipitation process using aqueous solution of iron(III) chloride hexahydrate, iron(II) chloride hexahydrate, and triethylamine[29,88]. For preparation of Fe_3O_4 particles coated with PEG (PEG-Fe_3O_4), 0.5 g of Fe_3O_4 powder in 5 g of water were sonicated at room temperature with an ultrasonic probe for 1.5 min (3 pulses of 30 s each, operated at 50 W, Qsonica Q700 sonicator). PEG 1500 solution (2 mL; 50% w/v, Sigma-Aldrich) was added with sonication for 30 s, and this process was repeated four times until the total amount of PEG 1500 was 8 mL. The PEG-Fe_3O_4 powders were washed and extracted by centrifuge separation (VWR Clinical 200) using acetone with speed of 6000 rpm for 5 min for 3 times. Thermogravimetric analysis (TGA) showed that PEG-Fe_3O_4 particles were composed of ~15 wt% PEG (**Figure 5**).

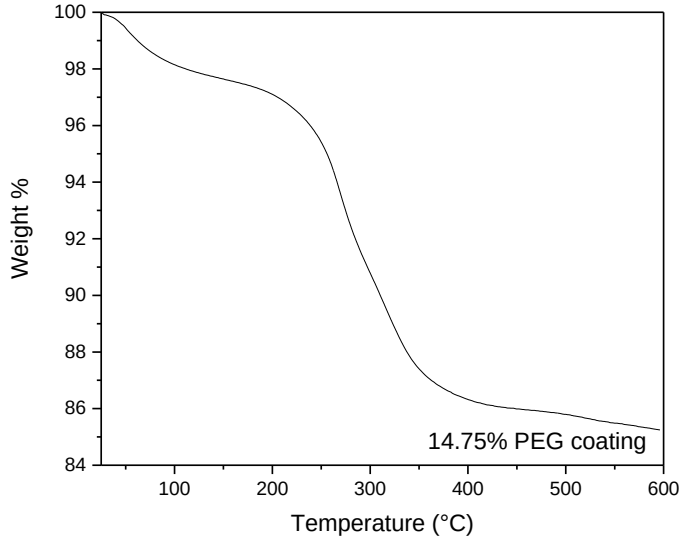

Figure 5: TGA profile of PEG coating, which is carried out in nitrogen in the temperature range of 25–600°C at a heating rate of 20°C/min, confirming 14.75 wt% PEG coating.

PPBT (M_w: 21 kDa, polydispersity: 2.2, head to tail regioregularity: 89%) was purchased from Rieke Metals Inc. The PPBT ion exchanged derivatives were prepared through a facile procedure. PPBT was dispersed in DI water (80 mg in 10 mL) and was combined with ion exchange resin (Amberlite™ IR120, H form, 5 g) in excess to remove the potassium salt and replace it with hydrogen at room temperature in air (12 h). Following the removal of the resin beads with a sieve (220-micron size mesh), sodium hydroxide (1 M, 388 µL, the molar equivalent to the amount of PPBT) was added to the P-H-BT solution to produce the ion exchanged PPBT, P-Na-BT. A yield of approximately 82% was achieved. The same process was utilized for lithium, ammonium and potassium. The hydrogen intermediate was produced from the first step of the ion exchange procedure.

2.2.2 Electrode Fabrication and Electrochemistry

The slurries for the electrodes were prepared by mixing PEG-Fe_3O_4 (0.1 g), carbon additives (0.02 g), and PPBT or ion exchanged derivatives in DI water (10 wt% solution, 0.2 g) with a weight ratio of PEG-Fe_3O_4:carbon:polymer = 71.4:14.3:14.3. The electrodes for field-emission scanning electron microscopy (FE-SEM, Zeiss Ultra-60) measurement, electrochemical evaluation and spectroscopy characterization were produced by blade coating (doctor blade, MTI corp). The electrodes were first allowed to dry at room temperature for 1 h, followed by 110 °C for 12 h in a vacuum oven.

Stainless-steel coin cells (2032-type) were used for electrochemical measurements. Lithium metal, purchased from MTI corp., was used as a counter electrode and 1 M $LiPF_6$ in ethylene carbonate (EC) and diethylene carbonate (DEC) (1:1 by weight), purchased from BASF, was used as the electrolyte. Before electrochemical testing, the capacity of each coin cell was confirmed by charging and discharging at a current density of 40 mAg^{-1} (~0.05 C). The tests were then proceeded for cycling and rate capability. Cyclic voltammetry (CV) was performed on half coin cells in the potential range of 0.01-3 V at the rate of 0.5 mV s^{-1} and electrical impedance spectroscopy (EIS, Metrohm Autolab PGSTAT101) measurements were conducted in the frequency range from 0.1 MHz to 0.1 Hz before and after cycling.

2.2.3 Microscopic Characterization

FE-SEM images were observed on the surface view of the electrodes using a Zeiss Ultra-60 FE-SEM with an accelerating voltage of 5 kV using the high vacuum mode at room temperature.

2.2.4 Spectroscopic Characterization

The electrode samples for spectroscopy measurements were prepared by removing powder samples from the prepared electrodes. Fourier transform infrared (FT-IR) spectra were recorded using a Thermo Scientific Nicolet iS50 FT-IR spectrometer. X-ray photoelectron spectroscopy (XPS) characterization was performed using a Thermo K-Alpha XPS system. The instrument was equipped with a monochromatic Al-K X-ray source (1468 eV). Spectra were collected using the flood gun and an X-ray spot size of 400 μm. Survey scans were collected with pass energy of 200 eV with 1 eV increments. High resolution scans (for specific elements) were collected with pass energy of 50 eV with 0.1 eV increments. For XPS analysis of the electrodes after 100 cycles, the delithiated electrodes were extracted from the cycled coin cells and carefully rinsed with DMC three times (5 mL in total) to remove residual electrolyte and then dried in a vacuum oven (80°C, 12 hr).

2.3 Results and Discussion

2.3.1 Ion Exchange Procedure and Verification

An ion exchanged polythiophene binder was used as a model polymer system to investigate the impact of cation size and structure on enhancing electrochemical performance in a magnetite anode system. Replacement of the potassium ion was conducted using a facile ion exchange procedure (**Figure 6**) to analyze the effects of lithium (P-Li-BT), sodium (P-Na-BT), hydrogen (P-H-BT) and ammonium (P-NH_4-BT) substitution. A control potassium sample was formulated by adding potassium hydroxide

to the ion exchanged P-H-BT to afford P-K-BT to confirm that the ion exchange process did not alter the structure of the thiophene based polymer.

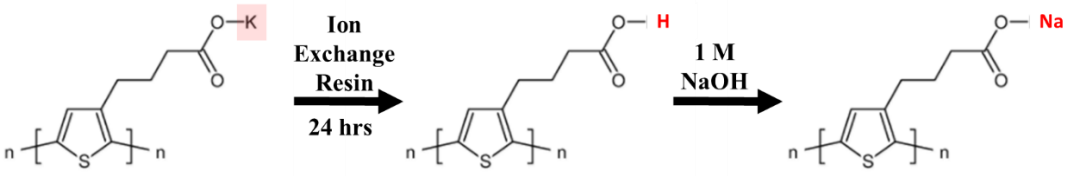

Figure 6: Schematic representation of the ion exchange procedure using sodium as an example.

X-ray photoelectron spectroscopy (XPS) verified the successful completion of the ion exchange procedure. Survey scans (**Figure 7a**) confirmed complete conversion of the potassium salt in P-Na-BT, P-Li-BT, P-H-BT and P-NH_4-BT. The presence of potassium was noted in both the parent PPBT and its P-K-BT control. All carboxylated polythiophenes reveal the presence of carbon and oxygen. P-Na-BT, P-NH_4-BT and P-Li-BT exhibit sodium, nitrogen, and lithium, respectively. XPS is unable to detect the presence of hydrogen, and as such the P-H-BT was solely verified on the bases of a lack of observable potassium. The atomic % from XPS (**Table 2**) further verified the ion exchange procedure by indicating that the proportion of ion to polymer present in each sample was essentially unchanged from the starting PPBT. These results provide corroborating evidence that excess ions from the hydroxide solutions neither absorbed nor adsorbed to the ion exchanged material.

Table 2: Peak table from survey scan to illustrate atomic % of ion in each polymeric binder.

Name	Atomic % (XPS)
K 1s (PPBT)	9.58 %
Na 1s (P-Na-BT)	9.45 %
K 1s (P-K-BT)	8.34 %
Li 1s (P-Li-BT)	8.87 %
N 1s (P-NH_4-BT)	8.11 %

A high-resolution XPS scan of carbon provides insight into the chemical interactions present in the PPBT derived polymers. The C 1s scan exhibits two clear carbon peaks at about 284.5 eV and 288 eV (**Figure 7b**), corresponding to C-O and C=O bonds, respectively and provides further confirmation that the PPBT side chains remained intact after the ion exchange process. These peaks are present for each ion exchanged polymeric binder. In PPBT and P-K-BT, two additional peaks are present (293 eV and 295.5 eV), which are associated with K[89].

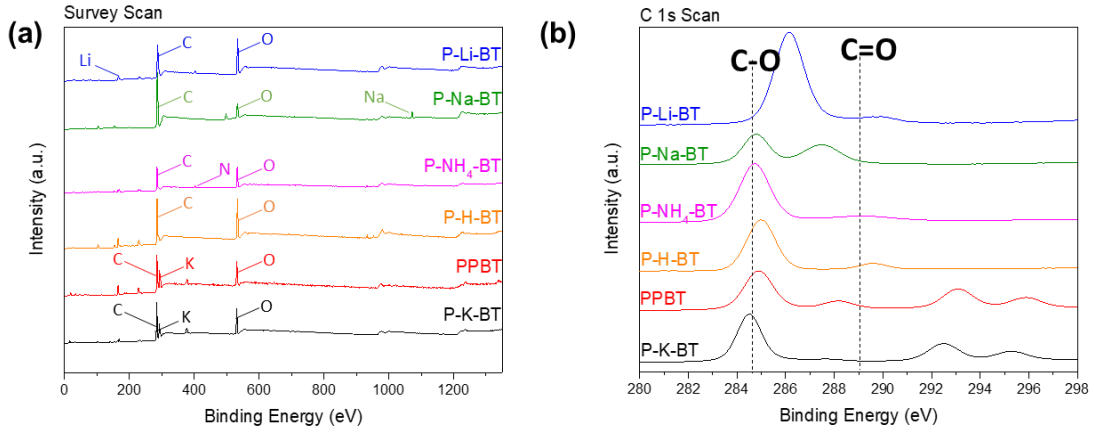

Figure 7: XPS characterization of ion exchanged derivatives of PPBT. (a) Survey scan of ion exchanged polymeric binders. (b) C scan of ion exchanged polymeric binders.

2.3.2 Stability of Ion Exchanged Polymers

The stability of the ion exchanged polymers was first evaluated using zeta potential measurements (**Figure 8**). In efforts to mimic the immediate environment surrounding the nanoparticles, they were dispersed in water through bath-type sonication process. The intermediate polythiophene, P-H-BT, was not sufficiently soluble in water for accurate zeta potential measurements. Values more negative than -30 mV are considered to represent the level of mutual repulsion needed to ensure the stability of a dispersion[90]. The ammonium derivative is the only polymer system to exhibit a zeta potential less negative than the -30 mV threshold, suggesting poor stability. The zeta potential results correlate well with cation size, where $K^+ > Na^+ > Li^+$, indicating that the size of the cation influences materials dispersion stability, which in turn will ultimately impact electrochemical performance.

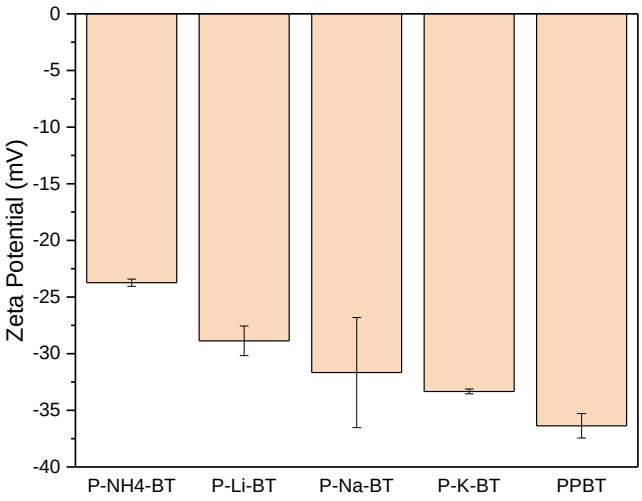

Figure 8: Zeta potential measurements of ion exchanged derivatives of PPBT.

2.3.3 Microscopic Characterization

To evaluate how the polymer dispersion characteristics of a given ion exchanged polymer in aqueous medium impacts composite electrode morphology, electrodes were fabricated with PEG-Fe_3O_4, carbon additives and the respective PPBT analogs (P-Na-BT, P-Li-BT, P-NH_4-BT, P-H-BT, and P-K-BT) in the same manner as reported previously[30]. The morphology was then visualized using FE-SEM (**Figure 9**). While the zeta potential results suggested minimal impact on morphology, with the ammonium and sodium salts expected to exhibit some degree of agglomeration, the sodium analog to PPBT, P-Na-BT, appears somewhat more uniformly dispersed than either the parent or alternative ion exchanged derivatives, and exhibits less variation in size and no large aggregates present (**Figure 9b**). The improved dispersion of P-Na-BT may derive from enhanced interactions between the sodium carboxylate and PEG coating on the magnetite surface. While limited to Na^+ and Li^+ as alkali metal ions, Maltesh and Somasundaran[91] used steady state fluorescence spectroscopy to demonstrate that Na^+ has a substantially stronger affinity to PEG than its Li^+ counterpart. The enhanced degree of dispersion is expected to enhance ion diffusion within the system and contribute positively to rate capability performance[30].

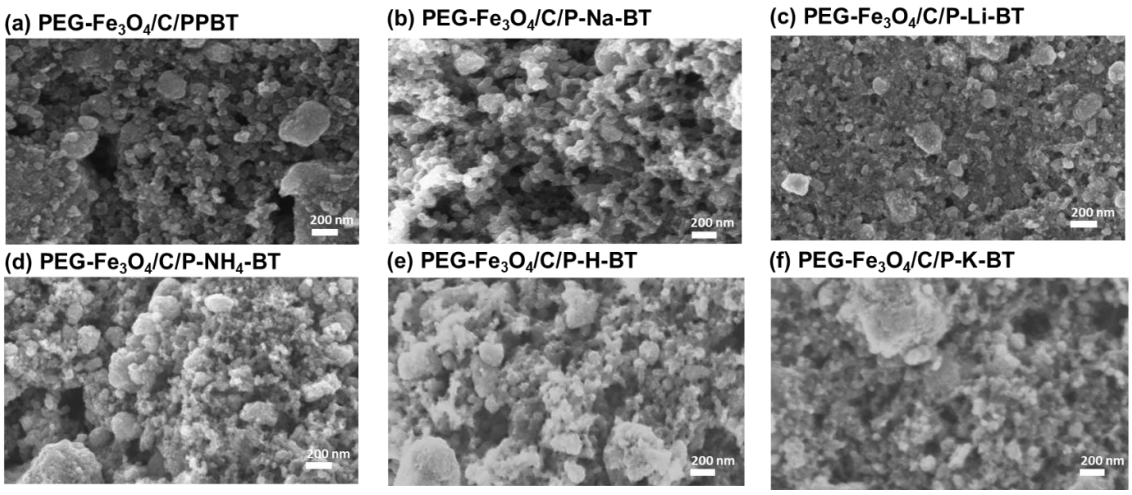

Figure 9: FE-SEM top view images of electrodes: (a) PEG-Fe_3O_4/C/PPBT (b) PEG-Fe_3O_4/C/P-Na-BT (c) PEG-Fe_3O_4/C/P-Li-BT (d) PEG-Fe_3O_4/C/P-NH_4-BT (e) PEG-Fe_3O_4/C/P-H-BT (f) PEG-Fe_3O_4/C/P-K-BT

2.3.4 Electrochemical Characterization

Coin cells were fabricated to explore the impact of counterion on the electrochemical performance of composite anodes comprised of PEG-Fe_3O_4 active material, carbon additives, and polymeric binder in a 71.4:14.3:14.3 mass ratio, Li metal served as the counter electrode, and 1 M $LiPF_6$ in ethylene carbonate (EC) and diethylene carbonate (DEC) (1:1 by weight) was used as the electrolyte. The mass ratio was chosen based on prior results to facilitate direct comparison[38]. Charge-discharge cycling (**Figure 10a**) was conducted at a current density of 240 mA g^{-1} (~0.3 C) to determine the capacity retention of each system for 100 cycles. Galvanostatic profiles are provided in **Figure 11**.

With respect to capacity retention upon cycling, the carboxylic acid, P-H-BT (orange) and ammonium carboxylate, P-NH_4-BT (pink) polythiophene based electrodes performed poorly. The results for P-NH_4-BT may derive from weak interactions between

NH_4^+ and PEG[91], which is expected to influence ion transport within the electrode, despite the ability of the binder to facilitate a similar, well-dispersed morphology to its ion exchanged analogs. Conceivably, the low zeta potential obtained for P-NH_4-BT may be an early indicator of performance since the value suggests that dispersions of the polymer would be unstable. The poor capacity retention for P-H-BT is believed to result from its poor solubility in water leading to more heterogeneous dispersions and morphologies.

The alkali metal carboxylates display distinctly different behavior, whereby they exhibit moderately high capacity which is more effectively retained during cycling. While P-Li-BT (blue), the lithium carboxylate exhibits the highest capacity (886 mAh g^{-1}), that capacity is not maintained during cycling and fades by approximately 26% after 100 cycles (653 mAh g^{-1}). This initial capacity may derive from a somewhat elevated concentration of Li^+ ions present in the composite electrode in the early stages: the polymeric binder accounts for 14.3 wt% of the overall electrode composition, approximately 5 wt% of which is the ion. With continued cycling, the additional lithium introduced via the binder no longer dominates, and capacity appears to decrease steadily during cycling.

The sodium salt, P-Na-BT (green) exhibited the lowest initial capacity, namely 637 mAh g^{-1}; however as cycling progressed, a gradual increase in capacity was observed until an apparent steady state was reached after about 60 cycles. This initial delay in capacity may be a result of slow reaction kinetics. Whereas the increase in capacity is believed due to the affinity of Na^+ to PEG limiting the size of Fe_3O_4 aggregates, thereby enhancing dispersion of the components and increasing the surface area of the active material. With respect to the latter, increased active material surface area would be expected to facilitate

Li^+ insertion, resulting in a steady increase in capacity during cycling, effectively overcoming initially slower reaction kinetics, *vide infra* (**Figure 12**).

The next higher homolog of the alkali metal series, namely PPBT (red) and its ion-exchanged control P-K-BT (black), exhibit the most stable capacity throughout 100 cycles with both samples exhibiting similar capacity and capacity retention. The improved cycling performance of the potassium carboxylates is likely due to the size of the cation, in relation to the lower atomic number Li^+ and Na^+ counterparts. Notably, Elabd[92] and Long[93] demonstrated that materials comprising alkali metal salts with an overall larger cation exhibit higher ionic conductivity. They speculated that incorporation of the larger metal ion led to suppression of the materials' glass transition temperature (T_g). The T_g for the polymers under investigation could not be measured due to the 89% regioregularity of the PPBT used. Previous studies using regiorandom polymers indicate that no crystalline reflections are observed in DSC,[94] as was observed for the ion exchanged derivatives. However, we surmise that the enhanced capacity and capacity retention of the potassium polythiophene carboxylate, PPBT and P-K-BT is directly related to its ionic conductivity. To measure the ionic conductivity a lithium and an electron dopant are needed and the baseline ionic conductivity of the polymers could not be measured. Conceivably, the larger atomic radius cation may also facilitate formation of a somewhat more porous morphology that supports ion transport through the composite electrode. Note, we previously established that both electron and ion transport are vital for enhanced electrochemical performance[11].

Newly fabricated half cells were subjected to rate capability experiments (**Figure 10b**), where cells were lithiated at a constant current density of 80 mA g^{-1} (~0.1 C) and

delithiated over a wide range of current densities (80 – 1600 mA g^{-1}) between a voltage range of 0.01 – 3 V. Rate capability testing was limited to P-Na-BT, P-Li-BT and PPBT based electrodes given that the ammonium salt and carboxylic acid systems exhibited poor capacity/capacity retention performance (**Figure 10a**). As discussed above, the highest initial capacity was observed for the P-Li-BT (blue) electrodes, which is most likely facilitated by the presence of Li^+ within the pristine composite electrode that may enhance transport at the early stages of cycling. As cycling continued however, the impact of the embedded Li ions was diminished: when the coin cell was cycled back to 0.1 C, the capacity dropped from the starting 1040 mAh g^{-1} to 848 mAh g^{-1}. In the case of Na^+, P-Na-BT electrodes exhibited a lower starting capacity of 850 mAh g^{-1}, which increased to 910 mAh g^{-1} upon cycling back to 0.1 C. These results mirror the behavior of the sodium carboxylate during cycling, and will be discussed further below. Notably, P-Na-BT based electrodes exhibited the best rate capability performance, particularly at higher current densities (1 C and 2 C).

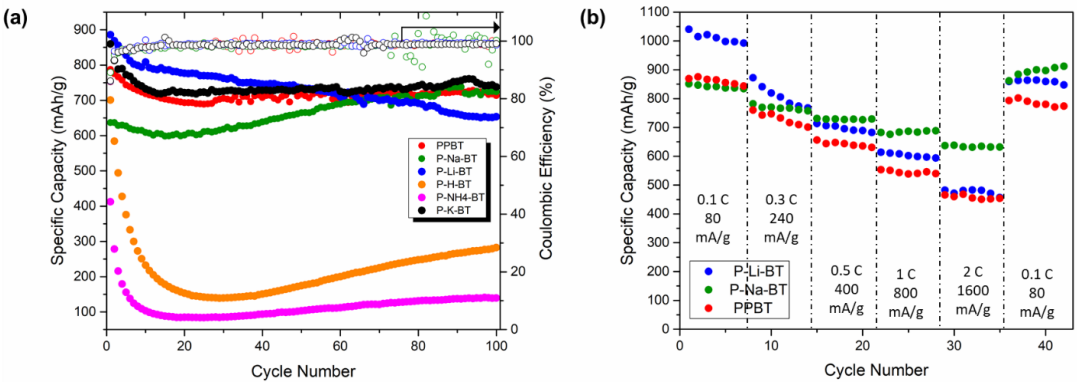

Figure 10: (a) Cycling performance (capacity retention as a function of cycle number) comparing different ion exchanged polymer binders cycled at 240 mA g^{-1} (~0.3 C) between 0.01 and 3 V. (b) Delithiation rate capability, where cells were lithiated a constant current density of 80 mA g^{-1} (0.1 C) and delithiated at different current densities between 0.01 and 3 V.

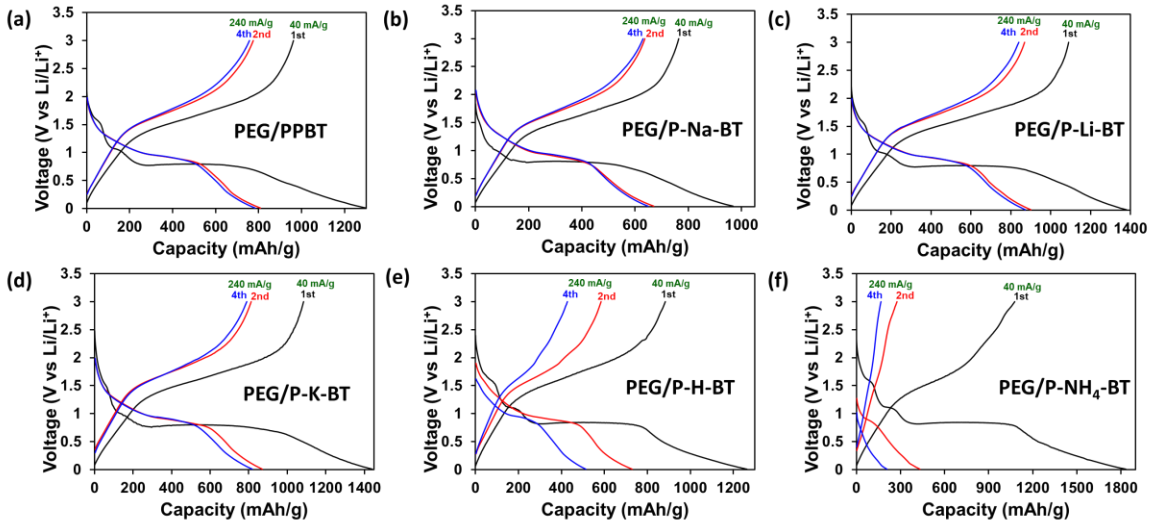

Figure 11: Galvanostatic profiles of (a) PEG/PPBT, (b) PEG/P-Na-BT, (c) PEG/P-Li-BT, (d) PEG/P-K-BT, (e) PEG/P-H-BT, and (f) PEG/P-NH_4-BT.

Cyclic voltammetry (CV) profiles performed at different scan rates (v) (**Figure 12a-c**) provided insight into electrode kinetics and helped to elucidate further how cation characteristics can impact the performance of the carboxylated polythiophene binder. The kinetic data was characterized by analyzing the voltammetric response of the polymeric binders at various scan rates according to $I_{pc} = av^b$, where the measured peak current (I_{pc}) and the potential scan rate (v) obey a power-law relationship[95–99]. The slope from the plot of log (I_{pc}) *vs.* log (v) provided the value of b, which is correlated with Li^+ diffusion[95,98]. The fitting results are summarized in **Figure 12d**; a higher value of b suggests faster kinetics. PPBT electrodes exhibited b = 0.927, compared with b = 0.814 and 0.691 for the Li^+ and Na^+ alternatives, respectively. These results support the trends observed in the cycling and rate capability studies suggesting that the potassium carboxylate offers

opportunities for enhanced electrochemical performance vs. the analogous Li^+ and Na^+ based binder systems. Na exhibits the lowest value (b = 0.691), which verifies cycling and rate capability trends discussed above and indicates the presence of Na^+ in the pristine electrode hinders electrode kinetics. The value for the lithium salt falls between the K^+ and Na^+ analogs, which may help elucidate the steady decrease in capacity during cycling and rate capability testing.

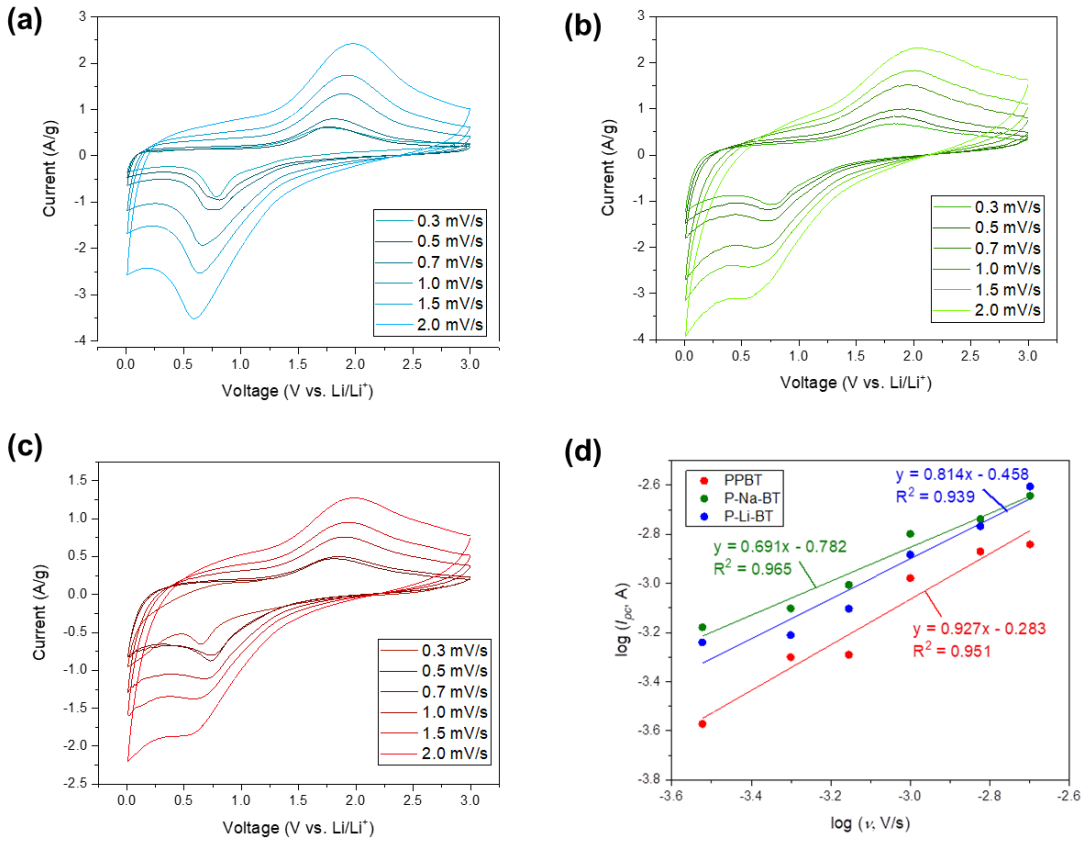

Figure 12: CV profiles with various scan rates (v) of (a) PEG/P-Li-BT, (b) PEG/P-Na-BT, (c) PEG/PPBT and (d) Plot of log (I_{pc}) vs. log (v), which were plotted from the results of cathodic peak currents of CV curves with different scan rates (v).

Further insight into the impact of counterion size and structure on the performance of the carboxylated binders can be obtained from analysis of EIS results (**Figure 13**), whereby the cells used for the study correspond to those cycled between 0.01 and 3V. Impedance testing was performed in the frequency range of 0.1 MHz to 0.1 Hz before cycling at 3V and after 100 cycles at their open-circuit voltage (OCV). The Nyquist plots support the cycling and rate capability data presented in **Figure 10** above. Superior battery electrode performance can be attributed to decreased charge transfer resistance (R_{ct}), which is estimated from the diameter of the high-frequency semicircle[100]. Prior to cycling (**Figure 13a**), P-Li-BT exhibited the lowest charge transfer resistance, followed closely by P-Na-BT; while the potassium analog, PPBT, displayed the largest R_{ct}. The initially reduced charge transfer resistance for the Li^+ analog as compared to the K^+ carboxylate corresponds well with the observed cycling and rate capability performance.

After 100 cycles (**Figure 13b**), the results were dramatically different. Charge transfer resistance for both the potassium and sodium carboxylated polythiophene based composite electrodes decreased significantly, while R_{ct} increased in the case of the Li^+ counterpart. The EIS results after cycling correlate well with the observed stabilized capacity retention for both the potassium and sodium systems and the capacity fade in capacity for the lithium carboxylate binder.

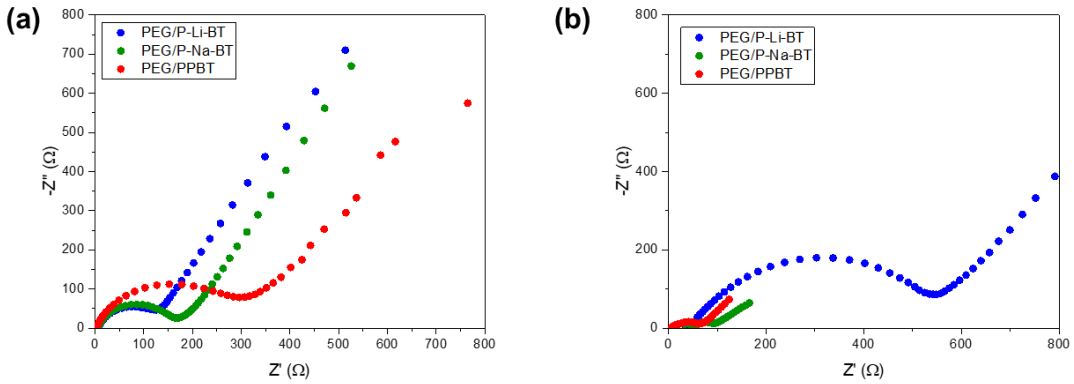

Figure 13: Impedance spectra measured (a) at 3V before cycling and (b) at open-circuit voltage (OCV) after 100 cycles in the frequency range from 0.1 MHz to 0.1 Hz.

2.3.5 Spectroscopic Characterization

The composite electrodes were further evaluated by XPS after 100 cycles **(Figure 14**) to explore differences in chemical composition. The results offer evidence for the formation of a stable SEI layer, which can be deduced from the fraction of LiF present in the electrode[95,101]. The survey scans presented in **Figure 14a** demonstrate that a simple change in counterion can lead to substantial differences in chemical composition of the corresponding electrodes. Note that the ions associated with the carboxylated binder were absent after cycling. **Figure 14b** provides the F 1s scan, where that the potassium containing PPBT based system exhibited a substantially more intense peak, while the Na and Li analogs appeared to have similar, lower levels of F^-. The higher fraction of LiF in the cycled PPBT-based electrodes suggests formation of a stable SEI layer and helps to validate the electrochemical results discussed above. As evidenced by the C 1s and O 1s data (**Figure 14c, d**), the proportion of organic compounds within the SEI layer was

relatively higher when P-Na-BT was used as the binder in comparison to either the PPBT or P-Li-BT containing composites. These results may explain why the Na-based electrodes stabilized to the same level as the PPBT alternatives by 100 cycles.

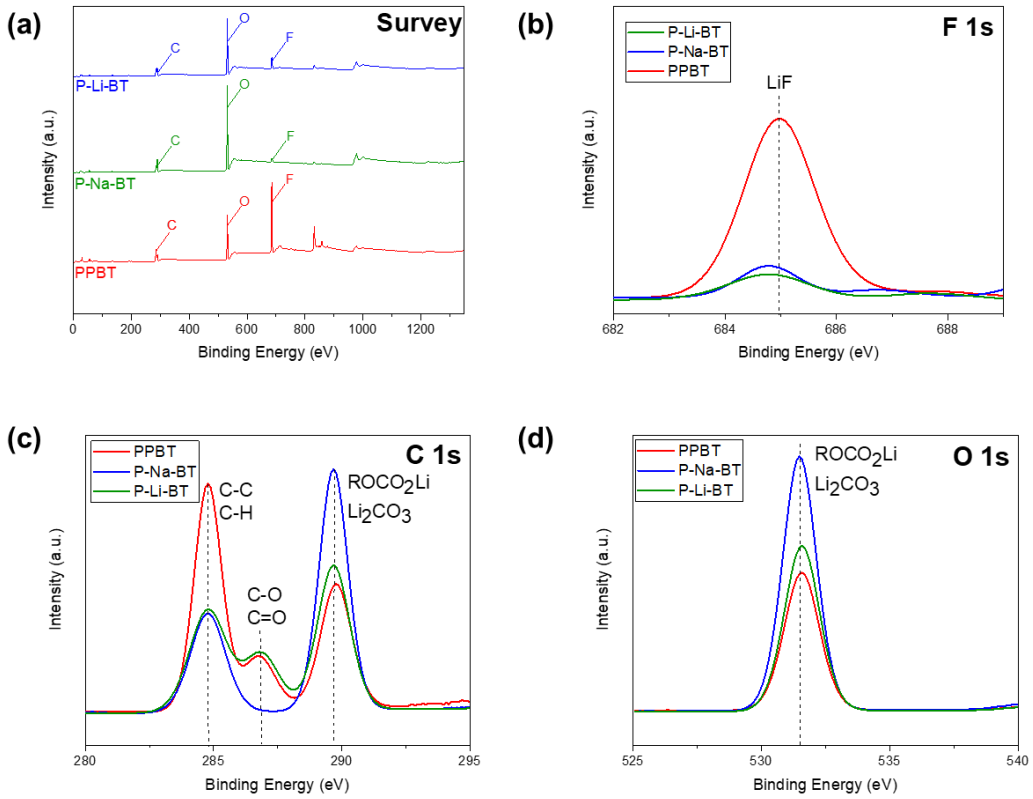

Figure 14: XPS analysis of SEI layer after 100 cycles: (a) Survey scan, (b) F 1s scan, (c) C 1s scan, and (d) O 1s scan.

In addition to chemical composition, molecular interactions between the active material and polymeric binders are expected to impact electrochemical performance. To that end, Fourier infrared (FT-IR) spectroscopy provides a convenient tool to uncover differences in how the electrode components interact. The PPBT carboxylate moieties exhibit vibrational bands at 1556 and 1400 cm^{-1}, which correspond respectively to the O-

C-O asymmetric and symmetric stretching modes (**Figure 15a**)[11,71]. These same bands appeared in all ion-exchanged derivatives of PPBT (**Figure 15a-f**), providing support for successful ion-exchange with no impact on the base polymer structure. To further elucidate relevant chemical/molecular interactions within the composite systems, FT-IR samples were prepared by scraping powder samples from the electrodes for direct comparison to the individual components (PEG-Fe_3O_4 and PPBT ion exchanged polymeric binder). New, lower intensity peaks not present in the raw materials were observed at around 1766 cm^{-1}, corresponding to a C=O stretching vibration. In addition, upon incorporation into the composite, the polythiophene carboxylate O-C-O asymmetric stretching vibration underwent a shift to higher energy, namely from roughly 1556 cm^{-1} in the parent polymer to 1530 cm^{-1} in the composite for each analog. The shift to lower frequency (higher energy) suggests weakening due to Fe-carboxylate bonding[16]. **Figure 15g**[15] provides a schematic representation of how the 1766 cm^{-1} and 1530 cm^{-1} bands are believed to correspond to a Fe-carboxylate bond between the active material and polymeric binder. The FT-IR results support the presence of intermolecular interactions between the polythiophene binder carboxylate moiety and Fe_3O_4 not only in PPBT[15], but in all ion exchanged carboxylate salts. In the case of the ammonium salt, P-NH_4-BT (**Figure 15d**), the intensity of the C=O band was significantly lower than its alkali metal alternatives, perhaps due to weaker Fe-carboxylate interactions. Further, these interactions were absent in composite prepared with the carboxylic acid derivative, P-H-BT (**Figure 15e**). Interactions between the binder and high capacity active material have previously been reported as critical factors influencing electrode stability[11,71].

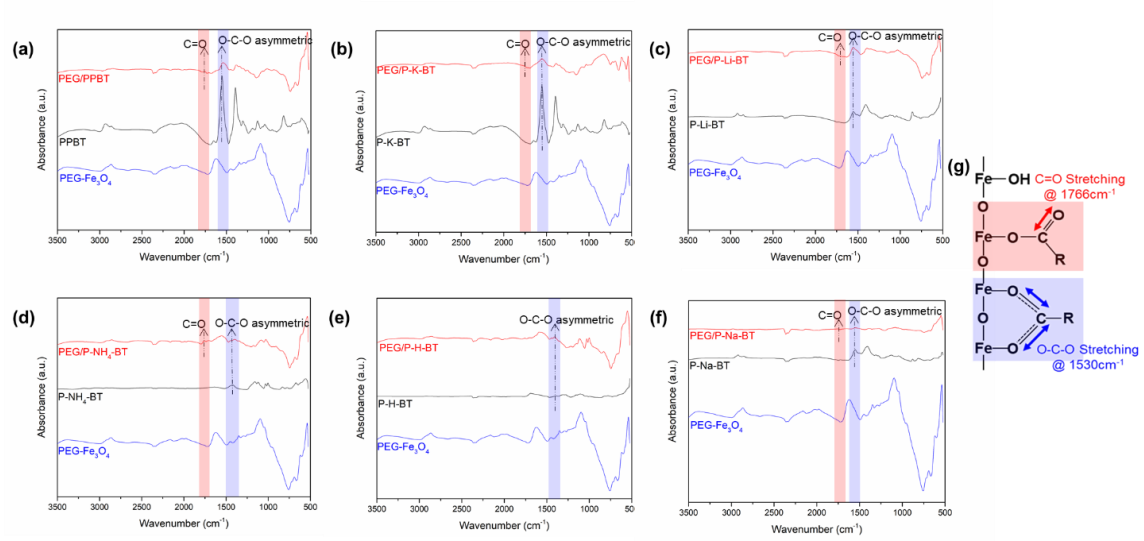

Figure 15: FT-IR spectra of raw materials (PEG-Fe_3O_4, polymeric binder) and electrode slurry. (a) FT-IR spectra of PPBT binder. (b) FT-IR spectra of P-K-BT control binder. (c) FT-IR spectra of P-Li-BT binder. (d) FT-IR spectra of P-NH_4-BT binder. (e) FT-IR spectra of P-H-BT binder. (f) FT-IR spectra of P-Na-BT binder. (g) Proposed chemical interactions between Fe_3O_4 and polymeric binder in electrode slurries. Adapted with permission from ref [11].

Support for the presence of bonding between PPBT and the Fe_3O_4 surface can be attained from XPS analysis, specifically of the Fe 2p core level (**Figure 16**). The observed peaks at ~712 and ~724 eV correspond to Fe $2p_{3/2}$ and Fe $2p_{1/2}$ orbitals, respectively; while the absence of a peak mid-way between and associated with Fe^{3+}, confirms a pure magnetite phase[102]. The appearance of this shakeup satellite peak in PEG-Fe_3O_4/PPBT electrode slurries confirms the presence of chemical/bonding interactions between PPBT and the Fe_3O_4 surface. This peak was observed for electrode slurries prepared with the lithium, sodium and potassium analogs. The absence of interactions between the active material and P-H-BT and P-NH_4-BT may negatively affect electrode stability thereby hindering electrochemical performance.

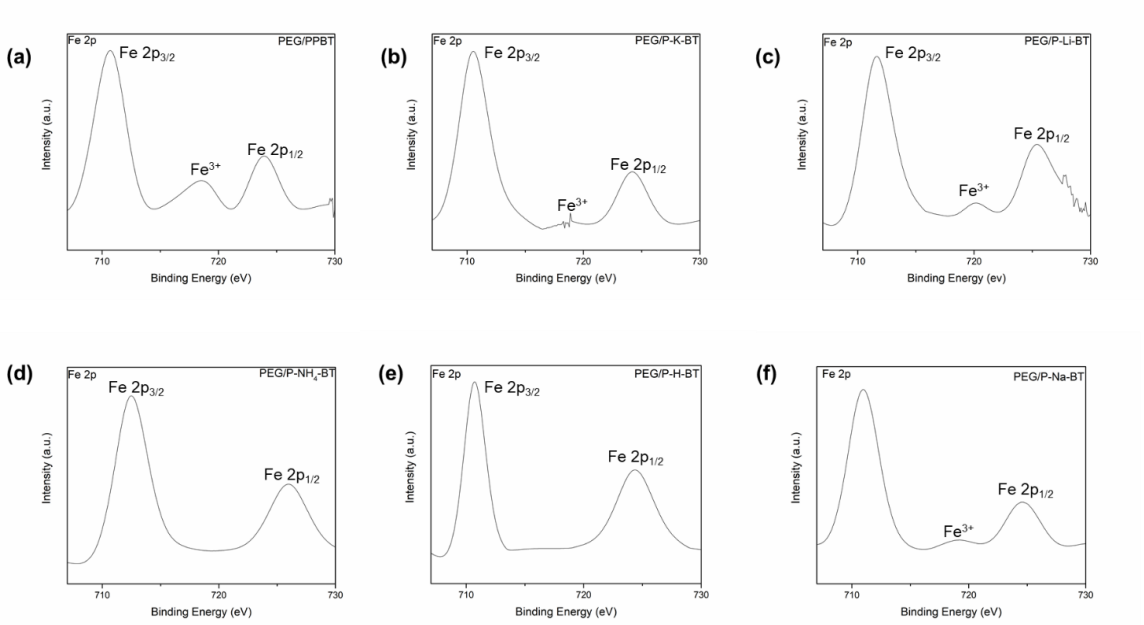

Figure 16: XPS spectra of electrode slurries. (a) XPS spectra of PPBT electrode slurry. (b) XPS spectra of P-K-BT control electrode slurry. (c) XPS spectra of P-Li-BT electrode slurry. (d) XPS spectra of P-NH_4-BT electrode slurry. (e) XPS spectra of P-H-BT electrode slurry. (f) XPS spectra of P-Na-BT electrode slurry.

2.4 Conclusions

The results presented in this investigation demonstrate the impact of cation size effects on overall electrochemical performance. In all discussed systems, PEG aids in limiting magnetite aggregation, as previously demonstrated[15,27]. New to this study is the inquiry into the affinity of the cation to the PEG surface coating, where Na^+>Li^+ (with further evidence needed for K^+), which improved dispersion of the active material within the binder. Improved dispersion noticeably impacted rate capability performance, particularly at high current densities (1C and 2C), and allowed the capacity of the sodium derivative to improve as a result of a steady increase in the active material surface area.

Increased cation size positively impacted kinetics, capacity retention, SEI layer formation and charge transfer resistance. Cation size was previously shown to improve ionic conductivity[92,93] and may also impact porosity within the electrode, which would subsequently affect ion transport. The largest cation in this study, potassium, exhibited the most stable performance, which could be a result of a more porous morphology that is able to support ion transport. Deviations from the proposed correlation between cation size and improved performance can be explained from lithium derivatives exhibiting an artificially high capacity at the start of testing, which would impact initial capacity values, charge transfer resistance before cycling, and kinetics. The positive, initial effects from lithium are intrinsically due to its importance in the overall system and not a reflection on the cation size effects. Lithium is smaller in size causing a more tightly packed system, which may ultimately be limiting ion transport. Since potassium and sodium are larger cations, they are positively improving ion transport, as evidenced through electrochemical testing.

Using PEG in conjunction with a carboxylated polythiophene binder for high-capacity composite battery electrodes, we demonstrated that cation size and structure impacts interfacial interactions and chemical binding between the components of the composite. These, in turn, significantly affect the overall electrochemical performance of the system. Unexpectedly, while the lithium salt analog exhibited initial higher capacity, that capacity was not retained upon cycling. Alternatively, the larger potassium cation based composite exhibited reduced charge transfer resistance and stable SEI layer formation, which improved cycling performance and rate capability. Furthermore, interactions between PEG, introduced to limit aggregation of the active material, and the counterion present in the polymeric binder can facilitate materials dispersion, leading to

enhanced rate capability at higher current densities. The strategies discussed here in determining how ions present within a composite electrode can either aid or hinder transport create a framework for the future design of polymeric binders for high performance high capacity electrodes. Simultaneously, the results provide insight into how the molecular structure of the individual components of composite electrodes can be manipulated to optimize the interfacial interactions/interfacial chemistries that markedly influence overall electrochemical performance.

CHAPTER 3. TUNING SEMICONDUCTING POLYMERS FOR BINDER APPLICATIONS

3.1 Introduction

To meet societal expectations of light-weight consumer electronics with extended battery lifetimes and electric vehicles able to traverse hundreds of miles on a single charge, new materials designs that effect an increase the energy density of battery technologies are imperative.[5] Current state-of-the-art lithium-ion technology relies on graphite-based anodes, which have a relatively low theoretical capacity of 372 mAh g^{-1}.[4] Alternative active materials, such as transition metal oxides providing multiple electron transfers per formula unit, promise markedly higher specific capacities (~500-1000 mAh g^{-1})[1], but most of these oxides suffer from poor conduction. Fe_3O_4 (magnetite) and RuO_2, are notable exceptions that exhibit high electronic conductivities,[77–79] with Fe_3O_4 having additional advantages in terms of being earth abundant, low cost and environmentally friendlier.[1,77–79] The practical implementation of magnetite, however, is limited by its poor cycling stability due to significant volume changes during continuous charging/discharging that are directly related to its conversion mechanism.[31,103]

To ameliorate the large volume changes experienced by magnetite and other active materials that occur during cycling, it has been suggested that the polymeric binder component of the composite electrode can help reinforce the system, thereby helping to preserve active material and electrode integrity during cycling.[56,71] The prevailing polymeric binder used in battery electrode applications, poly(vinylidene difluoride)

(PVDF), is robust and readily available; however, as a result of weak van der Waals interactions between the active material and the polymer, it is unable to effectively accommodate large volume changes in spacing between particles that inevitably occur during cycling.[50] Thus, further advancements in polymeric binder design are needed, given their critical role in maintaining both electronic and mechanical integrity of battery electrodes.[61]

While PVDF represents a workhorse polymer frequently used to bind the active material and conducting agents together in composite electrodes, water soluble alternatives are beginning to emerge as attractive, low cost and more sustainable alternatives. For instance, carboxymethyl cellulose (CMC) and polyacrylic acid (PAA) enable aqueous processing, obviating the need for toxic solvents, and further, it has been suggested that hydrogen bonding interactions between the carboxylate moiety on the polymer and surface hydroxyl groups on the active material (i.e. Si, Fe_3O_4), may help promote ion transport.[50,52–57] Other alternatives, including semiconducting and conducting polymers, which provide for varying degrees of electronic conductivity have also been reported.[49,83,104,105] For instance, semiconducting polymers that can be doped during battery cycling thereby supporting electronic conductivity within the electrode, have been explored, and it has been suggested that conductive binders may reduce the need for the incorporation of conductive additives, such as Super P or Carbon Black.[60] With respect to the latter, use of conductive polymeric, poly(9,9-dioctylfluorene-co-fluorenone-co-methylbenzoic ester), as the binder component for SiO anodes obviated the need for conductive additives.[64] The ongoing development of polymeric binders, whether water-soluble or conductive, has demonstrated that binder chemistry is integral to the design and development of high-

performance anodes,[62] and ideally, in addition to serving as an adhesive to preserve electrode mechanical integrity, the binder component should facilitate electronic/ionic conductivity.[61]

While several alternative polymers have been reported to positively impact high capacity anode electrochemical performance, especially assisting in enhancing conduction, systematic studies that explore the roles of particular chemical functionalities are lacking. For instance in silicon anode systems, a water-soluble conductive binder consisting of carboxymethyl cellulose (CMC) and poly(3,4-ethylenedioxythiophene): poly(styrenesulfonate) (PEDOT:PSS) showed improved electrochemical performance,[55] while in magnetite systems, poly(3-potassium-4-butanoate thiophene) (PPBT) used in conjunction with polyethylene glycol (PEG) has proven effective.[106] The non-conjugated carboxylated polymer, PAA, has also been investigated as a binder for silicon-based anodes.[50,56,57,59] This low cost, water soluble, acidic polymer readily binds to the active material surface, facilitating improved electrode stability coupled with "green" electrode fabrication.[57] In comparison to CMC, it was suggested that the higher concentration of carboxylate functional groups enabled the improved performance of PAA electrodes.[50]

Here, we investigate the role of carboxylate functionalities and the ability of the binder to support electronic conduction on performance of magnetite-based anodes for Li-ion battery applications. Specifically, the potassium salt of the insulating acrylate PAA, named PAA-K, was used to explore electrode electrochemical characteristics in the presence of carboxylate, while PPBT served as a carboxylated semiconducting polymer control. Two conducting polymers were evaluated to investigate possible synergies between carboxylation and electronic conductivity that support electrode performance,

namely, PEDOT:PSS and a carboxylated derivative, a water-soluble alternating copolymer of a functionalized 3,4-propylenedioxythiophene unit with a 2,2'-bis(3,4-ethlyenedioxythiophene) unit (WS-PE_2). Electrodes fabricated with each of these polymers were characterized by examining their specific capacity and capacity retention upon cycling, coulombic efficiency, rate capability, and electrode kinetics. The results provide fundamental insights into the role and importantly, impact of functional groups present on binders used for high-capacity composite anodes in promoting efficient electron and ion transport pathways.

3.2 Materials and Methods

3.2.1 Materials

Fe_3O_4 nanoparticles (~10 nm) were synthesized by a previously reported coprecipitation process using aqueous solution of iron(III) chloride hexahydrate, iron(II) chloride hexahydrate, and triethylamine.[29,88] For preparation of Fe_3O_4 particles coated with PEG (PEG-Fe_3O_4), 0.5 g of Fe_3O_4 powder in 5 g of water were sonicated at room temperature with an ultrasonic probe for 1.5 min (3 pulses of 30 s each, operated at 50 W, Qsonica Q700 sonicator). PEG 1500 solution (2 mL; 50% w/v, Sigma-Aldrich) was added with sonication for 30 s, and this process was repeated four times until the total amount of PEG 1500 was 8 mL. The PEG-Fe_3O_4 powders were washed and extracted by centrifuge separation (VWR Clinical 200) using acetone with speed of 6000 rpm for 5 min for 3 times.

PPBT (M_w: 21 kDa, polydispersity: 2.2, head to tail regioregularity: 89%) was purchased from Rieke Metals Inc. WS-PE_2 was synthesized through a previously described method.[107] PAA (M_w: 1180.5 kDa, polydispersity: 2.03) was purchased from Sigma

Aldrich and M_w was determined by size exclusion chromatography (**Figure 18**). To produce the potassium salt form of PAA, the polymer was dispersed in water, excess KOH (1 M, 3 mL) and allowed to mix for 30 min. Excess K ions were removed with dialysis for a 3-day period in a total of 3 L of DI water. The PAA-K polymer was verified through XPS (**Figure 17**). The C 1s scan reveals a shifting to lower binding energies of C-O and C=O bonds, which would result from the additional K^+ present. In PAA-K, two additional peaks are present (293 eV and 295.5 eV), which are associated with K and confirm a successful ion exchange.[89] The same shifting of binding energies is observed in the O 1s scan, providing further confirmation.

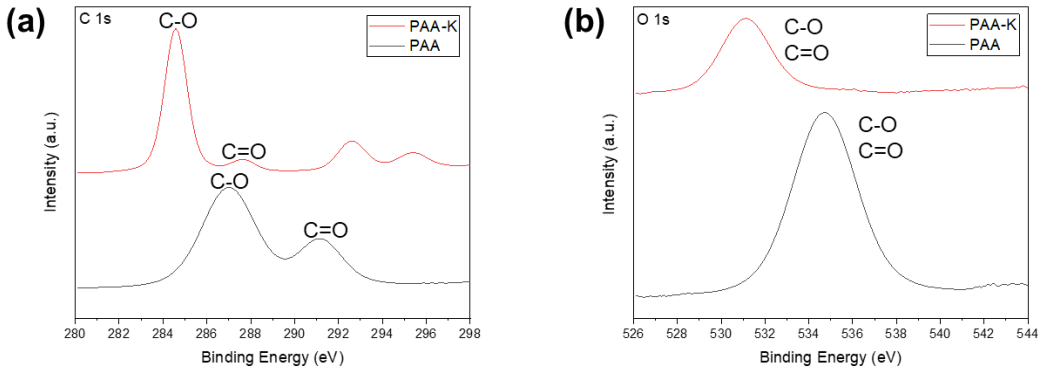

Figure 17: XPS spectra of PAA and PAA-K. (a) C 1s scan and (b) O 1s scan.

3.2.2 Size Exclusion Chromatography

A SEC-multi-angle light scattering (MALS) setup was used to determine the molecular weight and polydispersity of PAA. A 20 µL injection of 2.5 mg/mL PAA dispersed in a buffer of pH 9 (0.3 M $NaNO_3$, 0.1 M H_2NaPO_4, and 0.02% NaN_3 w/v) was used. The SEC system consisted of an Agilent 1260 Infinity II with ISO Pump and 1260

Vialsampler. An Agilent PL aquagel guard column was followed by two Agilent PL aquagel-OH MIXED-H columns (8um 300 x 7.5mm). The MALS system consisted of a Wyatt DAWN HELEOS-II and Otpilab T-rEX. Analysis was completed using Astra 7.1 software. The reported chromatograms displayed the light scattering trace from the 90° detector (**Figure 18**). The dn/dc value for PAA used was 0.17 mL g^{-1}.

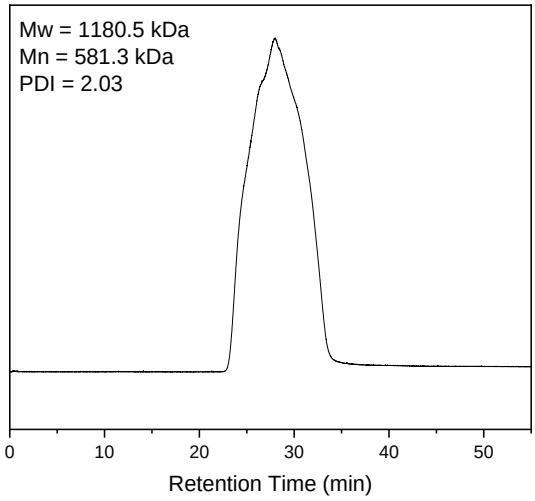

Figure 18: SEC curve of PAA.

3.2.3 Electrode Fabrication and Electrochemistry

The slurries for the electrodes were prepared by mixing PEG-Fe_3O_4 (0.1 g), carbon additives (0.02 g), and PPBT (10 wt% solution, 0.2 g) with a weight ratio of PEG-Fe_3O_4:carbon:polymer = 71.4:14.3:14.3. The slurries for WS-PE_2 and PAA-K electrodes were prepared with the same weight loading, but concentrations of solutions varied based on viscosity differences in the polymers. WS-PE_2 was added at a 2.5 wt% solution and PAA-K was used in a 5 wt% solution. The electrodes for field-emission scanning electron

microscopy (FE-SEM, Zeiss Ultra-60) measurement, electrochemical evaluation and spectroscopy characterization were produced by blade coating (doctor blade, MTI corp). The electrodes were first allowed to dry at room temperature for 1 h, followed by 110 °C for 12 h in a vacuum oven.

PEDOT:PSS electrodes were fabricated using a monodispersed spherical Fe_3O_4 (sFe_3O_4), using a previously reported solvothermal synthesis method.[108] The sFe_3O_4/PEDOT:PSS electrode and sFe_3O_4/carbon/PEDOT:PSS electrode were prepared in a weight ratio of 96.2:3.8 and 71.4/14.3/14.3, respectively, and were blade-coated onto a Cu foil substrate. These compositions were determined through conductivity testing, based on the conductivity threshold. The electrodes were first allowed to dry at room temperature for 1 h, followed by 110 °C for 12 h in a vacuum oven.

Stainless-steel coin cells (2032-type) were used for electrochemical measurements. Lithium metal, purchased from MTI corp., was used as a counter electrode and 1 M $LiPF_6$ in ethylene carbonate (EC) and diethylene carbonate (DEC) (1:1 by weight), purchased from BASF, was used as the electrolyte. Before electrochemical testing, the capacity of each coin cell was confirmed by charging and discharging at a current density of 40 mAg^{-1} (~0.05 C), using an Arbin battery cycler. The tests were then proceeded for cycling and rate capability. Cyclic voltammetry (CV) was performed in the potential range of 0.01-3 V at the rate of 0.5 mV s^{-1} and electrical impedance spectroscopy (EIS, Metrohm Autolab PGSTAT101) measurements were conducted in the frequency range from 0.1 MHz to 0.1 Hz.

3.2.4 Electronic Conductivity Measurements

Measurements followed the same procedure as previously detailed.[38] For these measurements, the electrode devices with two bottom contacts (channel width = 10 μm and length = 50 μm) were used for electrical characterization, where composite film were deposited via mold-casting on a silicon wafer with a 300 nm thick SiO_2. The characterization process follows from a previously detailed procedure[109]: Au was used for the source and drain contacts that were fabricated using a standard photolithography based on a lift-off process, followed by Denton Explorer E-beam evaporation of 3 nm thick Cr as the adhesive layer and sequentially Au contact with 50 nm thickness. Before casting, all devices were exposed in a UV-ozone cleaner (Novascan PSD-UV) for 15 min to completely remove any organic contaminants. The prepared composite electrodes were casted via a mold-casting technique[38] and were tested in a nitrogen ambient glovebox using a semiconductor parameter analyzer (Agilent 4155 C). Composite electrode conductivity is measured simultaneously at three different points. Two voltage probes between the source and drain electrodes monitor the potential along the conductive channel. The resulting electronic conductivity was calculated by:

$$\sigma = \frac{L}{W \times t}\frac{I_D}{V_D}$$

where W (10 μm), L (50 μm), and t are the channel width, length, and film thickness, respectively. V_D is the drain voltage and I_D is the drain current.

3.2.5 Microscopic Characterization

FE-SEM images were observed on the surface view of the electrodes using a Zeiss Ultra-60 FE-SEM with an accelerating voltage of 5 kV using the high vacuum mode at room temperature.

3.2.6 Spectroscopic Characterization

The electrode samples for spectroscopy measurements were prepared by removing powder samples from the prepared electrodes. X-ray spectroscopy (XPS) characterization was performed using a Thermo K-Alpha XPS system. The instrument was equipped with a monochromatic Al-K X-ray source (1468 eV). Spectra were collected using the flood gun and an X-ray spot size of 400 µm. Survey scans were collected with pass energy of 200 eV with 1 eV increments. High resolution scans (for specific elements) were collected with pass energy of 50 eV with 0.1 eV increments. For XPS analysis of the electrodes after 100 cycles, the delithiated electrodes were extracted from the cycled coin cells and carefully rinsed with DMC three times (5 mL in total) to remove residual electrolyte and then dried in a vacuum oven (80°C, 12 hr).

3.2.7 Hansen Solubility Parameter Analysis

3.2.7.1 Solubility Tests for Hansen Solubility Parameter (HSP)

Five mg of polymer (PAA, WS-PE_2, PPBT and PEG) were placed into a vial with 2 mL of a test solvent. The vial was heated at 70°C for 3 h and sonicated for 60 min. After, the vials were permitted to stand and observed for 6 h in ambient temperature. The solubility was examined by these solutions via visual observation. In the case of the

polymer, solvents would be considered as poor if they were unable to dissolve the polymer after dissolving process and good if they were able to dissolve it. On the basis of visual examination, HSPs (δ_D, δ_P, and δ_H) and the radius value (R_0) of the sphere of interaction were calculated and fitted by HSPiP software (Hansen Solubility Parameters in Practice, 3rd edition).

3.2.7.2 Hansen Solubility Parameter Analysis

To evaluate whether or not a solvent belongs to a sphere of high physical affinity, the distance R_a between the solvent and material is calculated by the below equation:[38,110]

$$(R_a)^2 = 4(\delta_{D1} - \delta_{D2})^2 + (\delta_{P1} - \delta_{P2})^2 + (\delta_{H1} - \delta_{H2})^2$$

where the subscripts 1 and 2 represent the solute and solvent, respectively. The relative energy difference (RED = R_a/R_0) provides an estimate of whether two materials will be miscible (miscible when RED < 1, partially when RED = 1, and immiscible when RED > 1)[110]. Good solvents are defined as solvents which can dissolve more than 2.5 mg/mL of the polymer, were assigned a score of "1", while poor solvents were assigned a value of "0".

3.2.7.3 Solubility Test Results

The solubility of the various polymers in this investigation in a wide range of solvents is summarized below.

Table 3: Good and bad solvents in tests of PPBT surface affinity and their RED values. (δ_D = 19.05 $MPa^{1/2}$, δ_P = 25.96 $MPa^{1/2}$, δ_H = 26.85 $MPa^{1/2}$, R_o = 19.9 $MPa^{1/2}$, Data fit 0.976).

Solvent	δ_D ($MPa^{1/2}$)	δ_P ($MPa^{1/2}$)	δ_H ($MPa^{1/2}$)	Surface Affinity	RED
1,2,4-Trichlorobenzene	20.2	4.2	3.2	Bad	1.629
Acetone	15.5	10.4	7	Bad	1.314
Chlorobenzene	19	4.3	2	Bad	1.664
Chloroform	17.8	3.1	5.7	Bad	1.578
Ethanol	15.8	8.8	19.4	Bad	1.002
Hexane	14.9	0	0	Bad	1.924
Tetrahydrofuran	16.8	5.7	8	Bad	1.414
Toluene	18	1.4	2	Bad	1.766
Tricholoroethylene	18	3.1	5.3	Bad	1.59
Diethylene Glycol	16.6	12	19	Good	0.848
Dimethyl Formamide	17.4	13.7	11.3	Good	1.01
Dimethyl Sulfoxide	18.4	16.4	10.2	Good	0.967
Ethylene Glycol	17	11	26	Good	0.796
Water	15.5	16	42.3	Good	1.001

Table 4: Good and bad solvents in tests of PEG1500 surface affinity and their RED values. (δ_D = 19.39 $MPa^{1/2}$, δ_P = 24.56 $MPa^{1/2}$, δ_H = 27.24 $MPa^{1/2}$, R_o = 19 $MPa^{1/2}$, Data fit 1.000).

Solvent	δ_D ($MPa^{1/2}$)	δ_P ($MPa^{1/2}$)	δ_H ($MPa^{1/2}$)	Surface Affinity	RED
1,2,4-Trichlorobenzene	20.2	4.2	3.2	Bad	1.66
Acetone	15.5	10.4	7	Bad	1.363
Chlorobenzene	19	4.3	2	Bad	1.704
Chloroform	17.8	3.1	5.7	Bad	1.609
Dimethyl Formamide	17.4	13.7	11.3	Bad	1.037
Ethanol	15.8	8.8	19.4	Bad	1.001
Hexane	14.9	0	0	Bad	1.988
Tetrahydrofuran	16.8	5.7	8	Bad	1.444
Toluene	18	1.4	2	Bad	1.809
Tricholoroethylene	18	3.1	5.3	Bad	1.622
Diethylene Glycol	16.6	12	19	Good	0.844
Dimethyl Sulfoxide	18.4	16.4	10.2	Good	1
Ethylene Glycol	17	11	26	Good	0.76
Water	15.5	16	42.3	Good	0.999

Table 5: Good and bad solvents in tests of PAA surface affinity and their RED values. (δ_D = 19.67 MPa$^{1/2}$, δ_P = 6.08 MPa$^{1/2}$, δ_H = 15.62 MPa$^{1/2}$, R_o = 12.7 MPa$^{1/2}$, Data fit 1.000).

Solvent	δ_D (MPa$^{1/2}$)	δ_P (MPa$^{1/2}$)	δ_H (MPa$^{1/2}$)	Surface Affinity	RED
Acetone	15.5	10.4	7	Bad	1.004
Chlorobenzene	19	4.3	2	Bad	1.087
Hexane	14.9	0	0	Bad	1.519
Toluene	18	1.4	2	Bad	1.164
Water	15.5	16	42.3	Bad	2.336
1,2,4-Trichlorobenzene	20.2	4.2	3.2	Good	0.993
Chloroform	17.8	3.1	5.7	Good	0.867
Diethylene Glycol	16.6	12	19	Good	0.723
Dimethyl Formamide	17.4	13.7	11.3	Good	0.777
Dimethyl Sulfoxide	18.4	16.4	10.2	Good	0.94
Ethanol	15.8	8.8	19.4	Good	0.711
Ethylene Glycol	17	11	26	Good	0.998
Tetrahydrofuran	16.8	5.7	8	Good	0.752
Tricholoroethylene	18	3.1	5.3	Good	0.886

Table 6: Good and bad solvents in tests of WS-PE2 surface affinity and their RED values. (δ_D = 15.92 MPa$^{1/2}$, δ_P = 14.01 MPa$^{1/2}$, δ_H = 30.64 MPa$^{1/2}$, R_o = 11.9 MPa$^{1/2}$, Data fit 1.000).

Solvent	δ_D (MPa$^{1/2}$)	δ_P (MPa$^{1/2}$)	δ_H (MPa$^{1/2}$)	Surface Affinity	RED
1,2,4-Trichlorobenzene	20.2	4.2	3.2	Bad	2.552
Acetone	15.5	10.4	7	Bad	2.011
Chlorobenzene	19	4.3	2	Bad	2.593
Chloroform	17.8	3.1	5.7	Bad	2.309
Dimethyl Formamide	17.4	13.7	11.3	Bad	1.644
Dimethyl Sulfoxide	18.4	16.4	10.2	Bad	1.779
Ethanol	15.8	8.8	19.4	Bad	1.041
Hexane	14.9	0	0	Bad	2.836
Tetrahydrofuran	16.8	5.7	8	Bad	2.032
Tricholoroethylene	18	3.1	5.3	Bad	2.344
Toluene	18	1.4	2	Bad	1.164
Diethylene Glycol	16.6	12	19	Good	0.999
Ethylene Glycol	17	11	26	Good	0.499
Water	15.5	16	42.3	Good	0.997

3.3 Results and Discussion

While PAA, PPBT and PEDOT:PSS have been investigated as alternative binders for high-capacity Li-ion battery electrode applications, a systematic investigation leading to understanding of the role of carboxylate and conjugated functionalities has yet to emerge. Both PAA and PEDOT:PSS have been reported to enhance silicon anode performance,[50,55–57,59] while PPBT has been shown effective for a range of metal oxide active components.[11,86,95,108] To elucidate the impact of the predominant functionalities, the performance of electrodes fabricated with PAA, PPBT and PEDOT:PSS are described below.

3.3.1 PEDOT:PSS Electrochemical Characterization

Preliminary investigation into PEDOT:PSS, confirmed conclusions drawn from studies using poly(3-hexylthiophene) (P3HT) that while electronic conductivity is a factor to consider in the design of a binder for composite electrode materials, it is not a sufficient criterion.[38] As presented in **Figure 19a** in comparison to P3HT, PPBT and PVDF, PEDOT:PSS is highly conductive (55 S/cm). Yet counter to PVDF and the thiophenes, the conducting polymer does not undergo a significant increase in conductivity upon incorporation of carbon (**Figure 19b**).[38] When used as a binder for magnetite-based electrodes, PEDOT:PSS (**Figure 19c**) exhibited poor capacity retention at 0.3 C between 0.01 and 3V and poor overall performance, even with the addition of carbon to promote electron transport. SEM images (**Figure 19d**) suggest that PEDOT:PSS adopts a morphology that may hinder ion transport, illustrating that high electronic conductivity is

an insufficient criterion for achieving enhanced electrochemical performance and ion transport must be a prime consideration.[11,38]

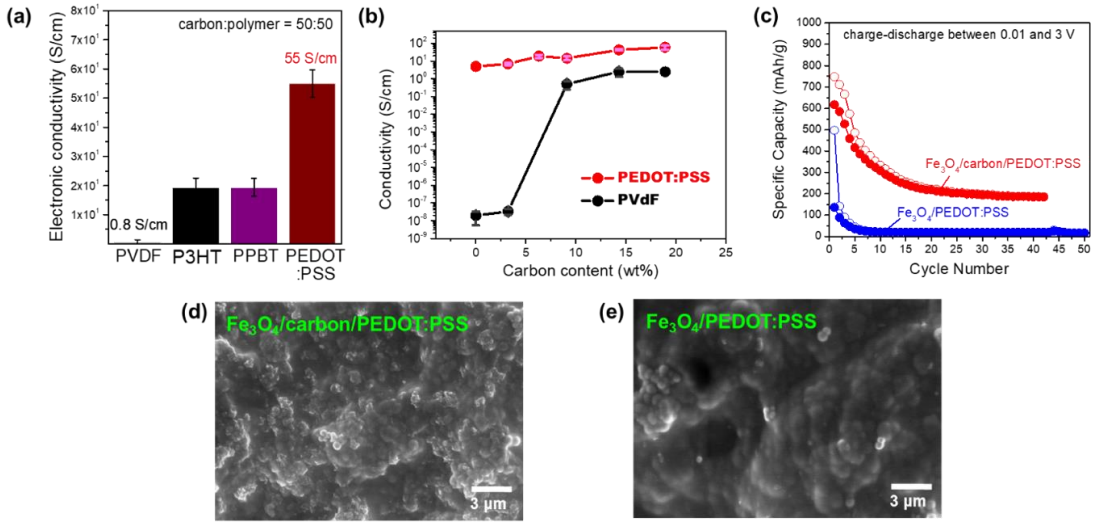

Figure 19: PEDOT:PSS conductivity and composite electrode characteristics. (a) Conductivity measurements (b) Conductivity as a function of carbon loading (c) Capacity retention (capacity vs. cycle number) at 0.3 C between 0.01 and 3 V (d) SEM image of electrode surface for Fe_3O_4/carbon/PEDOT:PSS (e) SEM image of electrode surface for Fe_3O_4/PEDOT:PSS.

3.3.2 Polymers of Interest

The incorporation of carboxylate functionalities facilitated the investigation of how the polar substituent can impact electrochemical performance, both in the presence and absence of conjugated moieties that can support electron transport. Specifically, three water-soluble, carboxylated polymers (**Figure 20**) investigated here included the potassium salt of PAA (PAA-K), PPBT and the PEDOT:PSS derivative, WS-PE_2, which is a water soluble (WS) copolymer comprising a functionalized 3,4-propylenedioxythiophene unit (P_x) with a 2,2'-bis(3,4-ethylenedioxythiophene) unit (E_x).

Compared to the parent PEDOT:PSS, the polar side chains on the solvent resistant form of PE_2 were reported to allow for enhanced ion transport. WS-PE_2 exhibited low oxidation potential, broad redox-active potential window, rapid charge transport, and high capacitance values in supercapacitor applications.[107] In order to mitigate active particle aggregation and improve particle dispersion, polyethylene glycol (PEG) was physically introduced onto the Fe_3O_4 particle surface,[11,30,43,84] where resultant PEG-Fe_3O_4 particles were composed of ~11 wt% PEG (TGA analysis, **Figure 21**). Control studies were also performed in the absence of PEG.

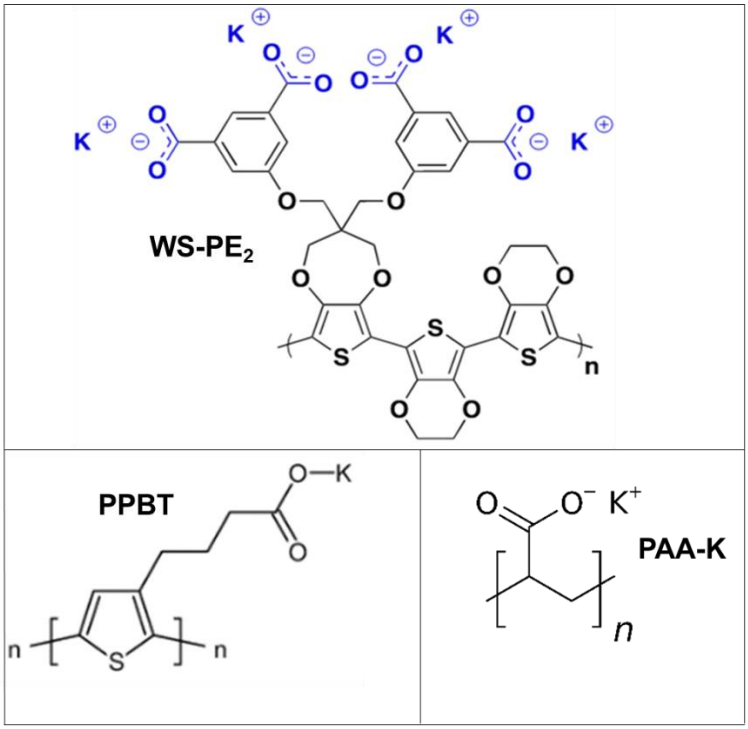

Figure 20: Polymers of interest: WS-PE_2, poly[3-(potassium-4-butanoate)thiophene] (PPBT), and the potassium salt form of polyacrylic acid (PAA-K).

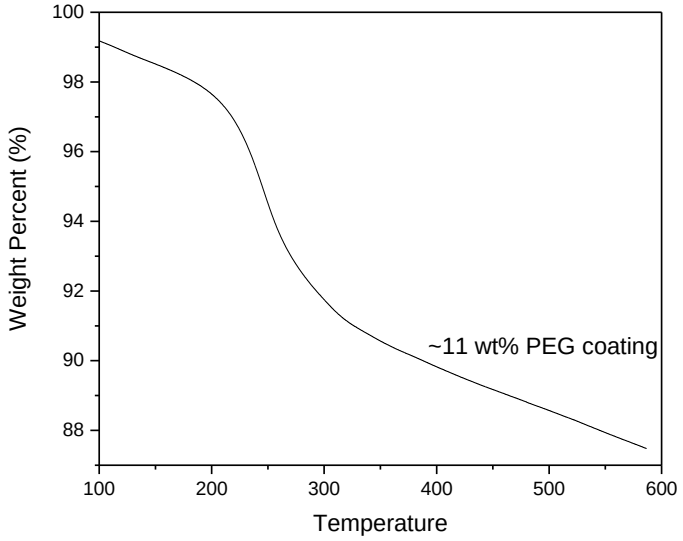

Figure 21: TGA profile of PEG coating, which is carried out in nitrogen in the temperature range of 25–600°C at a heating rate of 10°C/min, confirming ~11 wt% PEG coating.

3.3.3 Microscopic Characterization

Electrodes were prepared with Fe_3O_4 active material, carbon additives, and polymeric binder in the same manner as previously described.[38] Since transport limitations at the aggregate level can significantly impact Fe_3O_4 electrochemistry,[111] composite morphology was evaluated through SEM (**Figure 22**), and as anticipated, electrodes fabricated without PEG to inhibit active material aggregation generally comprised larger aggregates (**Figure 22a-c**).[11,30] Use of PEG (**Figure 22d-e**) afforded electrodes with more uniform morphology and significantly fewer larger aggregates.

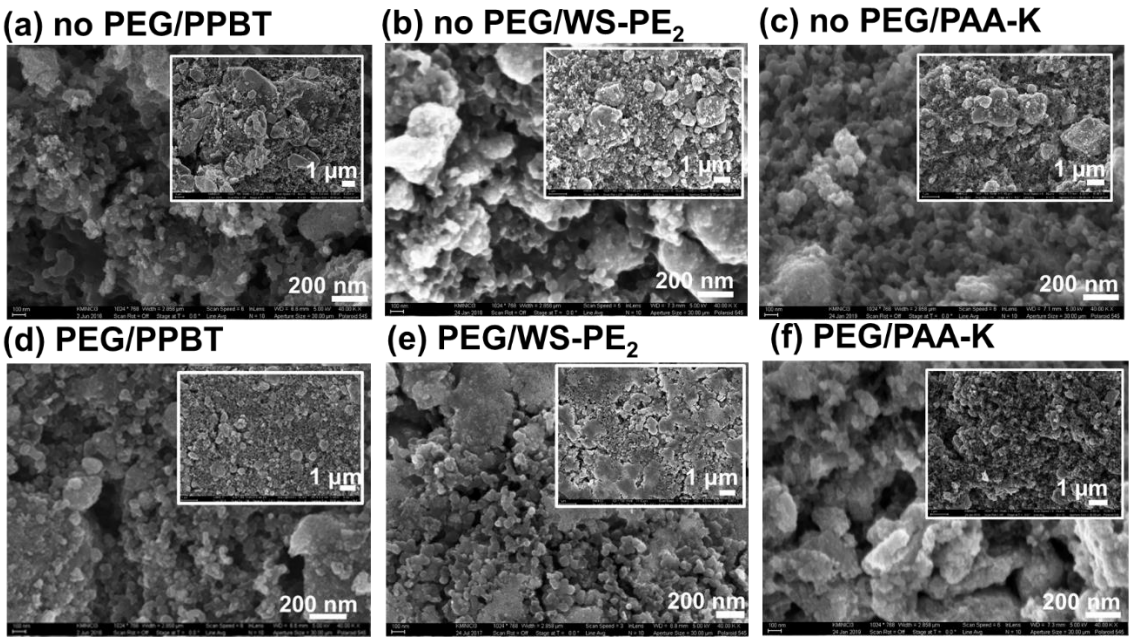

Figure 22: SEM images of electrode surface.

3.3.4 Hansen Solubility Parameter Analysis

The physical compatibility between electrode constituents was further evaluated using Hansen solubility parameter (HSP) analysis which enables estimation of the physical affinity between different materials.[38] Specifically, materials with similar HSP values exhibit high physical affinities, which correlates well with compatibility.[38] HSPs were calculated using the respective polymer solubility in a range of solvents with known HSP values. HSPs (dispersion, polar, and hydrogen bonding parameters, δ_D, δ_P, δ_H, respectively) and the radius (R_0) of the sphere of interaction for the materials was obtained through Abbott and Hansen software.[112] Solvents within R_0 are expected to disperse/dissolve the solute, whereas solvents outside of R_0 are not expected to be effective.[110,113,114] The details associated with the calculations along with the solubility of the various polymers in a wide

range of solvents is summarized above in Materials and Methods. The calculated HSP values for the carboxylated polymers and PEG are summarized in **Table 7**.

Table 7: Hansen solubility parameters (HSPs) of the active material coating, PEG, and various polymeric binders.

Material	δ_D (MPa$^{1/2}$)	δ_P (MPa$^{1/2}$)	δ_H (MPa$^{1/2}$)	R_0 (MPa$^{1/2}$)	Data fit
PPBT	19.05	25.96	26.85	19.9	0.976
PEG 1500	19.39	24.56	27.24	19	1.000
WS-PE$_2$	15.92	14.01	30.64	11.9	1.000
PAA	19.67	6.08	15.62	12.7	1.000

RED values calculated for PEG with respect to WS-PE$_2$, PPBT, and PAA were 13.1, 1.6, and 21.8, respectively. A lower RED value is an indication of better materials miscibility, where the physical affinity with PEG follows the trend: PPBT > WS-PE$_2$ > PAA based on the RED values. The Hansen spheres (**Figure 23**) present the relationship of interactions for PEG/WS-PE$_2$, PEG/PAA, and PEG/PPBT. Generally, when regions of affinity of different materials are superimposed, the components are expected to experience very high physical attraction.[115] Together with their RED value, in order to confirm the extent of overlap between two spheres of interaction, the sphere intersection volume (V_{int}) was calculated and the superimposed volume portion (%V_{int}) for each polymer volume was obtained by $V_{int}/V_{polymer}$, as illustrated in **Figure 23**. Values close to 100% indicate mutual compatibility, but values that are low suggest that two phases could readily form upon mixing. The HSP results strongly suggest that the physical affinity between PEG and PPBT is substantially more favorable that between PEG and either WS-PE$_2$ or PAA.

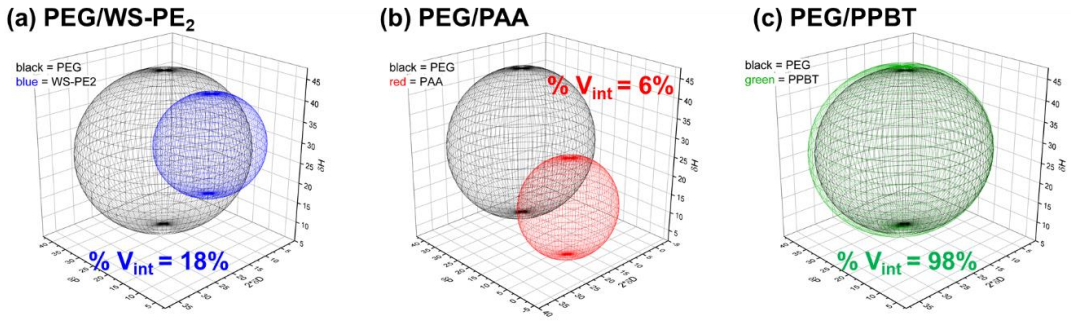

Figure 23: Hansen solubility parameter (HSP) spheres of interaction for (a) PEG 1500 and WS-PE$_2$, (b) PEG 1500 and PAA, (c) PEG 1500 and PPBT. %V$_{int}$ refers to the superimposed volume portions in which PEG is occupied by the other polymer.

3.3.5 Electrochemical Characterization

The impact of carboxylate and conjugated functionalities in polymeric binders used in the fabrication of magnetite-based anodes, in the presence/absence of PEG was further elucidated through electrochemical characterization. Tests were performed using coin cells fabricated with Li metal counter electrodes and working electrodes prepared with Fe_3O_4 active material (with/without PEG coating), carbon additives and polymeric binder in a 71.4:14.3:14.3 mass ratio, which was chosen based on prior results to facilitate direct comparison.[38] The electrolyte was 1 M $LiPF_6$ in ethylene carbonate (EC) and diethylene carbonate (DEC) (1:1 by weight). Charge-discharge cycling (**Figure 24a**) was conducted at a current density of 240 mA g^{-1} (~0.3 C) for 100 cycles to determine capacity retention. Corresponding Coloumbic efficiency is provided in **Figure 24b**, while galvanostatic profiles are provided in **Figure 25**. Repeatability over three separate coin cells is demonstrated in **Table 8**.

PEG/PPBT provided for the most stable electrode performance over 100 cycles, while PAA-K (red) results were clearly inferior. In contrast, the carboxylated PEDOT:PSS analog,WS-PE_2 (blue) exhibited intermediate cycling performance that was notably improved compared to its parent PEDOT:PSS (**Figure 19c**). After 100 cycles, PPBT and WS-PE_2 appeared to exhibit similar capacity values, which prompted determination of capacity retention of the WS-PE_2 electrode for 200 cycles. As presented in **Figure 24c,** despite having a lower capacity, PEG/WS-PE_2 electrode performance appears to stabilize over 200 cycles. The impact of PEG on cycling was most significant with PPBT as the binder, highlighting the need to consider materials physical affinity when designing composite materials for electrode applications. While PEG/PPBT resulted in significantly improved cycling performance, the incorporation of PEG led to a decrease in PAA-K and WS-PE_2 performance, perhaps due to its poor physical affinity with the polymers, particularly the PAA-K system.

Newly fabricated half cells were subjected to rate capability experiments (**Figure 24d**) where cells were lithiated at a constant current density of 80 mA g^{-1} (~0.1 C) and delithiated over a wide range of current densities (80 – 1600 mA g^{-1}) between a voltage range of 0.01 – 3 V. PEG/PPBT and PEG/PAA-K exhibited similar performance, particularly at higher current densities (1 C and 2 C); and the corresponding no PEG analogs presented similar trends, although at lower capacity values. Conceivably, PEG facilitated materials dispersion, which in turn led to enhanced rate capability performance.[30] Despite its enhanced cycling stability at 0.3C, WS-PE_2 exhibited poor overall rate capability performance.

The improved rate capability performance of PAA-K is attributed to the concentration of carboxylic groups, as compared to WS-PE_2 and PPBT. Magasinski *et al*. previously noted the improvement of PAA with respect to CMC in Si-based anodes is due to the higher concentration of carboxylic groups.[50] They speculated that a certain fraction of the COOH groups in PAA form strong hydrogen bonds with OH groups on the active material surface and therefore, the remaining carboxyl groups are able to form COOLi groups to protect the anode electrical conductivity from degradation. The concentration of carboxylic groups per repeat unit of each polymer was calculated to be 66.9 wt%, 39.9 wt%, and 34 wt% for PAA-K, PPBT, and WS-PE_2, respectively. The trend in increasing carboxylic group concentration corresponds well with rate capability data.

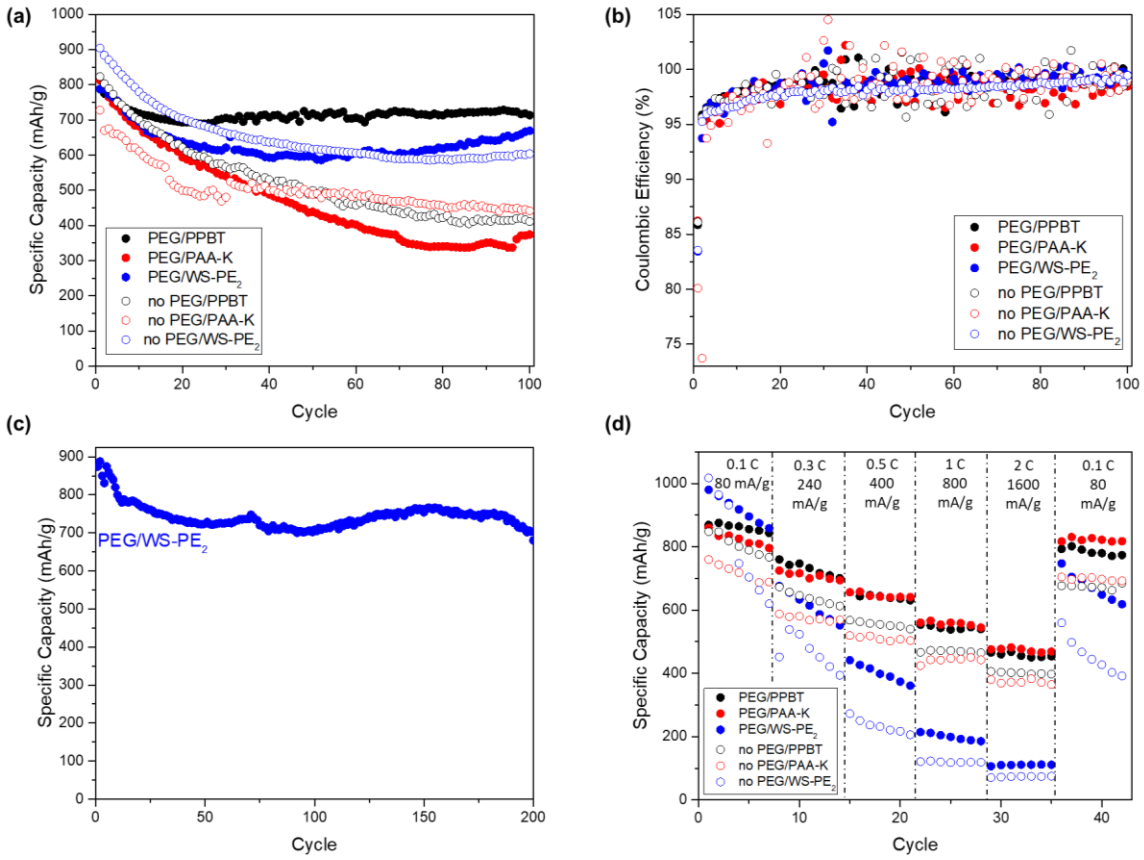

Figure 24: (a) Cycling performance comparing different polymeric binders with and without PEG cycled at 240 mA g^{-1} (~0.3 C) between 0.01 and 3 V. (b) Coulombic efficiency corresponding to cycling performance in (a). (c) Cycling performance of PEG/WS-PE_2 over 200 cycles at 240 mA g^{-1} (~0.3 C) between 0.01 and 3 V. (d) Delithiation rate capability, where cells are lithiated at a constant current density of 80 mA g^{-1} (0.1 C) and delithiated at different current densities between 0.01 and 3 V.

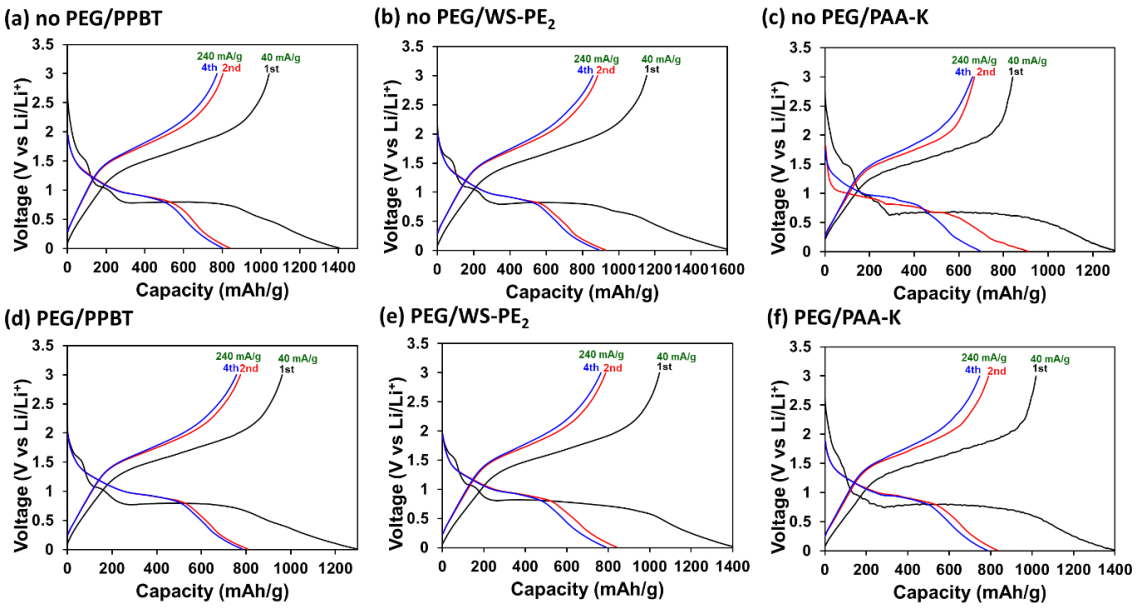

Figure 25: Galvanostatic profiles of various polymeric binders.

Table 8: Composite Anodes with Different Polymeric Binders (averaged over three coin cells)

Anode System	Initial Delithiation Capacity (mAh/g)	Cycle 100 Delithiation Capacity (mAh/g)	Initial Coulombic Efficiency (%)	Cycle 100 Coulombic Efficiency (%)
PEG/PPBT	826 ± 40	739 ± 43	85.6 ± 0.4	99.1 ± 0.3
PEG/PAA-K	788 ± 22	342 ± 36	85.5 ± 0.8	98.7 ± 0.6
PEG/WS-PE_2	775 ± 74	658 ± 47	84.0 ± 2.0	98.8 ± 0.6
No PEG/PPBT	797 ± 37	342 ± 36	86.0 ± 0.8	99.3 ± 0.6
No PEG/PAA-K	705 ± 32	435 ± 9	80.6 ± 0.7	99.0 ± 0.1
No PEG/WS-PE_2	870 ± 30	556 ± 43	83.7 ± 0.1	99.6 ± 0.2

Further insight into the performance differences between the carboxylated polymers can be discerned from analysis of EIS results (**Figure 26**), whereby the cells used here correspond to those cycled between 0.01 and 3V (**Figure 24a**). Impedance testing was performed in the frequency range of 0.1 MHz to 0.1 Hz before cycling at 3V and after 100

cycles at their open-circuit voltage (OCV). Superior battery electrode performance can be attributed to decreased charge transfer resistance (R_{ct}), which is estimated from the diameter of the high-frequency semicircle.[100] Prior to cycling, the two conjugated polymers, PPBT and WS-PE_2 (in the absence of PEG) exhibited the lowest charge transfer resistance, while PEG/PAA-K presented with the largest charge transfer resistance, consistent with its low initial capacity. The other systems showed the following trend of charge transfer resistance: no PEG/PAA-K > PEG/WS-PE_2 > PEG/PPBT. After cycling (**Figure 26b, c**), all composites exhibited a decrease in charge transfer resistance, but the trends differed. Charge transfer resistance was the lowest for the electrode fabricated with PAA-K in the absence of PEG, which is attributed to the concentration of carboxylic functional groups, *vide supra*. The other systems changed in trend of charge transfer resistance as compared to before cycling: no PEG/WS-PE_2 > PEG/WS-PE_2 = PEG/PAA-K > no PEG/PPBT = PEG/PPBT. The increased charge transfer resistance for WS-PE_2 may aid in the explanation for poor rate capability performance.

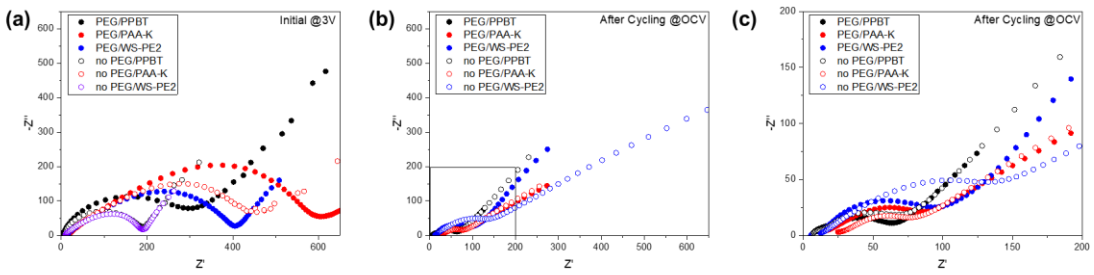

Figure 26: Electrical impedance spectroscopy (EIS) (a) before cycling at 3V, (b) after 100 cycles at OCV, and (c) zoomed in after 100 cycles at OCV in the frequency range from 0.1 MHz to 0.1 Hz.

Electrode kinetics was evaluated using cyclic voltammetry (CV) performed at different scan rates (v) (**Figure 27**) to further characterize differences between the polymeric binders. The kinetic data was characterized by analyzing the voltammetric response of the polymeric binders at various scan rates according to $I_{pc} = av^b$, where the measured peak current (I_{pc}) and the potential scan rate (v) obey a power-law relationship.[95–99] The slope from the plot of log (I_{pc}) *vs.* log (v) provided the value of *b*, which is correlated with Li^+ diffusion.[95,98] The fitting results are summarized in **Figure 28**, where a higher value of *b* suggests faster kinetics. Values of *b* for all systems are provided in **Table 9**. The impact of the PEG surface coating is clearly dependent on interactions between PEG and the polymer binder, as illustrated in HSP analysis (**Figure 23**). Due to the strong interactions between PEG and PPBT, large deviations are observed for systems with and without PEG. The PEG/PPBT system exhibits a much higher value of *b* as compared to its no PEG counterpart. As evidenced in HSP, the interactions between PEG and WS-PE_2 and PAA-K are weak in comparison, and the PEG coating in these systems may hinder electrochemical performance. PAA-K and WS-PE_2 exhibit higher values of *b* in the absence of PEG vs the same polymers used in conjunction with the oligomeric ether used to limit active materials aggregation. These values strongly correlate with the trends observed in cycling and rate capability studies suggesting the importance of physical affinity between active material coatings and polymeric binder.

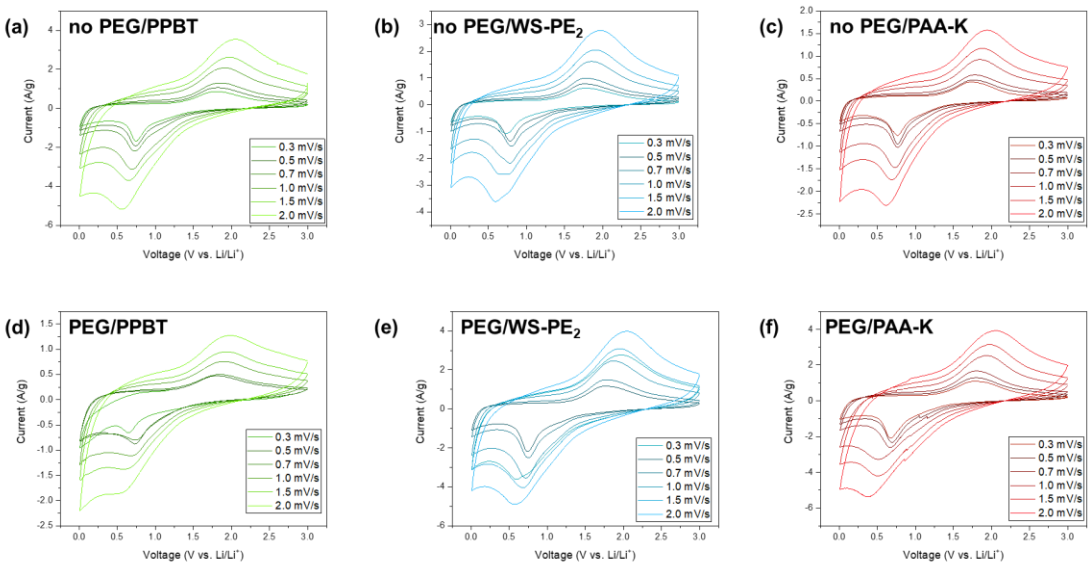

Figure 27: CV profiles with various scan rates (v) of (a) no PEG/PPBT, (b) no PEG/WS-PE_2, (c) no PEG/PAA-K, (d) PEG/PPBT, (e) PEG/WS-PE_2, and (f) PEG/PAA-K.

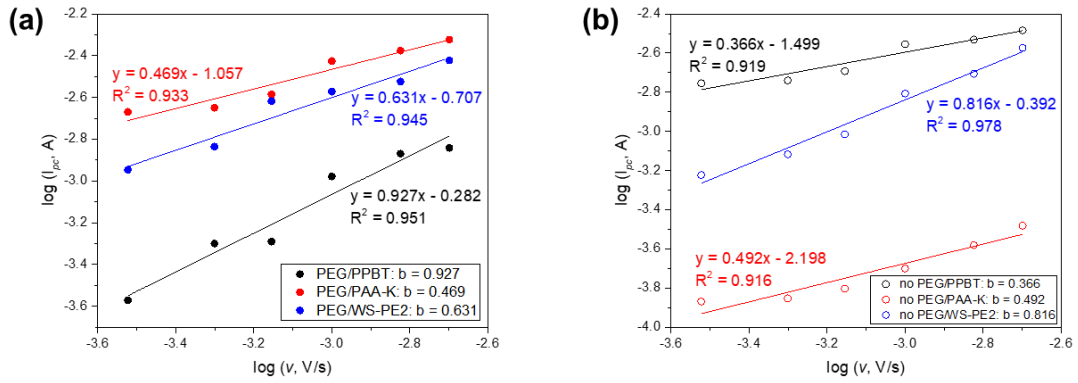

Figure 28: Plot of log (I_{pc}) vs. log (v), which were plotted from the results of cathodic peak currents of CV curves with different scan rates (v) for (a) electrodes with PEG coating on Fe_3O_4 surface and (b) electrodes without PEG coating Fe_3O_4 surface.

Table 9: Kinetic information for the polymeric binders with and without the PEG coating.

System	Slope (b)
PEG/PPBT	0.927
PEG/PAA-K	0.469
PEG/WS-PE2	0.631
No PEG/PPBT	0.366
No PEG/PAA-K	0.492
No PEG/WS-PE2	0.816

3.3.6 Spectroscopic Characterization

X-ray photoelectron spectroscopy (XPS) spectra after 100 cycles (**Figure 24a**) revealed information regarding the SEI layer formation. The survey scan (**Figure 29a**) illustrates that only C, O and F remain on the electrode surface after cycling. The F 1s scan (**Figure 29b**) reveals information regarding the stability of the SEI layer through the LiF peak.[95,101] The intensity of the peak correlates well with the electrochemical performance of each system discussed above. PEG/PPBT exhibited the most stable performance and subsequently has the highest intensity LiF peak present. No PEG/PAA-K and no PEG/WS-PE_2 show similar peak intensities. PEG/WS-PE_2 and no PEG/PPBT have similar and lower levels of F^-. Finally, the PEG/PAA-K system showed the lowest intensity peak, and corresponding worst electrochemical performance. It should be noted that the no PEG systems for WS-PE_2 and PAA-K have higher intensity peaks compared to their PEG counterparts, which further correlates to the importance of physical affinity. Although WS-PE_2 showed similar electrochemical performance, with and without PEG, PEG appears to negatively impact the formation of a stable SEI layer. Further evidence of a stable SEI layer is derived from C 1s and O 1s data (**Figure 29c, d**), where a higher proportion of organic compounds is desired. Here we see that WS-PE_2, with and without PEG, has a higher

organic fraction than PEG/PPBT (**Figure 29c**), which may explain why this polymeric binder was able to stabilize to similar levels of PPBT after 100 cycles.

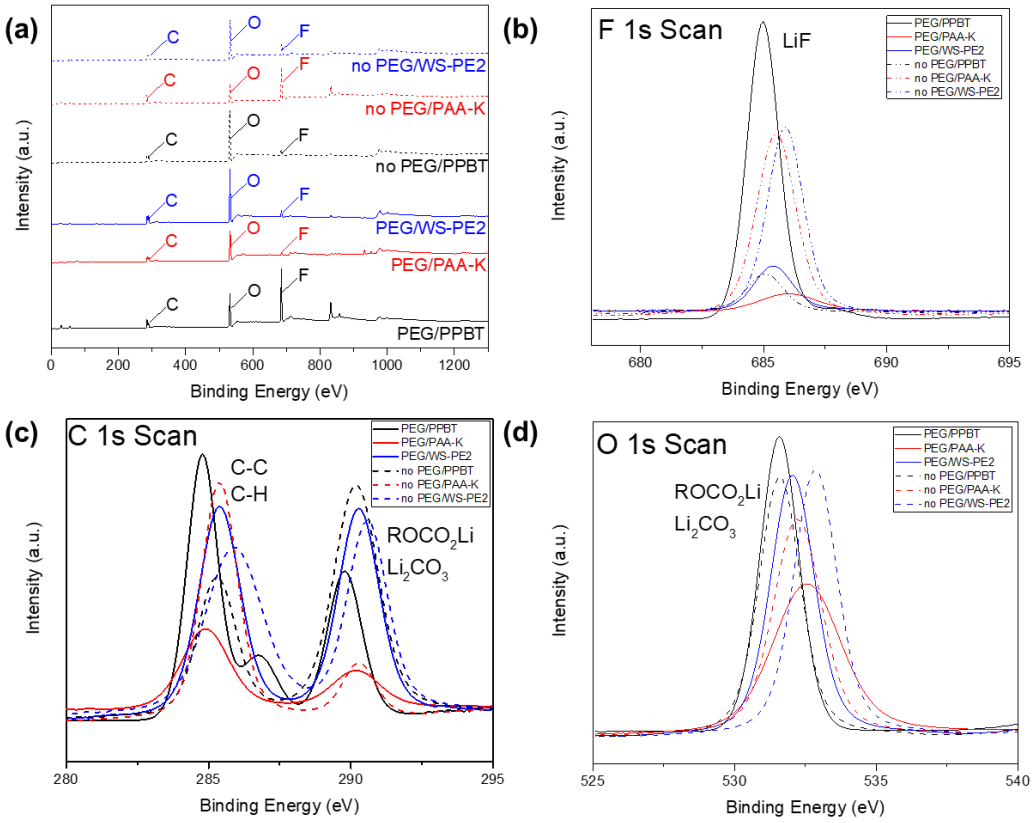

Figure 29: XPS analysis of SEI layer after 100 cycles: (a) Survey scan, (b) F 1s scan, (c) C 1s scan, and (d) O 1s scan.

The XPS spectra of the Fe 2p core level provides preliminary information on the chemical interactions present in the various polymeric binder systems with and without PEG coating (**Figure 30**). The peaks at ~712 and ~724 eV correspond to Fe $2p_{3/2}$ and Fe $2p_{1/2}$ orbitals, respectively. The absence of the middle peak, associated with Fe^{3+}, confirms a pure magnetite phase.[102] The presence of this satellite peak illustrates interactions between polymeric binder and active material surface. This peak is present in PEG/PPBT

and WS-PE2 electrode slurries. The absence of interactions between the active material and polymeric binder, as seen without PEG coating and in PAA-K electrode systems, correlated with poorer electrochemical performance, attributed to reduced electrode stability (**Figure 24a**).

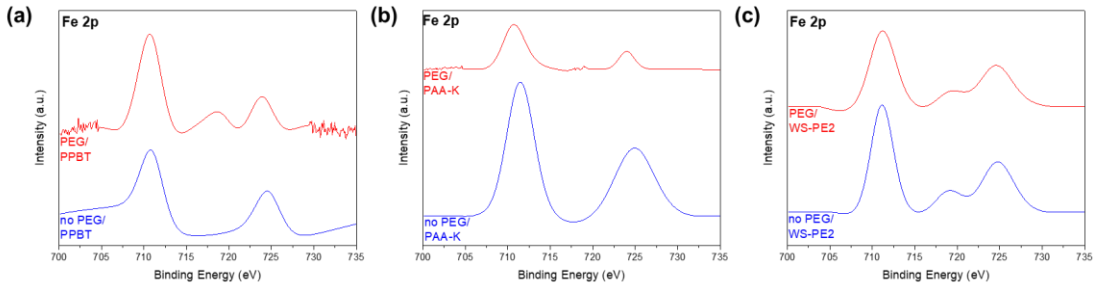

Figure 30: XPS spectra of electrode slurries. (a) XPS spectra of PPBT electrode slurry with and without PEG coating. (b) XPS spectra of PAA-K electrode slurry with and without PEG coating. (c) XPS spectra of WS-PE2 electrode slurry with and without PEG coating.

3.4 Conclusions

The PEG/PPBT system demonstrated the most stable performance in cycling, rate capability, and SEI layer formation. This is attributed to its high electronic conductivity as a result of the polythiophene binder undergoing electrochemical doping during cycling and its high physical affinity with PEG. WS-PE2 showed significant improvement over PEDOT:PSS, which is attributed to improved ion transport, in conjunction with its high electrical conductivity. WS-PE2 stabilized to similar levels of PPBT in cycling, but was not able to maintain performance in rate capability testing. The poor rate performance, particularly at high current densities (1 C and 2 C), is attributed to its bulky chemical structure and lower concentration of carboxylic groups. PAA-K demonstrated cycling

performance similar to no PEG/PPBT, which is a noteworthy improvement compared to the traditional PVDF,[11,30] but underperforms compared to PEG/PPBT and WS-PE_2. However, PAA-K exhibited comparable rate capability performance to PEG/PPBT and the lowest charge transfer resistance after 100 cycles, which is believed due to its high concentration of carboxylic groups.

The results presented here highlight the imperative to consider materials chemistry and functional group characteristics in complex composites in an integrated system approach. In the case of high-capacity electrodes for battery applications, the molecular structure of the polymeric binder and its chemical and physical interactions with the electrode constituents significantly impacts electrochemical performance. For instance, while PEG aided in limiting magnetite aggregation,[11,30] the physical affinity of the binder with the PEG active material coating proved important when designing composite electrodes. As elucidated through HSP analysis, PEG and PPBT demonstrated the highest physical affinity, which in turn led to enhanced electrochemical performance. Alternatively, WS-PE_2 and PAA exhibited limited physical affinity with PEG, and as a direct result, saw no improvements in electrochemical performance when used in conjunction with the coating and showed kinetic limitations. In contrast to the cycling performance and kinetics results, use of PEG appeared to afford enhanced rate capability performance in all polymer systems examined here.

High physical affinity between the polymeric binder and coating, as determined by HSP analysis, can be utilized to predict cycling stability, kinetics, and SEI layer formation, whereas, morphology is foretelling for rate capability performance, as demonstrated through PEG coating dispersion. The ideal polymeric binder aids in both electron and ion

transport through electronic conductivity and high concentration of carboxyl groups, as evidenced through electrochemical testing.

Using a variety of water-soluble, carboxylated binders for high-capacity composite battery electrodes, we demonstrated how functional group chemistries impact the critical interfaces and interactions between components in the system. Physical affinity between the polymeric binder and active material coating is an important consideration in the design of materials, which significantly impacts the overall electrochemical performance in a system. Poor physical affinity can lead to slower reaction kinetics, higher charge transfer resistance, and less stable SEI layer formation. Binder functional group chemistry also plays a key role. While a conjugated conducting backbone can facilitate electron transport within electrodes, high conductivity does not directly correlate to enhanced performance; additional factors, such as the presence of polar functionalities, such as carboxylates and their concentration are also important considerations. The strategies discussed here determine how conjugated polymers and carboxyl moieties can either aid or hinder transport within composite electrodes create a framework for the future design of binder materials chemistries for high performance, high capacity electrodes.

CHAPTER 4. PPBT MAGNETITE SURFACE FUNCTIONALIZATION AND POLYMERIC BINDER-CARBON INTERACTIONS

4.1 Introduction

Current lithium-ion battery technology relies on graphite-based anodes, which have a low theoretical capacity of 372 mAh g^{-1}.[4] Efforts to exceed this value have led to extensive research of alternative anode materials. Potential candidates, including silicon[61,116] and metal oxides,[13,74–76] exhibit superior capacities and have been considered for next generation Li-ion batteries. Among these materials, magnetite (Fe_3O_4) is low-cost, earth abundant, and environmentally friendly, with a theoretical capacity of ~925 mAh g^{-1}.[77] A challenge with implementation of Fe_3O_4 as an active material comes from its rapid capacity fading due to large volume changes during charging-discharging processes.[80] Thus, designing electrode materials to alleviate volume changes is the first step toward developing high-performance batteries.

Three main strategies have been previously discussed for improving the cycle-life of magnetite-based anodes and similar alloying-based systems, such as silicon. One approach has focused on active material synthesis to control crystallite size. The first investigation into magnetite crystallite size effects by Komaba *et al.*[37] revealed that nanocrystalline (10 nm) magnetite had the highest initial capacity. Sizing down particles to the nanoscales has been shown to shorten Li-ion diffusion pathways and increase

reversible capacity and rate capability.[18,20,38] In this study, we use a ~10 nm crystallite size active material.

Another approach for enhancing a magnetite-based system has been to introduce conductive carbon coatings onto the active material surface.[1,32,33] Carbon materials are often employed to enhance electrical conductivity, improve rate performance, and have been shown to improve electrochemical properties of Fe_3O_4 anodes, acting as a buffer to relieve volume changes during cycling.[1,20,31,32] A third strategy deals with incorporating water-soluble and/or semiconducting polymeric binders. The choice of binder is critical for maintaining contact between the active material and conductive additives in a composite electrode during repeated expansion/contraction of the active material during charging-discharging processes.[48] Water-soluble binders are emerging as an attractive, low-cost, and more environmentally friendly alternative to the traditional poly(vinylidene fluoride) (PVDF). Other alternatives to PVDF include semiconducting polymeric binders that can be doped during cycling and support electronic conductivity in the electrode.[60] A water-soluble, carboxylate-substituted polythiophene binder, poly[3-(potassium-4-butanoate) thiophene] (PPBT), combines the advantages of using water-soluble and semiconducting binders and was previously demonstrated to enhance electrochemical performance in magnetite-based anode systems.[11,30]

Here, we focus on combining the advantages of strategies two and three by functionalizing our active material surface with PPBT and exploring the overall role of the composite electrode. Two covalent attachment strategies, specifically an (3-aminopropyl)triethoxysilane (APTES) and 1-ethyl-3-(3-dimethylaminopropyl) carbodiimide (EDC)/N-hydroxysuccinimide (NHS) chemistry and a Fischer esterification

approach, are implemented for understanding how surface chemistry and functionalization strategy impacts overall electrochemical performance. Composite electrodes are investigated using the functionalized magnetite, carbon additives, and the PPBT polymeric binder. Furthermore, a closer look is given to electrodes consisting solely of the functionalized active material and carbon-polymer composites. The purpose of this investigation is to aid in the overall design framework strategies for achieving optimal electrochemical performance through composite electrode fabrication.

4.2 Materials and Methods

4.2.1 Materials

Fe_3O_4 nanoparticles (~10 nm) were synthesized by a previously reported co-precipitation process using aqueous solution of iron(III) chloride hexahydrate, iron(II) chloride hexahydrate, and triethylamine.[29,88] PPBT (M_w: 21 kDa, polydispersity: 2.2, head to tail regioregularity: 89%) was purchased from Rieke Metals Inc.

4.2.1.1 APTES Functionalization of Fe_3O_4 Nanoparticles

500 mg of magnetite (Fe_3O_4) nanoparticles were dispersed in 100 mL ethanol/water (4:1 v/v) in a round bottom flask with magnetic stirring. The suspension was brought to pH 4 with acetic acid before the dropwise addition of (3-aminopropyl)triethoxysilane (APTES) (36 mmol APTES/g Fe_3O_4). The flask was sealed with a rubber septum and allowed to stir for 5 hours at room temperature. The suspension was centrifuged at 6000 rpm for 10 min to isolate the functionalized nanoparticles, which were cleaned by redispersing and

centrifuging in ethanol (x1) and then acetone (x2). Finally, the nanoparticles were dried in a vacuum oven at 110 ºC overnight.

1-ethyl-3-(3-dimethylaminopropyl) carbodiimide (EDC)/N-hydroxysuccinimide (NHS) chemistry was used to "crosslink" the carboxyl functionality of poly[3-(potassium-4-butanoate)thiophene-2,5-diyl] (PPBT) with the amine functionality of the APTES-Fe_3O_4.

12.4 mg of PPBT was first dissolved in 30 mL of water (buffered at pH 5) in a round bottom flask with magnetic stirring at 70 ºC overnight. Then 15.3 mg EDC, 9.2 mg NHS, and 95 mg APTES-Fe_3O_4 were added to the flask. The flask was sealed with a rubber septum and the reaction proceeded at room temperature with stirring for 16 hours. The suspension was centrifuged at 6000 rpm for 20 min to isolate the nanoparticles, which were cleaned by redispersing and centrifuging in DI water (x2) and then acetone (x1). Finally, the nanoparticles were dried in a vacuum oven at 110 ºC overnight.

4.2.1.2 Fischer Esterification of Fe_3O_4 Nanoparticles

500 mg of magnetite (Fe_3O_4) nanoparticles were dispersed in 60 mL of deionized water with an ultrasonic probe (3 pulses of 30 seconds each, operated at 50 Watts, Qsonica Q700 sonicator). The Fe_3O_4 solution was then transferred to a 100 mL round bottom flask with a magnetic stir bar. *p*-Toluenesulfonic acid (1.4 g, 12% in acetic acid) and poly[3-(potassium-4-butanoate)thiophene-2,5-diyl] (PPBT, 78 mg) were added to the mixture, a condenser was attached to the flask, and the reaction was stirred vigorously (750 rpm) at 105 ºC for 24 hours. The solution was cooled to room temperature and was centrifuged at 6000 rpm for 20 min to isolate the nanoparticles, which were cleaned by redispersing and

centrifuging in DI water (x2) and then acetone (x1). Finally, the nanoparticles were dried in a vacuum oven at 110 ºC overnight.

4.2.2 Electrode Fabrication and Electrochemistry

4.2.2.1 PPBT/C Electrode Fabrication

PPBT/C electrodes were prepared at 60 wt%, 80 wt% and 90 wt% carbon loadings, with the remaining fraction consisting of the PPBT polymeric binder. The slurries for the 60 wt% electrodes were prepared by mixing Super P carbon (30 mg) and PPBT (10 wt% solution, 200 mg) with a weight ratio of carbon:polymer = 60:40. The slurries for the 80 wt% electrodes were prepared by mixing Super P carbon (40 mg) and PPBT (10 wt% solution, 100 mg) with a weight ratio of carbon:polymer = 80:20. The slurries for the 90 wt% electrodes were prepared by mixing Super P carbon (50 mg) and PPBT (10 wt% solution, 50 mg) with a weight ratio of carbon:polymer = 90:10. The electrodes for field-emission scanning electron microscopy (FE-SEM, Zeiss Ultra-60) measurement, electrochemical evaluation and spectroscopy characterization were produced by blade coating onto Cu foil (doctor blade, MTI corp). The electrodes were first allowed to dry at room temperature for 1 h, followed by 110 °C for 12 h in a vacuum oven.

4.2.2.2 PPBT-Fe_3O_4 Electrode Fabrication

The slurries for the electrodes were prepared by mixing PPBT-Fe_3O_4 (0.1 g), carbon additives (0.02 g), and PPBT (10 wt% solution, 0.2 g) with a weight ratio of PPBT-Fe_3O_4:carbon:polymer = 71.4:14.3:14.3. A higher active material loading composite electrode was prepared for the APTES-EDC functionalization method by mixing PPBT-

APTES-Fe_3O_4 (76 mg), carbon additives (7.6 mg), and PPBT (10 wt% solution, 19.6 mg) with a weight ratio of PPBT-Fe_3O_4:carbon:polymer = 89.25:8.45:2.3. The electrodes for field-emission scanning electron microscopy (FE-SEM, Zeiss Ultra-60) measurement, electrochemical evaluation and spectroscopy characterization were produced by blade coating onto Cu foil (doctor blade, MTI corp). The electrodes were first allowed to dry at room temperature for 1 h, followed by 110 °C for 12 h in a vacuum oven.

4.2.2.3 Electrochemistry

Stainless-steel coin cells (2032-type) were used for electrochemical measurements. Lithium metal, purchased from MTI corp., was used as a counter electrode and 1 M $LiPF_6$ in ethylene carbonate (EC) and diethylene carbonate (DEC) (1:1 by weight), purchased from BASF, was used as the electrolyte. Before electrochemical testing, the capacity of each coin cell was confirmed by charging and discharging at a current density of ~0.05 C. The tests were then proceeded for cycling and rate capability. Cyclic voltammetry (CV) was performed on half coin cells in the potential range of 0.01-3 V for magnetite-based electrodes and 0.01-1.5 V for carbon-based electrodes at the scan rates of 0.3, 0.5, 0.7, 1.0, 1.5 and 2.0 mV s^{-1}. Electrical impedance spectroscopy (EIS, Metrohm Autolab PGSTAT101) measurements were conducted in the frequency range from 0.1 MHz to 0.1 Hz before and after cycling.

4.2.3 Microscopic Characterization

FE-SEM images were observed on the surface view of the electrodes using a Zeiss Ultra-60 FE-SEM with an accelerating voltage of 3 kV for carbon-based electrodes using the high vacuum mode at room temperature. Elemental analysis was conducted using

energy dispersive x-ray spectroscopy (EDX, Oxford Aztec software) at an accelerating voltage of 10 kV.

4.2.4 Spectroscopic Characterization

The electrode samples for spectroscopy measurements were prepared by removing powder samples from the prepared electrodes. Fourier transform infrared (FT-IR) spectra were recorded using a Thermo Scientific Nicolet iS50 FT-IR spectrometer. X-ray photoelectron spectroscopy (XPS) characterization was performed using a Thermo K-Alpha XPS system. The instrument was equipped with a monochromatic Al-K X-ray source (1468 eV). Spectra were collected using the flood gun and an X-ray spot size of 400 μm. Survey scans were collected with pass energy of 200 eV with 1 eV increments. High resolution scans (for specific elements) were collected with pass energy of 50 eV with 0.1 eV increments. For XPS analysis of the electrodes after 100 cycles, the delithiated electrodes were extracted from the cycled coin cells and carefully rinsed with dimethyl carbonate (DMC) three times (5 mL in total) to remove residual electrolyte and then dried in a vacuum oven (80°C, 12 hr).

4.2.5 Brunauer-Emmett-Teller (BET) Surface Area

Physical adsorption of nitrogen was measured at 77 K and at relative pressures ranging from 0 to 100 kPa with a BELSORP-max (MicrotracBEL) analyzer. The polymer powders were degassed for 12 hours under a vacuum of -30 in Hg at 110 °C prior to analysis. BET surface area and density functional theory (DFT)-based pore size distributions were calculated from the obtained isotherms.

4.3 Results and Discussion

4.3.1 Understanding Polymeric Binder and Carbon Additive Interactions

4.3.1.1 Microscopic Characterization

To probe interactions between the polymeric binder and carbon additives, a preliminary investigation was conducted using composite electrodes fabricated with 60 wt%, 80 wt%, and 90 wt% carbon loading, namely Super P, in conjunction with the PPBT polymeric binder. FE-SEM (**Figure 31**) was used to evaluate how the higher and lower carbon loadings impact composite electrode morphology. Regardless of carbon loading, both systems demonstrated similar uniformity in particle size distribution.

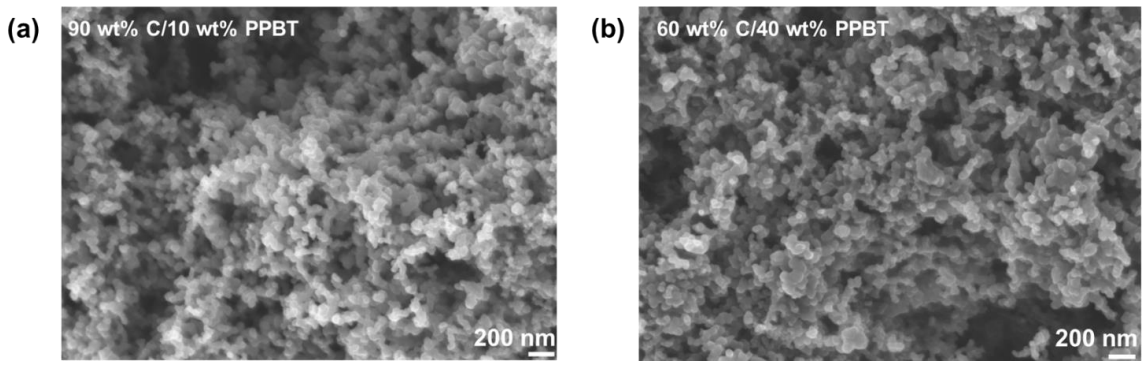

Figure 31: Morphology of (a) 90 wt% C/10 wt% PPBT and (b) 60 wt% C/40 wt% PPBT electrodes.

EDX SEM imaging and elemental (C, K, O and S) image mapping confirmed the presence of both carbon additives and the PPBT polymeric binder in the electrodes consisting of 60 wt% (**Figure 32**) and 90 wt% (**Figure 33**) carbon loading. The elemental mapping of K, O and S help elucidate the presence of the polymeric binder in the composite electrode. Despite differences in carbon loading, no phase separation was observed.

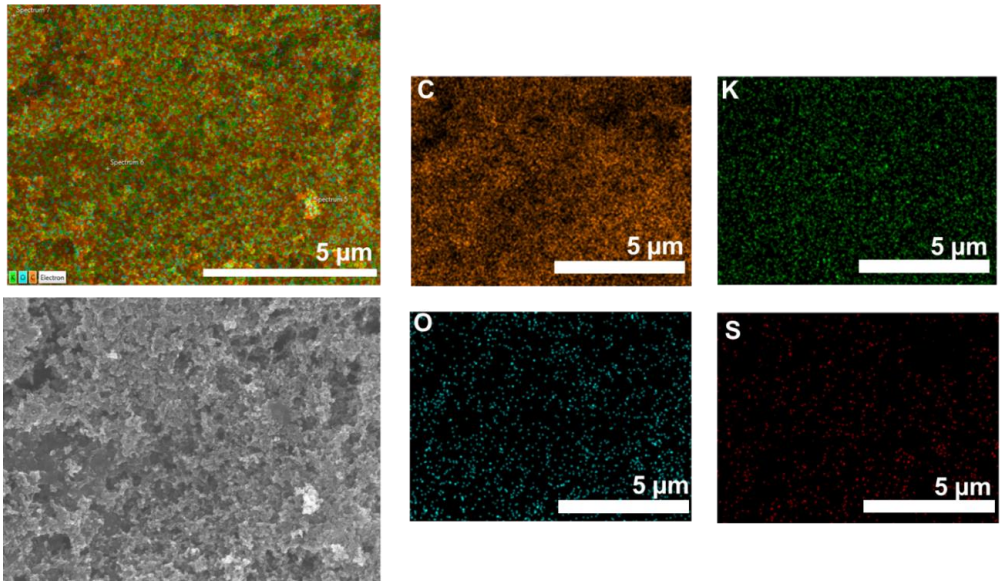

Figure 32: EDX SEM of 60 wt% C/40 wt% PPBT electrode with elemental mapping of C, K, O and S.

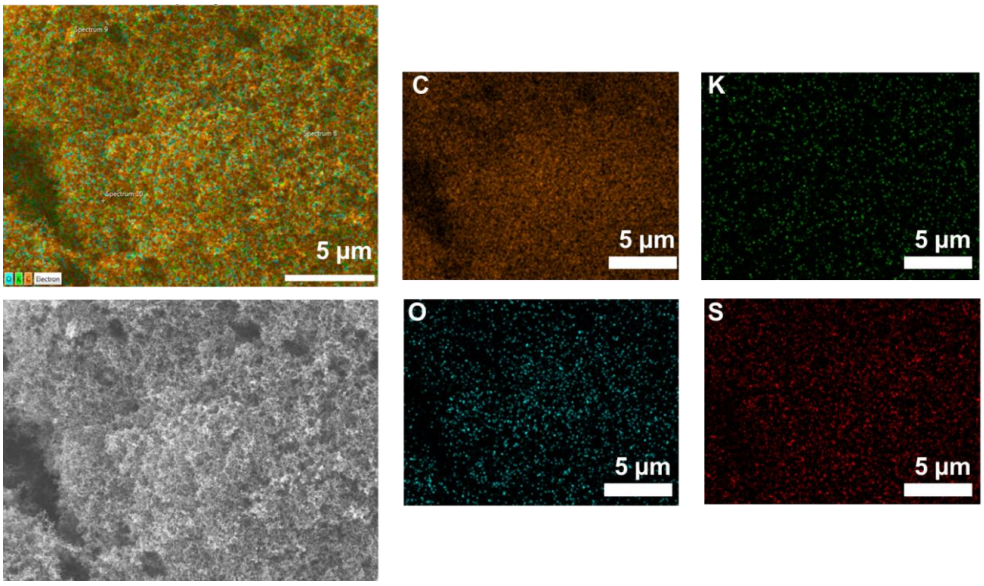

Figure 33: EDX SEM of 90 wt% C/10 wt% PPBT electrode with elemental mapping of C, K, O and S.

4.3.1.2 Electrochemical Characterization

The impact of carbon loading was evaluated through electrochemical characterization. Tests were performed using coin cells fabricated with Li metal counter electrodes and 1 M $LiPF_6$ in ethylene carbonate (EC) and diethylene carbonate (DEC) (1:1 by weight) was used as the electrolyte. Charge-discharge cycling (**Figure 34**) was conducted at a current density of 0.1 C to determine the capacity retention of each system for 50 cycles. In order to investigate PPBT binder electrochemical doping effects, a voltage window of 0.01 and 3 V was used. It was previously determined that PPBT has two oxidation peaks at 1.1 and 2.2 V and magnetite primarily operates in a higher voltage window, which established an interest in a higher voltage window of 3 V. A lower cutoff voltage of 0.01 V also demonstrated enhanced stability for PPBT in previous electrochemical characterization in a magnetite-based system.[106] Corresponding Galvanostatic profiles are provided in **Figure 35**Figure 35.

With respect to capacity retention upon cycling, the 90 wt% and 80 wt% systems demonstrated comparable performance. Initially, the 80 wt% electrode had a slightly higher capacity value of 310 mAh g^{-1}, but lowered to the performance of the 90 wt% system after approximately 20 cycles. Whereas, the 90 wt% electrode started at a lower capacity value of 261 mAh g^{-1}, but increased to 289 mAh g^{-1} after 50 cycles. The higher carbon loadings, 90 wt% and 80 wt%, demonstrated higher capacity retentions of 110% and 92%, respectively, compared to the 60 wt% system, with a value of 78%. Interestingly, the 60 wt% system demonstrated a significantly higher initial capacity of 505 mAh g^{-1}, but lowered to 394 mAh g^{-1} after 50 cycles. Despite a lower capacity retention, the 60 wt% system demonstrated enhanced capacity values compared to the higher carbon loadings,

which could be attributed to electrochemical doping effects from the higher polymeric binder content.

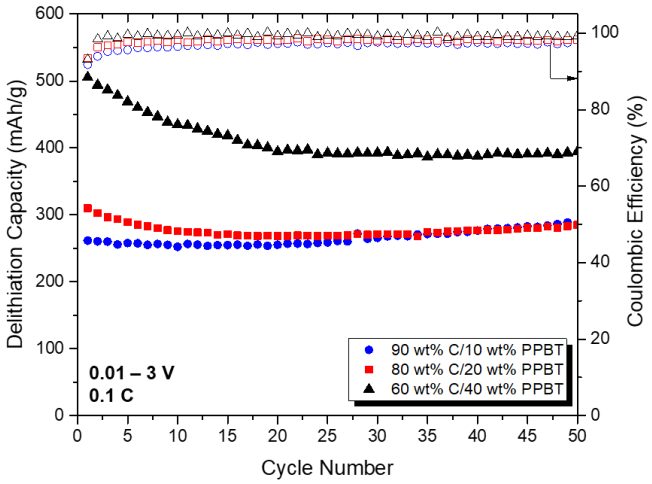

Figure 34: Cycling performance (capacity retention as a function of cycle number) comparing different carbon and polymer loadings cycled at 0.1 C between 0.01 and 3 V.

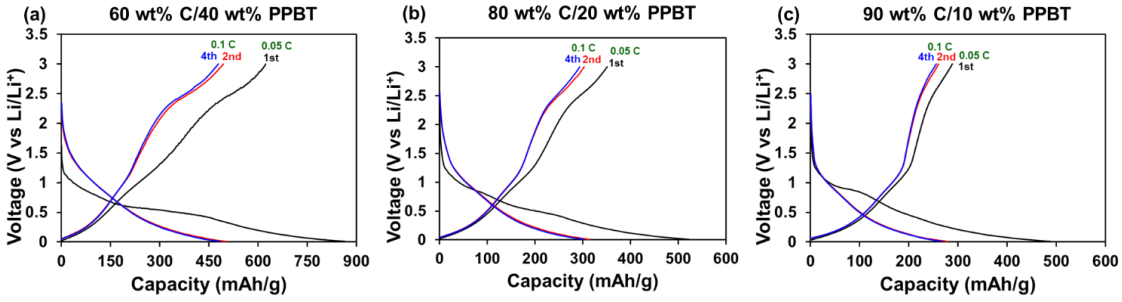

Figure 35: Galvanostatic profiles for (a) 60 wt% C/40 wt% PPBT, (b) 80 wt% C/20 wt% PPBT, and (c) 90 wt% C/10 wt% PPBT.

Electrode kinetics were evaluated using CV performed at different scan rates (v) to initially characterize the various carbon loadings, specifically 60 wt% and 80 wt% (**Figure 36**). The kinetic data was characterized by analyzing the voltammetric response of the polymeric binders at various scan rates according to $I_{pc} = av^b$, where the measured peak current (I_{pc}) and the potential scan rate (v) obey a power-law relationship.[95–99] The slope from the plot of log (I_{pc}) *vs*. log (v) provided the value of b.[95,98] The carbon-based electrodes demonstrated two peaks in the voltage range of 0.01-1.5 V, which were both used to extrapolate values of b, corresponding to Li^+ diffusion, where a higher value of b suggests faster kinetics.[95,98] Both peaks corresponded to similar b values. The 80 wt% system demonstrated a b = 1.2, as compared with b = 1.1 for the 60 wt% system. The results suggest that the higher carbon loading may have enhanced electrochemical performance with regards to Li^+ diffusion rate, which would aid in the understanding of capacity retention over 50 cycles, where the higher carbon loading systems demonstrated enhanced stability.

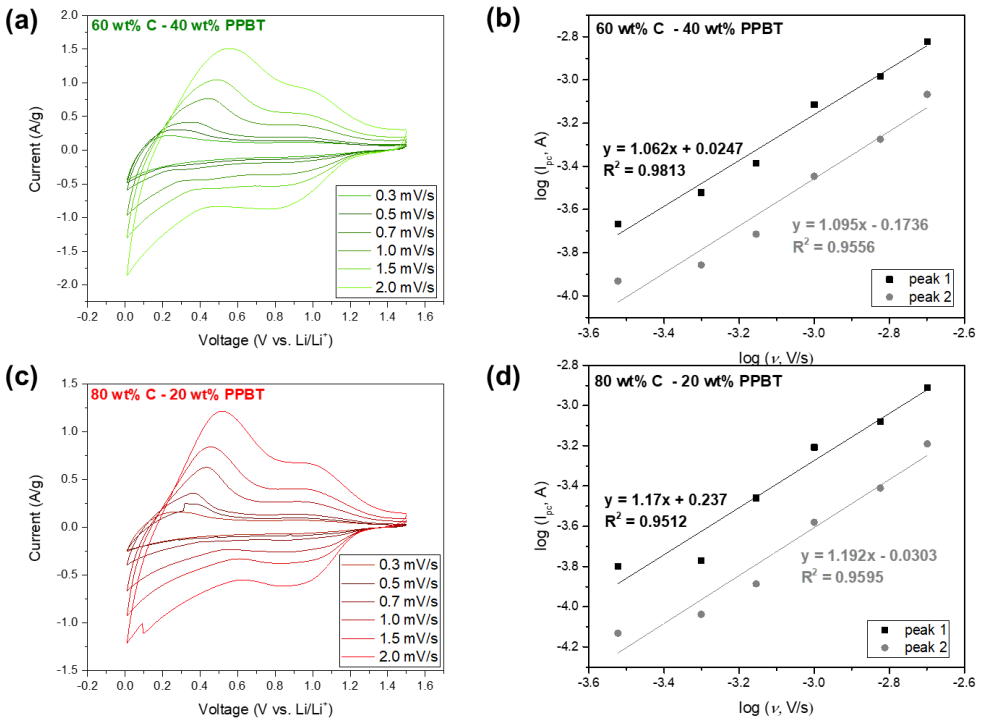

Figure 36: CV profiles with various scan rates (ν) of 60 wt% C/40 wt% PPBT electrode and 80 wt% C/20 wt% PPBT electrode, and corresponding plots of log (I_{pc}) vs. log (ν), which were plotted from the results of cathodic peak currents of CV curves with different scan rates (ν).

4.3.1.3 Spectroscopic Characterization

The composite electrodes were further evaluated by XPS after 50 cycles (**Figure 37**) to explore differences in chemical composition. The results offer evidence for the formation of a stable SEI layer, which can be deduced from the fraction of LiF present in the electrode.[95,101] The survey scans presented in **Figure 37a** demonstrate that only C, O and F remain in the corresponding electrode systems. **Figure 37b** provides the F 1s scan, where the 90 wt% loading exhibited a substantially more intense LiF peak, followed by the 80 wt% and 60 wt% systems, respectively. The 60 wt% system displays a higher binding

energy peak at ~ 689 eV, which is believed to correspond to degradation products of the $LiPF_6$ electrolyte salt, labeled $Li_xPF_yO_z$, and possibly a small contribution from the PPBT binder.[117] The higher fraction of LiF suggests formation of a stable SEI layer and helps to validate the stable cycling performance exhibited by the 90 wt% electrode after 50 cycles. As evidenced by the C 1s and O 1s scans (**Figure 37c, d**), the proportion of organic compounds within the SEI layer was relatively higher for the 90 wt% system, as compared to the 80 wt% and 60 wt% electrodes. These results further verify the stability of the 90 wt% system. Surprisingly, the 60 wt% system exhibits two additional peaks (293 eV and 295.5 eV), which could be associated with K.[89] Although not directly present in the survey scan, the presence of K in the 60 wt% electrode could indicate polymeric binder presence on the surface of the composite electrode, further confirming poor SEI layer formation. Unstable SEI layer formation further confirms the poor cycling stability of the 60 wt% system and clarifies the need for a higher level of carbon loading in the composite electrode.

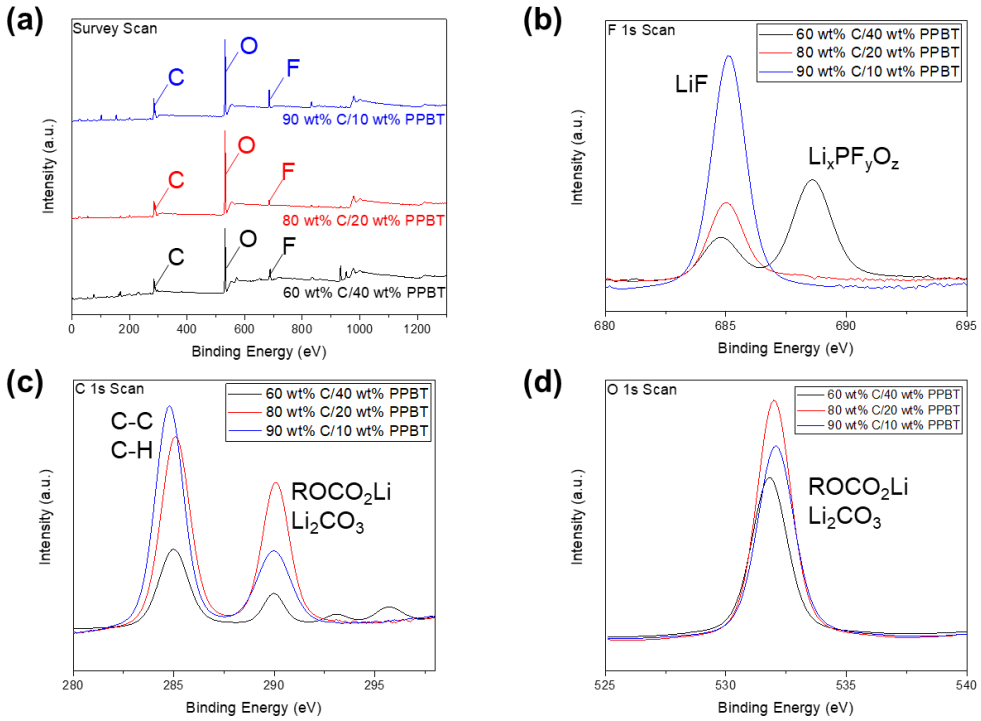

Figure 37: XPS analysis of SEI layer after 50 cycles: (a) Survey scan, (b) F 1s scan, (c) C 1s scan, and (d) O 1s scan.

4.3.2 PPBT Coated Magnetite Functionalization Methods

4.3.2.1 APTES/EDC Functionalization Method

A water-soluble carboxylated polythiophene binder, PPBT, was used as a model polymer to investigate the impact of surface functionalization techniques on enhancing electrochemical performance in a magnetite anode system. The magnetite surface was first coated with APTES, followed by an EDC/NHS chemistry to attach the PPBT (**Figure 38**). The final PPBT-coated particles from this approach are denoted PPBT-APTES-Fe_3O_4. APTES, or similar linkers, have previously been used in the literature to graft polymers

onto the hydroxyl surface of various active materials, including silicon and magnetite.[34,69,118–121]

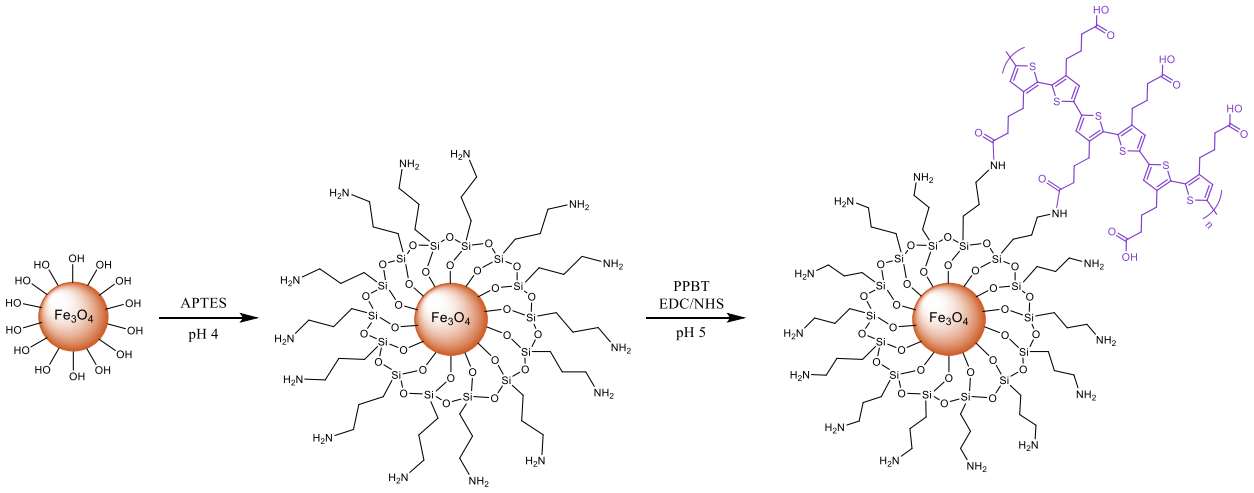

Figure 38: APTES and EDC functionalization of magnetite with PPBT to give PPBT-APTES-Fe_3O_4.

Both steps in the functionalization process were verified using TGA and FTIR (**Figure 39**). TGA on the PPBT-APTES-Fe_3O_4 demonstrated a 12 wt% PPBT coating on the final magnetite surface, however, there was 8 wt% APTES present, which could hinder electrochemical performance and will be discussed further below. PPBT carboxylic moieties exhibit peaks at 1556 and 1400 cm^{-1}, which correspond to O-C-O asymmetric and symmetric stretching.[122] The PPBT-APTES-Fe_3O_4 exhibits these same peaks, confirming the presence of PPBT on the active material surface.

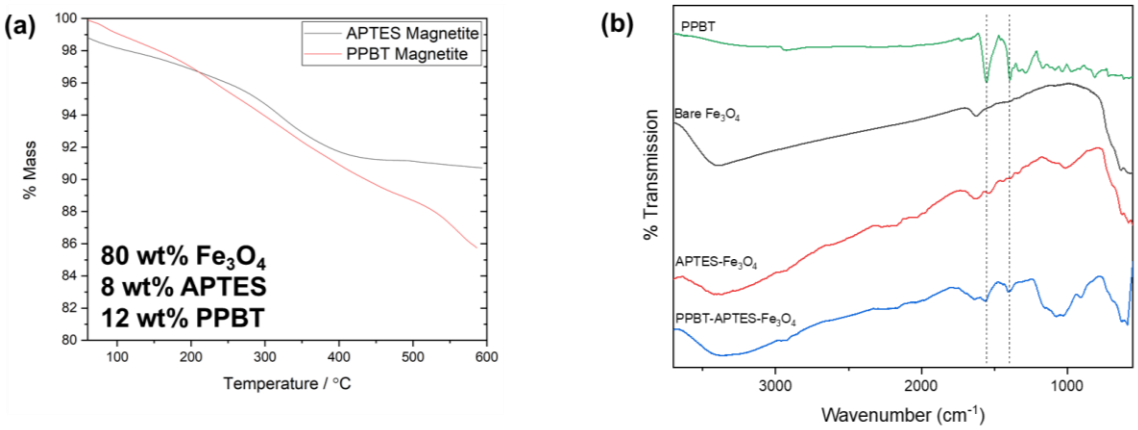

Figure 39: (a) TGA and (b) ATR-FTIR of bare magnetite, PPBT, APTES-Fe_3O_4, and PPBT-APTES-Fe_3O_4.

The impact of PPBT functionalization was evaluated through electrochemical characterization. Tests were performed using coin cells fabricated with Li metal counter electrodes and working electrodes prepared with PPBT-APTES-Fe_3O_4 active material, carbon additives, and polymeric binder in a 71.4:14.3:14.3 mass ratio, which was chosen based on previous results.[38] The electrolyte was 1 M $LiPF_6$ in ethylene carbonate (EC) and diethylene carbonate (DEC) (1:1 by weight). Electrode kinetics were evaluated using cyclic voltammetry (CV) performed at different scan rates (v) to initially characterize the PPBT-APTES-Fe_3O_4 (**Figure 40**). The kinetic data was characterized by analyzing the voltammetric response of the polymeric binders at various scan rates according to $I_{pc} = av^b$, where the measured peak current (I_{pc}) and the potential scan rate (v) obey a power-law relationship.[95–99] The slope from the plot of log (I_{pc}) *vs.* log (v) provided the value of b.[95,98] Here, we compared composite electrodes with carbon additives and PPBT polymeric binder to an electrode consisting of solely the functionalized active material. The PPBT-APTES-Fe_3O_4 electrode exhibited a b value of 0.477, as compared to the composite

electrode *b* value of 0.867. The *b* value is correlated to Li^+ diffusion, where a higher value of *b* suggests faster kinetics.[95,98] From this initial assessment, further electrochemical characterization was limited to the composite electrode.

Bridel *et al*. previously modified silicon particles with carboxymethyl cellulose (CMC) using 3-aminopropyl-trialkoxysilane (APTAS) to replace the necessity of a binder: an all-in-one particle approach. Despite surface modification, the electrochemical performance was similar to binder-free electrodes: demonstrating poor kinetics and a maximum capacity on the first cycle, resulting in immediate decay.[51]

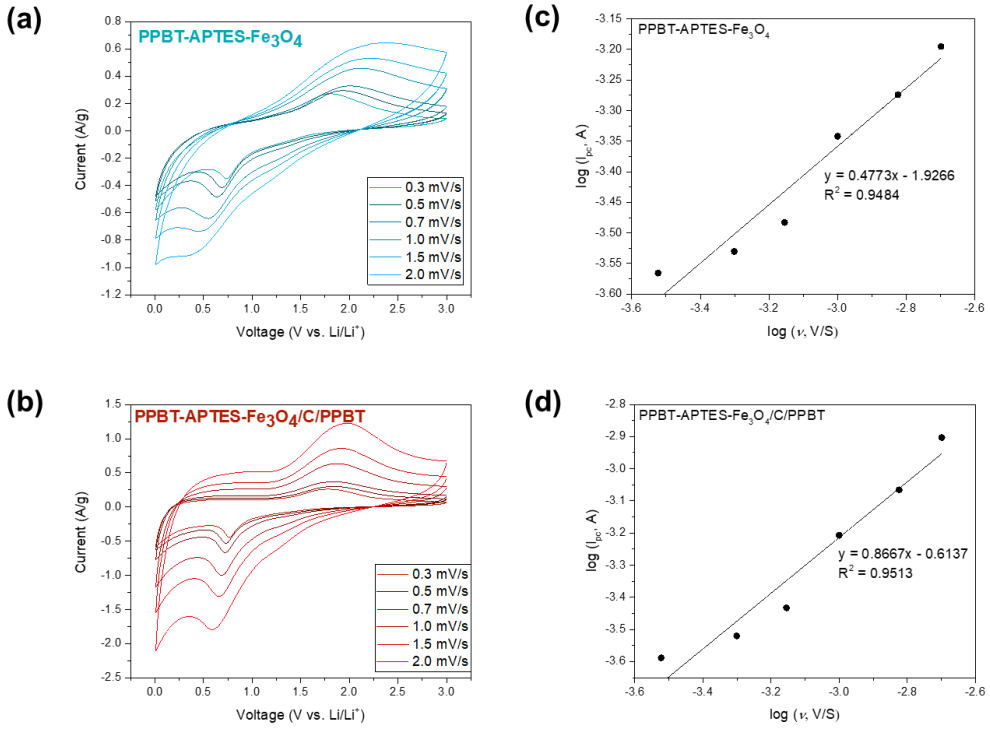

Figure 40: Effect of carbon additives and polymeric binder on kinetic performance of PPBT-APTES-Fe_3O_4. Cyclic voltammetry (CV) of (a) PPBT-APTES-Fe_3O_4 and (b) PPBT-APTES-Fe_3O_4/C/PPBT, with various scan rates, and corresponding plots of log (I_{pc}) vs. log (v), which were plotted from the results of cathodic peak currents of CV curves with different scan rates (v) for (c) PPBT-APTES-Fe_3O_4 and (d) PPBT-APTES-Fe_3O_4/C/PPBT.

Charge-discharge cycling (**Figure 41a**) was conducted at a current density of 240 mA g^{-1} (~0.3 C) for 100 cycles to determine capacity retention. The PPBT-APTES system demonstrated a lower capacity value than is typically seen for magnetite-based systems (395 mAh g^{-1} on the 1st cycle as compared to a theoretical capacity of ~925 mAh g^{-1}),[77] which could be attributed to the APTES linkers used in the functionalization technique. As cycling progressed, a gradual increase in capacity was observed until an apparent steady state was reached after about 80 cycles to a final capacity value of 488 mAh g^{-1}, which is still significantly lower than the theoretical capacity of magnetite. The phenomenon of gradual increase of capacity will be further discussed, *vide infra*.

As previously reported by Wang *et al*., APTES linkers are bulky, insulating, long-chains, which may hinder charge transport capabilities.[118] A covalent attached process between APTES capped magnetite nanoparticles and MWNTs were investigated as a potential anode material. Cycling and rate capability testing revealed poor electrochemical performance when compared to a π-π interaction attachment strategy. These results are also consistent with a study where covalent attachment of magnetite onto a glassy carbon electrode surface using APTES linker demonstrated a higher charge transfer resistance as compared to the bare glassy carbon surface.[119] Charge transport between nanoparticles and nanostructures is limited by the presence of bulky, non-conjugated ligands, serving as an undesirable barrier.

Newly fabricated half cells were subjected to rate capability experiments (**Figure 41b**), where cells were lithiated at a constant current density of 80 mA g^{-1} (~0.1 C) and delithiated over a wide range of current densities (80 – 1600 mA g^{-1}) between a voltage range of 0.01 – 3 V. At 0.1 C, the PPBT-APTES system exhibited a lower starting capacity

of 531 mAh g^{-1}, which increased to 609 mAh g^{-1} upon cycling back to the same current density. These results mirror the behavior observed during cycling.

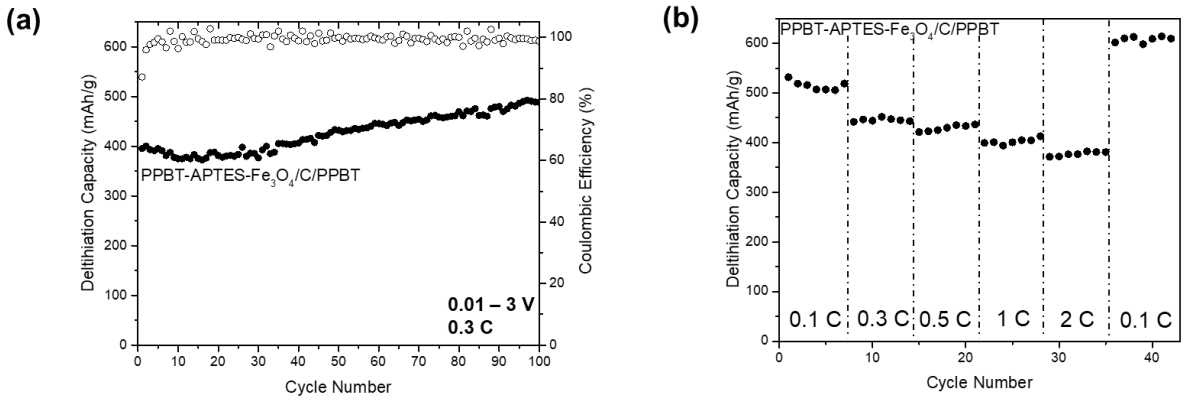

Figure 41: (a) Cycling performance (capacity retention as a function of cycle number) of PPBT-APTES- Fe_3O_4/C/PPBT cycled at 240 mA g^{-1} (~0.3 C) between 0.01 and 3 V. (b) Delithiation rate capability, where cells were lithiated a constant current density of 80 mA g^{-1} (0.1 C) and delithiated at different current densities between 0.01 and 3 V.

To improve the capacity value demonstrated by the PPBT-APTES-magnetite system, a higher active material loading was explored. Due to the additional APTES present, the magnetite loading was reduced. To compensate for the differences, the loading of PPBT-APTES-Fe_3O_4 was increased to 89.25 wt%, corresponding to 71.4 wt% active material, and was compared to the previous composite electrode, with an active material loading of 57.1 wt%. Electrode kinetics were evaluated using CV performed at different scan rates (v) to initially characterize the new active material loading of PPBT-APTES-Fe_3O_4 (**Figure 42**). The kinetic data was characterized by analyzing the voltammetric response of the polymeric binders at various scan rates according to $I_{pc} = av^b$, *vide supra*. The higher active material loading exhibited a b value of 0.788, as compared to the lower

active material loading *b* value of 0.867. The lower value of *b* from a higher active material loading is best attributed to the reduction in polymeric binder. It appeared that altering the active material loading would not improve the overall electrochemical performance of the PPBT-APTES-Fe_3O_4 electrode and alternative approaches were needed.

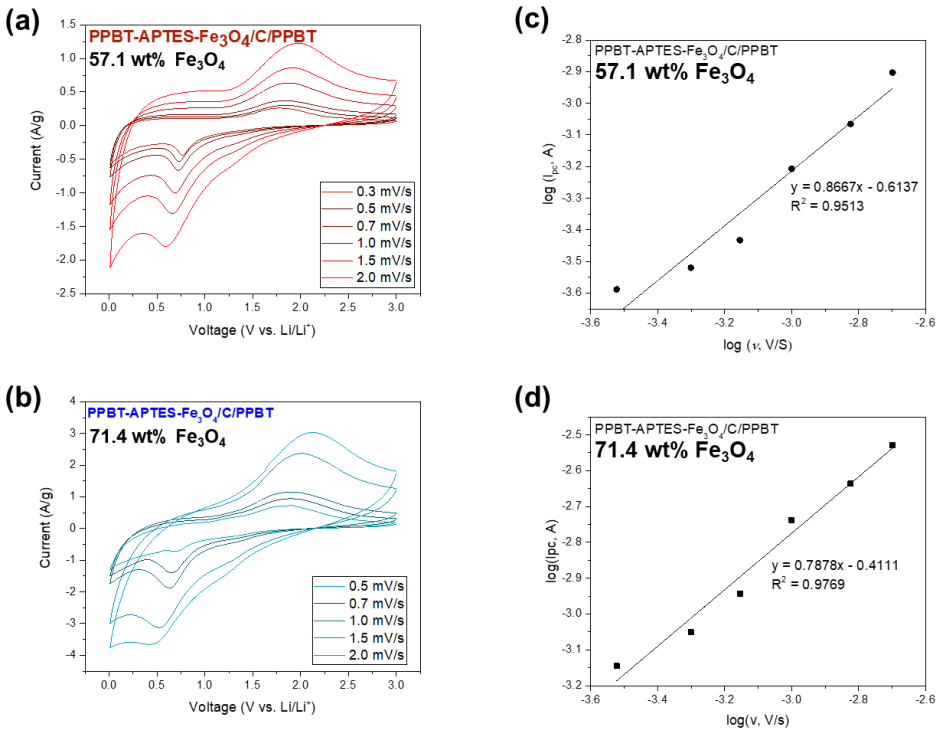

Figure 42: Effect of active material loading on kinetic performance in PPBT-APTES-Fe_3O_4/C/PPBT composite electrodes. Cyclic voltammetry (CV) of (a) 57.1 wt% Fe_3O_4 and (b) 71.4 wt% Fe_3O_4, with various scan rates, and corresponding plots of log (I_{pc}) vs. log (v), which were plotted from the results of cathodic peak currents of CV curves with different scan rates (v) for (c) 57.1 wt% Fe_3O_4 and (d) 71.4 wt% Fe_3O_4.

4.3.2.2 Fischer Esterification Functionalization Method

To further understand the effect of the PPBT-magnetite surface chemistry on the electrochemical performance of the magnetite active material surface, a Fischer esterification approach was used to attach the PPBT polymer directly onto the magnetite surface, denoted as PPBT-Fe_3O_4 (**Figure 43**).

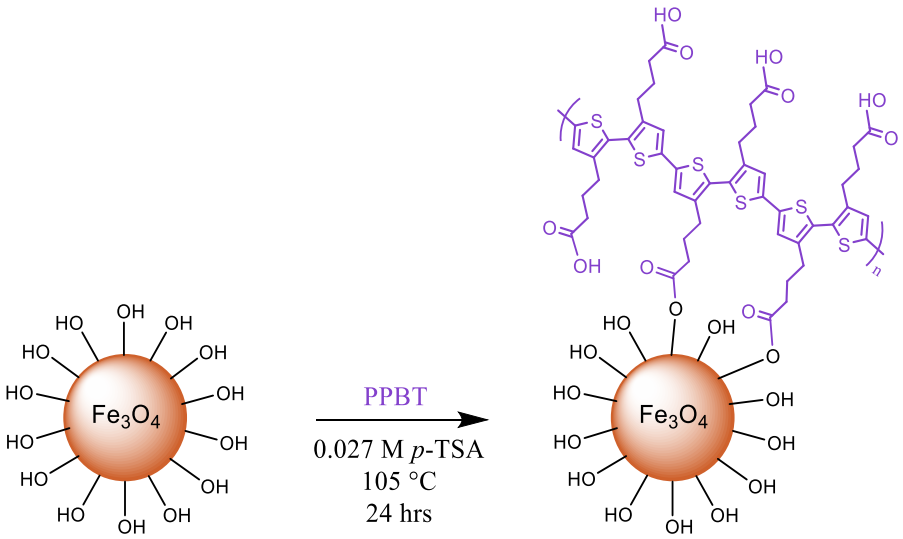

Figure 43: Schematic of magnetite functionalized with PPBT using a Fischer esterification to give PPBT-Fe_3O_4.

The Fischer esterification functionalization was confirmed using TGA and FTIR (**Figure 44**). TGA demonstrated a 14 wt% PPBT coating on the active material surface. PPBT carboxylic moieties exhibit peaks at 1556 and 1400 cm^{-1}, which correspond to O-C-O asymmetric and symmetric stretching.[122] The PPBT-Fe_3O_4 exhibits these same peaks, confirming the presence of PPBT on the active material surface. However, the O-C-O asymmetric peak was shifted to a lower frequency of 1530 cm^{-1}, which is believed to arise from the weakening of the O-C-O vibration. In addition to these peaks, a new peak was observed at 1767 cm^{-1}, which is associated with Fe-carboxylate C=O stretching.[106]

Together, these results indicate Fe-carboxylate bonding and confirm covalent bonding from the Fischer esterification functionalization.

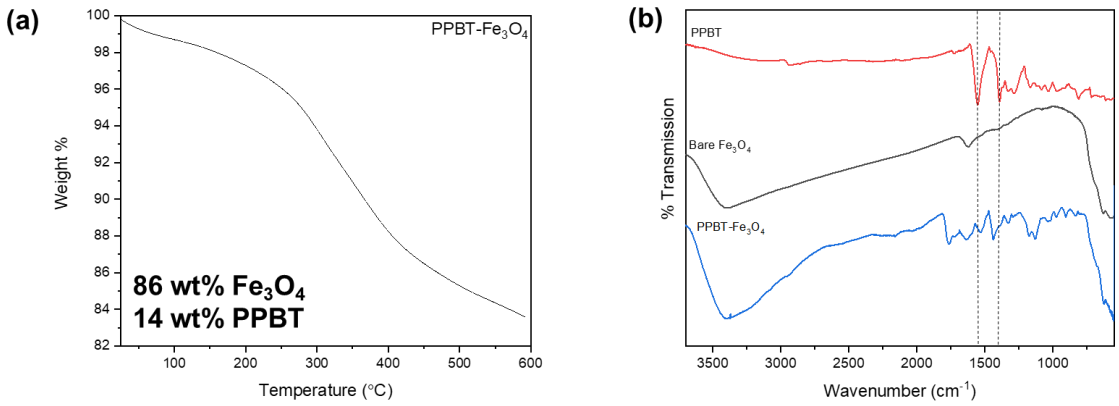

Figure 44: (a) TGA and (b) ATR-FTIR of bare magnetite, PPBT, and PPBT-Fe_3O_4 from a Fischer esterification.

The new PPBT functionalized magnetite and bare magnetite was probed by nitrogen isothermal adsorption/desorption measurements (**Figure 45**). The BET specific surface area of bare magnetite and PPBT-Fe_3O_4 was calculated to be 128 ± 1.54 m^2 g^{-1} and 106 ± 1.83 m^2 g^{-1}, respectively. These values indicate that the PPBT coating did not lead to an increase in surface area, as previously demonstrated with graphene-wrapped magnetite anodes.[121,123]

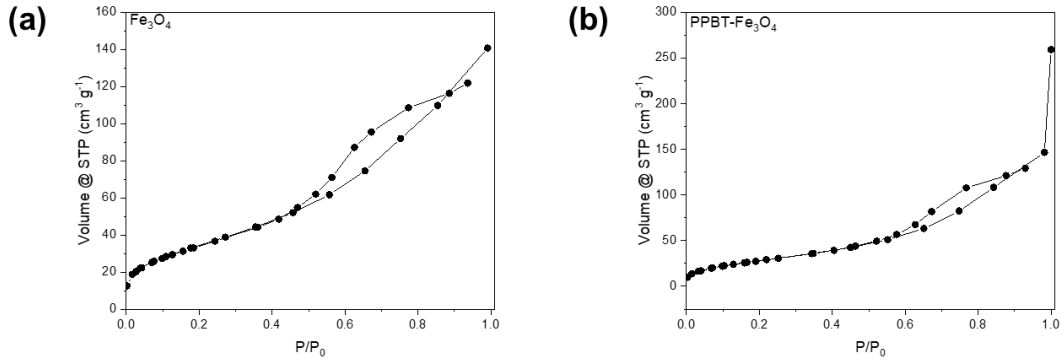

Figure 45: Nitrogen adsorption and desorption isotherm for (a) bare magnetite and (b) PPBT-Fe_3O_4 (Fischer esterification functionalization method).

The colloidal stability of the PPBT-Fe_3O_4 compared to the PPBT-APTES-Fe_3O_4 was evaluated using zeta potential and dynamic light scattering measurements (**Figure 46**). In efforts to mimic the immediate environment surrounding the nanoparticles, they were dispersed in water by stirring on a hot plate for 12 hours at 80 °C. Both magnetite solutions exhibited similar values of pH for comparable zeta potential measurements (pH~8). Typically, values more negative than -30 mV are considered to represent the level of mutual repulsion needed to ensure the stability of a dispersion.[90] The PPBT-APTES-Fe_3O_4 had a zeta potential of -38.27 ± 0.81 and the PPBT-Fe_3O_4 had a zeta potential of -33.13 ± 0.75. The magnetite functionalized using the APTES-EDC method displayed a more negative zeta potential and lower average aggregate size. APTES could aid in breaking up magnetite aggregates prior to the final functionalization with EDC and PPBT, producing smaller particle sizes.

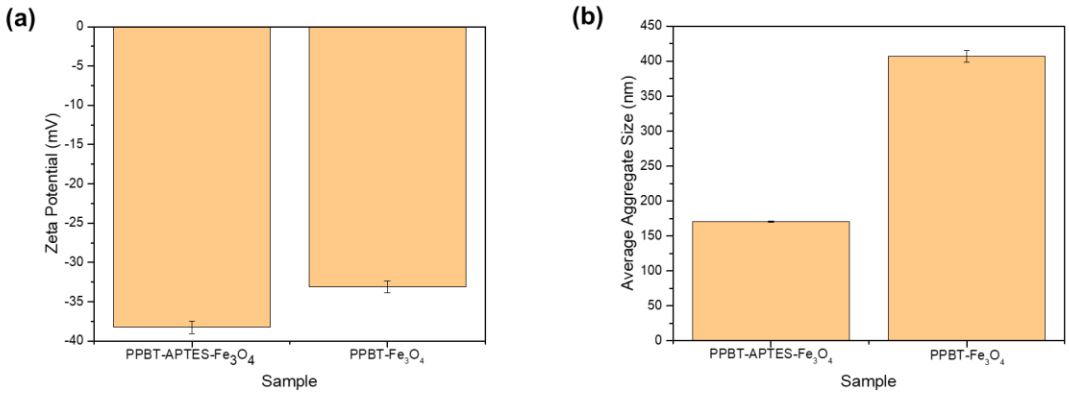

Figure 46: (a) Zeta potential and (b) average aggregate size of PPBT-APTES-Fe_3O_4 and PPBT-Fe_3O_4.

A preliminary aging study was conducted to examine the colloidal stability and average aggregate size over a three-week period (**Figure 47**). The zeta potential for the Fischer esterification functionalization resulted in values less negative than the -30 mV threshold, indicating a decrease in colloidal stability over time.[90] The PPBT-Fe_3O_4 had zeta potentials of -24 ± 0.92, -26.1 ± 0.52, and -28.1 ± 0.61, for the one-, two- and three-week periods, respectively. The zeta potential did not substantially change, but did not exhibit the same stability as the APTES functionalization method. The PPBT-APTES-Fe_3O_4 had zeta potentials of -35.2 ± 0.35, -37.1 ± 0.1, and -33.0 ± 0.8, for the one-, two-, and three-week periods, respectively. APTES remained more negative than the -30 mV threshold, which indicates stability of a dispersion. Similarly, the average aggregate size did not substantially change over three weeks. The Fischer esterification sample had an initial average aggregate size of 407 ± 8.8 that slightly decreased to 379.1 ± 4.1 after three weeks. Whereas, the APTES sample had an initial size of 171 ± 0.91 and slightly increased to 178 ± 1.1 after three weeks. Both samples retained their average aggregate sizes, with the

APTES system remaining lower in size. This aging study verified that the APTES could aid in breaking up magnetite particles, leading to enhanced colloidal stability and smaller aggregates.

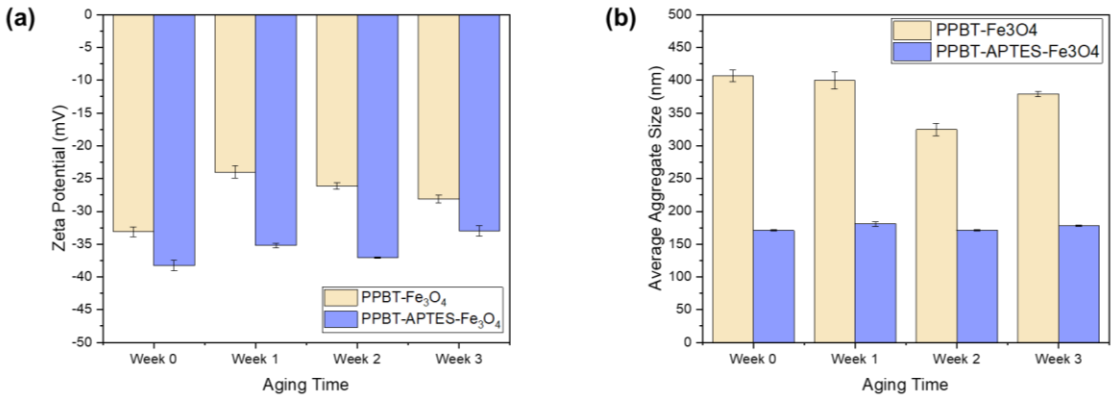

Figure 47: Three week aging study of functionalized PPBT coated magnetite. (a) Zeta potential and (b) average aggregate size of PPBT-APTES-Fe_3O_4 and PPBT-Fe_3O_4.

The morphology of electrodes prepared solely with PPBT-Fe_3O_4 as the active material and composite electrodes consisting of PPBT-Fe_3O_4 active material, carbon additives, and PPBT polymeric binder were evaluated through SEM (**Figure 48**). The PPBT polymeric binder was used to allow for direct comparison to the aforementioned PEG/PPBT system utilized in **Chapters 2** and **3.** As anticipated from DLS, the Fischer esterification functionalization method produced larger particles compared to the APTES/EDC procedure. Surprisingly, the composite electrodes displayed significantly different morphologies upon interactions with carbon additives and polymeric binder. The Fischer esterification functionalization produced an electrode with an overall more uniform morphology, with a few large aggregates present and should positively impact

electrochemical performance. In contrast, the PPBT-APTES-Fe_3O_4 system displayed a broader range of particle size distribution, with uneven surfaces, which could be a result of the APTES linkers acting as a barrier to the carbon additives and polymeric binder.

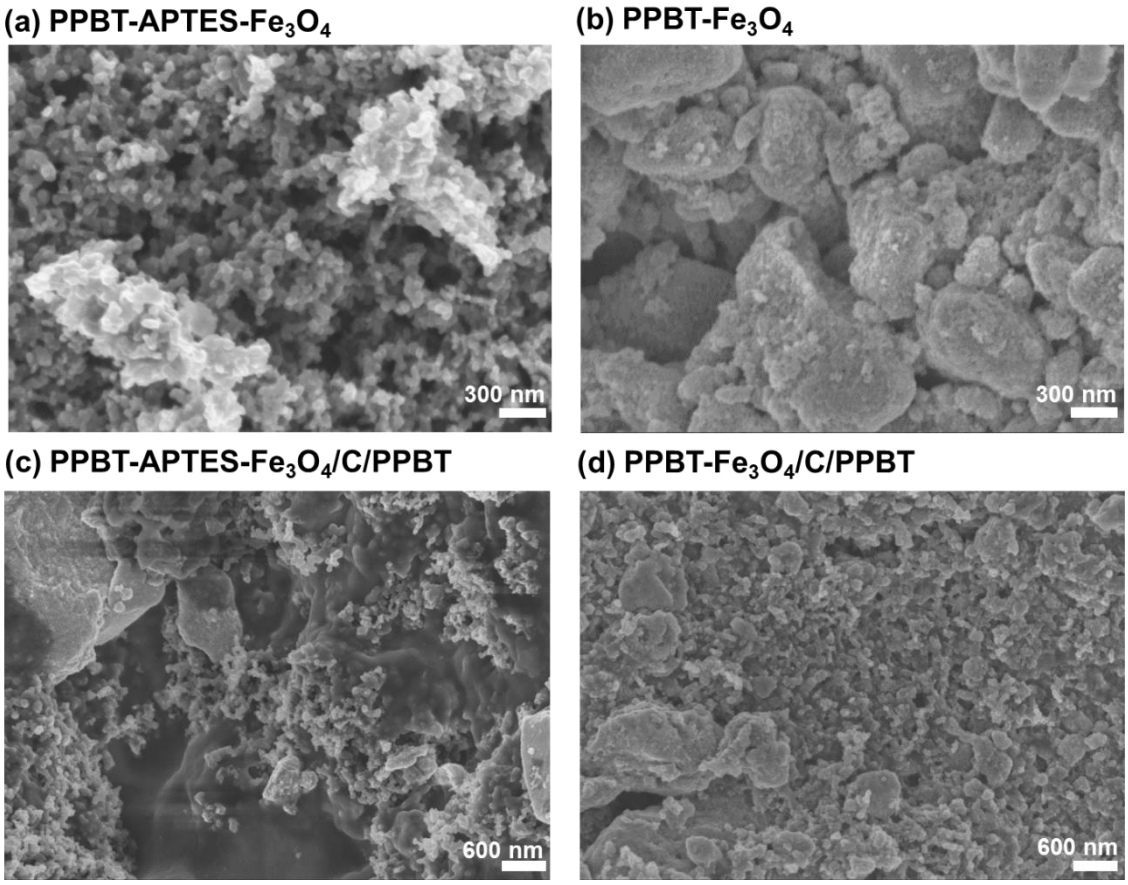

Figure 48: SEM of electrodes. (a) PPBT-APTES-Fe_3O_4 active material electrode, (b) PPBT-Fe_3O_4 active material electrode, (c) PPBT-APTES-Fe_3O_4/C/PPBT composite electrode, and (d) PPBT-Fe_3O_4/C/PPBT composite electrode.

The electrode kinetics were evaluated using CV performed at different scan rates (v) to initially compare the two functionalization methods (**Figure 49**). The kinetic data was characterized by analyzing the voltammetric response of the polymeric binders at various scan rates, as previously discussed. The new Fischer esterification

functionalization method exhibited a *b* value of 0.928, as compared to the APTES/EDC functionalization *b* value of 0.867. The *b* value for Fischer esterification functionalization corresponds to the PEG/PPBT system used in **Chapters 2 and 3**, which has a *b* value of 0.927. However, the PEG coating is not covalently attached to the magnetite surface and improvements in electrochemical performance result from the formation of a Fe-carboxylate interaction, resulting from the active material and polymeric binder. This initial electrochemical characterization is promising for enhanced performance with the new PPBT-Fe_3O_4 system, using the Fischer esterification functionalization.

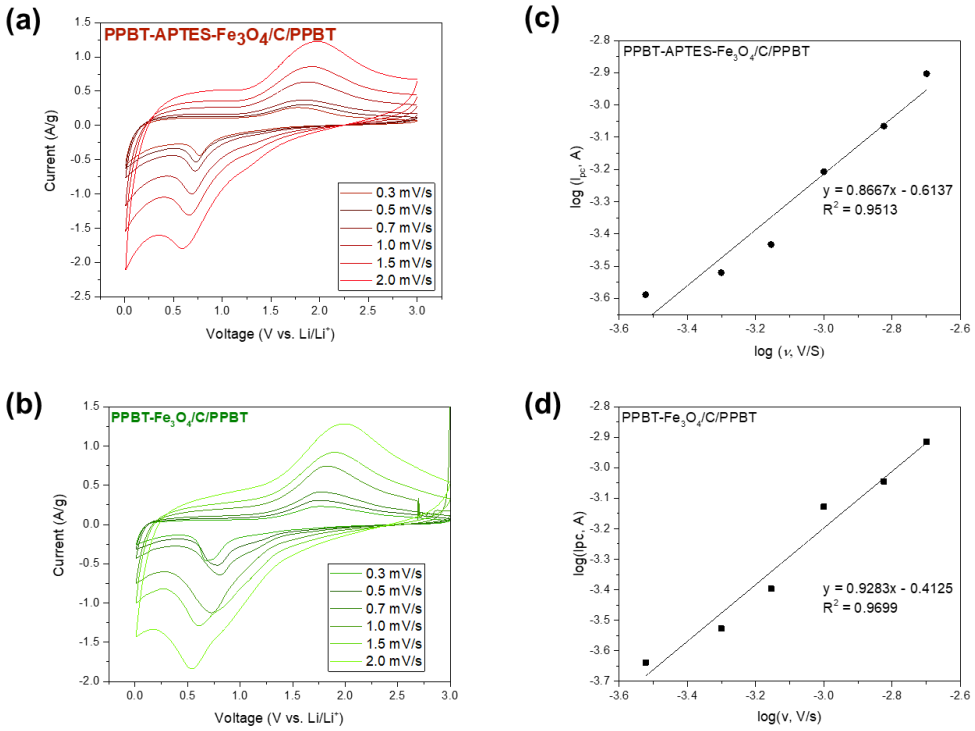

Figure 49: Comparing kinetic performance of PPBT-APTES-Fe_3O_4 and PPBT-Fe_3O_4 composite electrodes. Cyclic voltammetry (CV) of (a) PPBT-APTES-Fe_3O_4/C/PPBT and (b) PPBT-Fe_3O_4/C/PPBT, with various scan rates, and corresponding plots of log (I_{pc}) vs. log (v), which were plotted from the results of cathodic peak currents of CV curves with different scan rates (v) for (c) PPBT-APTES-Fe_3O_4/C/PPBT and (d) PPBT-Fe_3O_4/C/PPBT.

Coin cells were fabricated to explore the impact of the two magnetite functionalization techniques, using composite anodes composed of PPBT-Fe_3O_4 active material, carbon additives, and PPBT binder in a 71.4:14.3:14.3 mass ratio, Li metal served as the counter electrode, and 1 M $LiPF_6$ in ethylene carbonate (EC) and diethylene carbonate (DEC) (1:1 by weight) was used as the electrolyte. The mass ratio was chosen based on prior results to facilitate direct comparison.[38] Charge-discharge cycling (**Figure 50a**) was conducted at a current density of 240 mA g^{-1} (~0.3 C) to determine the capacity retention of each system for 100 cycles. Galvanostatic profiles are also provided in **Figure 51** for both functionalization methods.

The PPBT-Fe_3O_4 electrode (blue) demonstrated a higher initial capacity value of 826 mAh g^{-1} as compared to the APTES system (black), with a value of 395 mAh g^{-1}, resulting in a 209% increase with the new functionalization method. These trends continued over 100 cycles, where the PPBT-Fe_3O_4 exhibits a value of 1045 mAh g^{-1}, compared to the APTES system's capacity value of 489 mAh g^{-1}. The improved capacity of the PPBT-Fe_3O_4 results from the direct attachment of PPBT onto the magnetite surface and is no longer hindered by bulky APTES linkers. However, in terms of Coulombic efficiency, both systems demonstrated an initial value of 87%. After 100 cycles, PPBT-Fe_3O_4 has a value of 99.3%, while the APTES system displayed a value of 98.7%.

The APTES and Fischer esterification functionalization methods exhibited similar cycling phenomenon, where a gradual increase in capacity was observed for both samples. Similar behavior has previously been observed in other metal oxide composites and is believed due to the reversible growth of the polymeric gel-like film by kinetically activated electrolyte degradation.[121,123–125] However, we believe this trend is best attributed to an

increase in surface area of the PPBT-magnetite samples and an activation process from covalently bonded functionalization. An increased surface area is beneficial for electrolyte access and lithium-ion diffusion[121,123] and an activating process of porous anodes has previously been reported to cause an increase in capacity.[126,127] This activation process is speculated to result from using a covalently bonded coating involving a conductive material. This phenomenon was not previously observed in our PEG-magnetite samples, which involved a physical, not electrically conductive coating, as illustrated in **Chapters 2 and 3**.[11]

Newly fabricated half cells were subjected to rate capability experiments (**Figure 50b**), where cells were lithiated at a constant current density of 80 mA g^{-1} (~0.1 C) and delithiated over a wide range of current densities (80 – 1600 mA g^{-1}) between a voltage range of 0.01 – 3 V. Similar trends were observed in rate capability testing, where the direct attachment of PPBT showed significant improvements in capacity. PPBT-Fe_3O_4 exhibited a lower starting capacity of 791 mAh g^{-1}, which increased to 818 mAh g^{-1} upon cycling back to 0.1 C, mirroring the behavior observed during cycling. APTES electrodes follow a similar pattern of an initial capacity value of 531 mAh g^{-1}, which increased to 609 mAh g^{-1} at the 37th cycle.

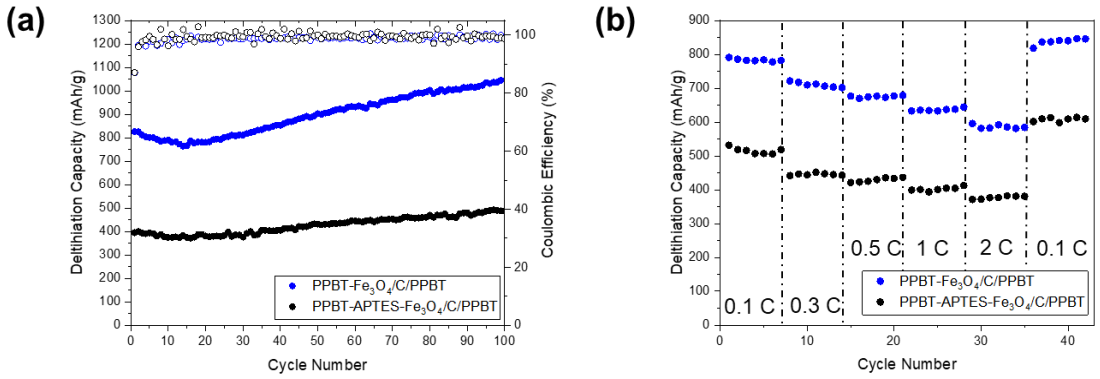

Figure 50: (a) Cycling performance (capacity retention as a function of cycle number) of PPBT- Fe_3O_4/C/PPBT as compared to PPBT-APTES- Fe_3O_4/C/PPBT cycled at 240 mA g^{-1} (~0.3 C) between 0.01 and 3 V. (b) Delithiation rate capability, where cells were lithiated a constant current density of 80 mA g^{-1} (0.1 C) and delithiated at different current densities between 0.01 and 3 V.

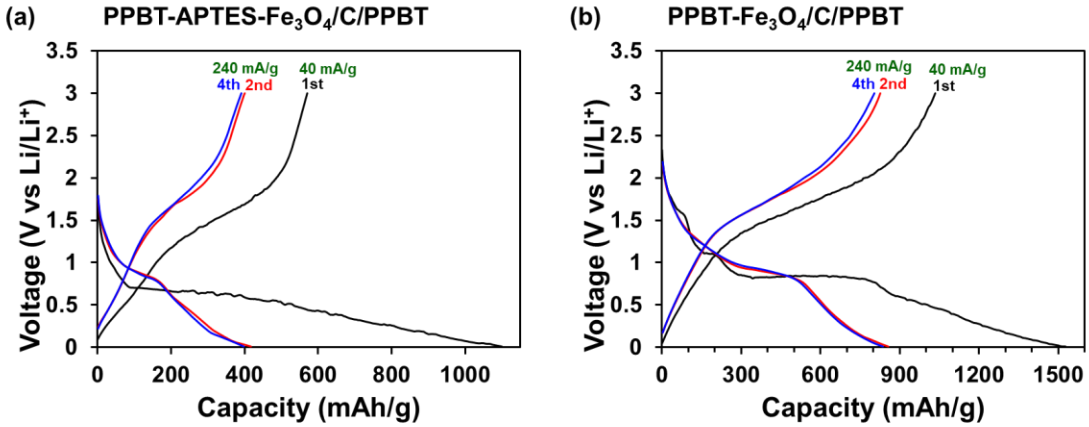

Figure 51: Galvanostatic profiles of (a) PPBT-APTES-Fe_3O_4/C/PPBT and (b) PPBT-Fe_3O_4/C/PPBT.

Further insight into the performance differences between the functionalization methods can be discerned from analysis of EIS results (**Figure 52**) whereby the cells used here correspond to those cycled between 0.01 and 3V (**Figure 50a**). Impedance testing was performed in the frequency range of 0.1 MHz to 0.1 Hz before cycling at 3V and after 100

cycles at their open-circuit voltage (OCV). Superior battery electrode performance can be attributed to decreased charge transfer resistance (R_{ct}), which is estimated from the diameter of the high-frequency semicircle.[100] Prior to cycling, the Fischer esterification system demonstrated a considerably lower charge transfer resistance as compared to the APTES system. As previously mentioned, APTES linkers are bulky, insulating, long-chains and previously demonstrated higher charge transfer resistances.[118,119] After cycling, the APTES system demonstrated a significant decrease in charge transfer resistance, whereas the Fischer esterification method remained relatively the same. The decrease for the APTES system could aid in the explanation of the increase in capacity phenomenon and proposed activation process.

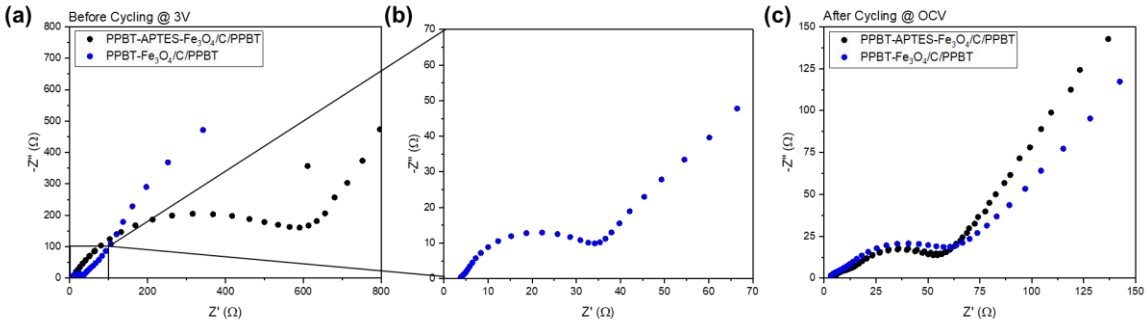

Figure 52: Electrical impedance spectroscopy (EIS) (a) before cycling at 3V, (b) zoomed into before cycling at 3V, and (c) after 100 cycles at OCV in the frequency range from 0.1 MHz to 0.1 Hz.

The composite electrodes were further evaluated by XPS after 100 cycles **(Figure 53**) to explore differences in chemical composition. The results offer evidence for the formation of a stable SEI layer, which can be deduced from the fraction of LiF present in the electrode.[95,101] The survey scans presented in **Figure 53a** demonstrate that only C, O

and F remain on the corresponding electrode surfaces after cycling. **Figure 53b** provides the F 1s scan, where the Fischer esterification electrode exhibited a substantially more intense peak as compared to the APTES system. The higher fraction of LiF in the cycled Fischer esterification functionalized electrodes suggests formation of a stable SEI layer and helps to validate the electrochemical results discussed above. As evidenced by the O 1s and C 1s data (**Figure 53c, d**), the proportion of organic compounds within the SEI layer was relatively higher for the APTES system. Surprisingly, the APTES system exhibited two additional peaks (293 eV and 295.5 eV), which could be associated with K.[89] Although not directly present in the survey scan, the presence of K in the APTES electrode could indicate the presence of polymeric binder on the surface of the composite electrode. Despite the higher fraction of organic compounds as compared to the Fischer esterification system, the significantly lower fraction of LiF and presence of K on the surface confirm unstable SEI layer formation.

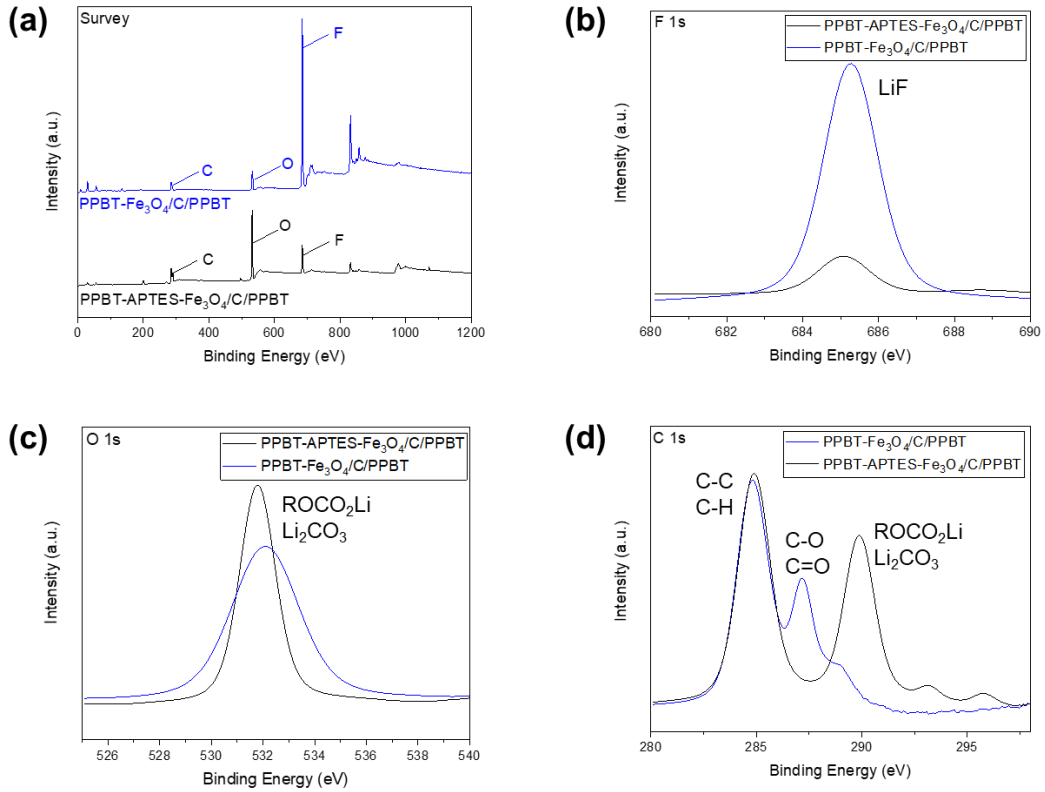

Figure 53: XPS analysis of SEI layer after 100 cycles. (a) Survey scan, (b) F 1s scan, (c) O 1s scan, and (d) C 1s scan.

Molecular interactions between the active material and polymeric binder are expected to positively impact electrochemical performance.[70,122] As such, Fourier infrared (FT-IR) spectroscopy provides a convenient tool to uncover further differences in the functionalization techniques (**Figure 54**). The PPBT carboxylate moieties exhibit vibrational bands at 1556 and 1400 cm^{-1}, which correspond respectively to the O-C-O asymmetric and symmetric stretching modes, and appear in electrode slurries of both functionalization methods.[11,71] A new peak not present in the PPBT binder was observed at around 1755 cm^{-1}, which corresponds to a C=O stretching vibration. Furthermore, a shoulder is observed at 1510 cm^{-1}, which was split from the 1556 cm^{-1} band, suggesting

coordination of carboxylate functionalities on the magnetite surface.[11] The presence of these peaks are only demonstrated in the PPBT-Fe_3O_4/C/PPBT system and are not observed from the APTES slurry. These FT-IR results should support enhanced electrochemical performance demonstrated from the direct attachment of PPBT on the magnetite surface and indicate that Fe-carboxylate interactions are present. Interactions between the binder and high capacity active material have previously been reported as critical factors influencing electrode stability.[11,71] These interactions are believed present between the active material and PPBT surface coating, but may also result from additional interactions between the PPBT surface coating and PPBT polymeric binder. Similar FT-IR results, indicating interactions between active material and polymeric binder, were demonstrated for the PEG/PPBT system, as discussed in **Chapter 2**. Future work will focus on using alternative binders, such as PAA, to differentiate between the surface coating and polymeric binder effects.

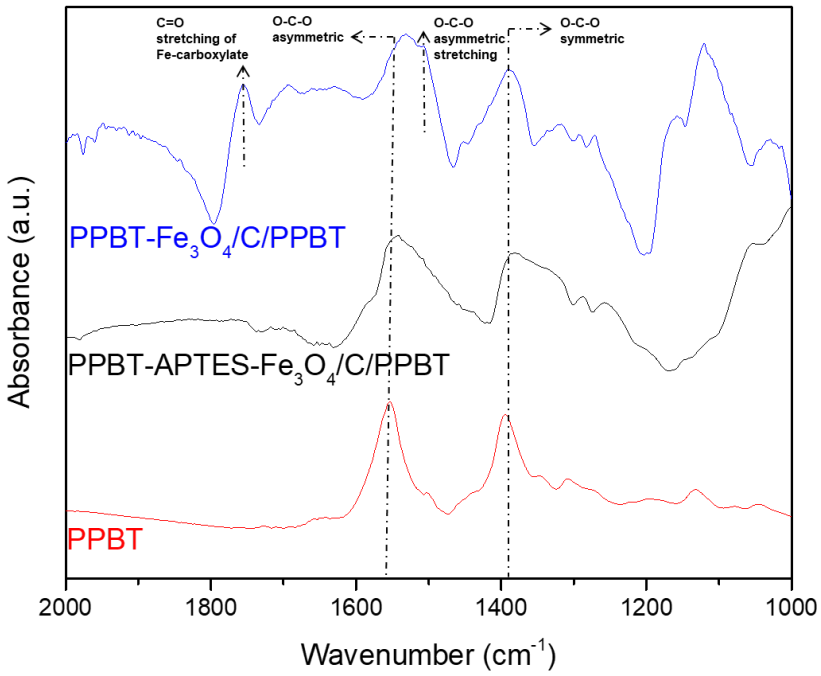

Figure 54: FT-IR spectra of polymeric binder (PPBT) and electrode slurries prepared by mixing PPBT-APTES-Fe_3O_4 or PPBT-Fe_3O_4 with PPBT binder and carbon additives.

Support for the presence of bonding between PPBT and the Fe_3O_4 surface can be attained from XPS analysis, specifically of the Fe 2p core level (**Figure 55**). The observed peaks at ~712 and ~724 eV correspond to Fe $2p_{3/2}$ and Fe $2p_{1/2}$ orbitals, respectively; while the absence of a peak mid-way between and associated with Fe^{3+}, confirms a pure magnetite phase.[102] The appearance of this satellite peak in PPBT-Fe_3O_4/C/PPBT electrode slurries confirms the presence of chemical/bonding interactions between PPBT and the Fe_3O_4 surface. This peak was not observed for the PPBT-ATPES system, which could hinder electrochemical performance. However, this peak was present in the PEG/PPBT system and could also point to interactions between the polymeric binder and active material. Further investigation into alternate binders is necessary to confirm this

hypothesis.

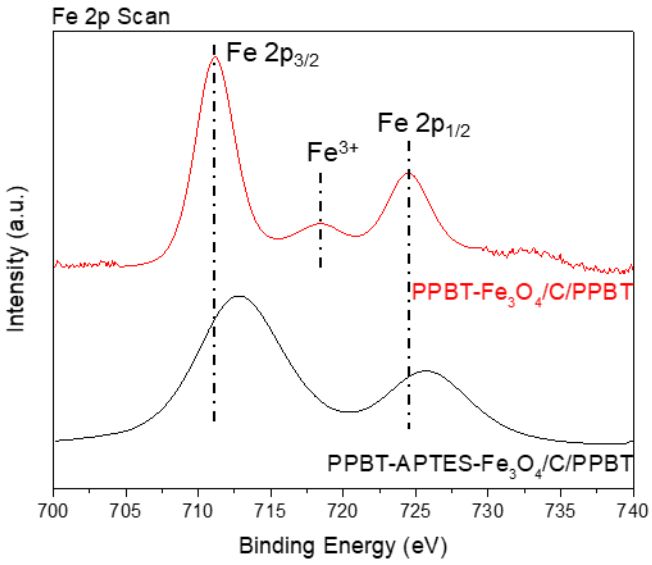

Figure 55: Fe 2p XPS spectra of electrode slurries.

4.4 Conclusions

The results presented in this investigation demonstrate the impact of carbon loading on carbon-polymer interactions in a composite electrode system. Regardless of carbon loadings, all systems demonstrated comparable particle dispersion and did not exhibit phase separation. A higher polymeric binder loading led to enhanced capacity value, as a result of electrochemical doping, but displayed lower capacity retention, lower Li^+ diffusion, and a less stable SEI layer formation. A higher carbon loading exhibited a lower capacity value, but a more stable performance. Further optimization is needed to determine a balance between carbon and polymeric loadings for ideal capacity and stability. In present composite electrode formation, a 50:50 loading is utilized for polymeric binder and carbon

loadings. From this preliminary investigation, it would appear that a higher carbon loading content could further impact electrode stability.

Two different surface chemistries were employed for the functionalization of magnetite with the polymeric binder, PPBT: APTES-EDC and Fischer esterification. The functionalization method significantly impacted overall electrochemical performance of composite electrodes. PPBT-APTES-Fe_3O_4 displayed a lower capacity and Li^+ diffusion rate, ultimately leading to poor performance. Although a commonly used surface modifier, APTES hindered the electrochemical performance as a result of its bulky and insulating nature. Optimization was attempted with the APTES system by incorporating carbon additives and polymeric binder, while increasing active material loading. All attempts resulted in poor performance compared to the control. Direct functionalization of PPBT onto the magnetite surface using a facile Fischer esterification technique, however, proved beneficial for electrode morphology and faster Li-ion diffusion, resulting in a higher capacity and improved rate capability performance. The observed attachment strategies from this investigation create a framework for the future design of high-capacity anode systems and can be applied to other active materials with alternative carboxylated polymeric binders for optimized performance.

Simultaneously, these results provide insight into composite electrode formation in optimizing surface functionalization techniques and carbon/polymer loading.

CHAPTER 5. CONCLUSION AND RECOMMENDATIONS

5.1 Summary and Conclusions

In this thesis, three polymeric binder designs were developed for use in magnetite-based anode systems.

In **Chapter 2**, a water-soluble carboxylated polythiophene polymer (PPBT) was utilized as a model system to analyze the effect of cation size on electrochemical performance. The cations studied included H^+, NH_4^+, K^+, Na^+, and Li^+. The hydrogen and ammonium derivatives exhibited poor electrochemical performance. P-H-BT demonstrated poor solubility in water leading to more heterogenous dispersions and morphologies, which ultimately led to poor capacity retention. The poor performance for P-NH_4-BT is believed to result from weak interactions between NH_4^+ and PEG. Potassium, sodium and lithium systems allowed for the investigation of cation size effects, where the largest cation size (K^+) demonstrated the most enhanced electrochemical performance through improvements to kinetics, capacity retention, SEI layer formation and reduced charge transfer resistance. The sodium derivative exhibited the most uniform morphology, leading to enhanced rate capability performance, as a result of interactions of the cation to the PEG surface coating. Deviations from the correlation between cation size and improved performance are attributed to artificially high capacity from the lithium system.

In **Chapter 3**, a series of carboxylated polymers with varying functional groups were analyzed as alternative polymeric binders. Polymers of interest included PEDOT:PSS, WS-PE_2, PPBT, and PAA-K. When compared to PEDOT:PSS, WS-PE_2

showed significant improvement, which is attributed to its ion transport enhancements, in conjunction with its high conductivity. Although demonstrating improved cycling performance, WS-PE_2 exhibited poor rate capability, particularly at high current densities, which is believed due to its bulky chemical structure and lower concentration of carboxylic groups. PAA-K underperformed in cycling compared to PPBT and WS-PE_2, but exhibited comparable rate capability performance relative to PPBT, which is thought a result of its high concentration of carboxylic groups. The PEG/PPBT system exhibited the best overall electrochemical performance, due to its electronic conductivity and high concentration of carboxyl groups. An important consideration from this investigation revealed the correlation between the necessity of a high physical affinity between the polymeric binder and coating, as determined by HSP analysis, which can be used to predict cycling stability, kinetics, and SEI layer formation, whereas morphology leads to enhanced rate capability performance.

In **Chapter 4**, the model polythiophene polymer was functionalized onto the magnetite surface using two functionalization methods, an APTES and EDC approach and Fischer-esterification. APTES linkers proved too bulky and insulating, ultimately hindering electrochemical performance. Direct attachment of the polymer onto the magnetite surface using Fischer-esterification led to enhanced performance. Additional work focused on understanding polymeric binder and carbon additive interactions for composite electrode design. A higher polymeric loading (40 wt%) enhanced capacity due to electrochemical doping of the polymer, but resulted in unstable SEI layer formation and poor capacity retention. A higher carbon loading (80-90 wt%) resulted in a lower capacity

value, but overall a more stable performance. Further optimization is needed to determine a balance between carbon and polymeric loading for ideal capacity and stability.

Altogether, these studies demonstrate frameworks for designing optimal polymeric binders to enhance performance of high-capacity anodes, often hindered by their large volume changes during cycling.

5.2 Recommendations and Future Work

5.2.1 Ion Exchanged Polymeric Binders

In **Chapter 2**, a model semiconducting carboxylated polythiophene, PPBT, was used to understand cation size effects on overall electrochemical performance. Preliminary cycling testing at 0.3 C between 0.01 and 3V was done comparing PAA and PAA-K with and without PEG coatings (**Figure 56**). The no PEG electrode systems are optimal for performance, due to limited physical affinity between the polymeric binder and coating, as discussed in **Chapter 3**. The PAA significantly outperformed the PAA-K, with and without PEG coating. The cation trends discussed in **Chapter 2** were only investigated with one polymeric binder. To further understand cation size effect trends, additional polymers should be investigated. Preliminary testing with PAA and PAA-K reveals different trends and additional characterization is needed to understand the different polymeric binder systems.

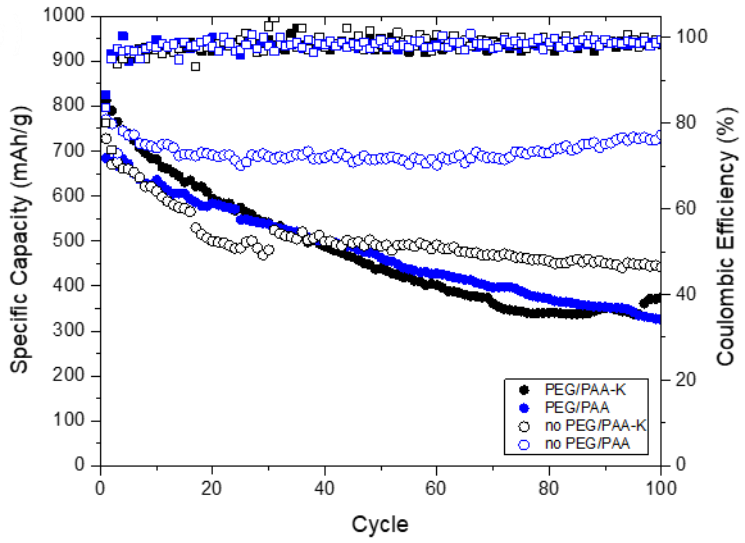

Figure 56: Cycling performance (capacity retention as a function of cycle number) of PAA and PAA-K polymeric binders with and without PEG coating at 240 mA g^{-1} (~0.3 C) between 0.01 and 3 V.

5.2.2 Tuning Polymeric Binders

In **Chapter 3**, PAA was investigated as an alternative, water-soluble, carboxylated polymeric binder. The molecular weight of PAA has been explored in silicon anode systems.[57,59] Hu *et al.* concluded the optimal PAA molecular weight range is 24-150 kDa to maintain cohesion in the electrodes over many cycles.[57] Whereas, Kasinathan *et al.* investigated a different range of molecular weights (250, 450, 1250 kDa) and found highest rate performance and long term stability at 250 kDa.[59] Kasinathan noted that the PAA of 1250 kDa had a very high viscosity, making it difficult for electrode fabrication and was discarded from the investigation. Due to the difficult processing of high molecular weight PAA, limited information exists on its properties in batteries. An alternative technique to

understanding high molecular weight performance of PAA and overcoming processing issues would be a polymer blend approach of combining high and low molecular weights, as previously done by McBride *et al*.[128] Blending different molecular weight polymers would aid with viscosity issues and allow for a more comprehensive study of molecular weight effects in polymeric binders, which is rarely investigated.

Enhancements in cycling performance was previously demonstrated using acidic water conditions in electrode fabrication.[129] This improvement was attributed to physical cross-linking of CMC chains in a solution of pH 3. Mazouzi *et al.* demonstrated that by altering the pH, SiOH groups were able to react with the COOH groups present on the CMC surface, leading to enhanced cycling stability.[48] This mechanism is pH dependent, where a pH value lower than the isolectric point of active material particles (here silicon) and pK_a of CMC is necessary for electrode preparation. Using PAA in acidic conditions could aid in the reaction between active material –OH groups and COOH on the binder. In our magnetite-based system, interactions between the polymeric binder and active material surface were not initially observed for PAA. Processing PAA in acidic conditions could positively impact its performance and improve cycling stability.

A comprehensive study of PAA as a polymeric binder has been limited to silicon-based systems and information on its performance in magnetite is limited. Understanding molecular weight influence and acidic electrode fabrication conditions could enhance the poor cycling performance that was observed in **Chapter 3** and offer a cost-effective alternative to PPBT.

5.2.3 PPBT Magnetite Surface Functionalization

5.2.3.1 Alternative Functionalization Techniques

In the surface functionalization methods used in **Chapter 4**, the amount of PPBT loading on the magnetite surface was not optimized. It would be useful to control the functionalization methods and explore how varying amounts of PPBT loading impact electrochemical performance. A higher loading of PPBT on the surface may allow for steps towards optimizing the system to move away from needing additional polymeric binder and conductive additives to aid in the design of flow battery systems.

In **Chapter 4**, only covalent attachment strategies were explored. Wang *et al.* previously demonstrated the feasibility of non-covalent π-π interaction strategies in magnetite-based systems.[118] Here, a π-π interaction process was used between Fe_3O_4 nanoparticles and multi-walled carbon nanotubes (MWNTs), where Fe_3O_4 nanoparticles were first functionalized with 4-mercaptobenzoic acid linkers. When compared to a covalent attachment and physical sonication, the non-covalently attached magnetite electrodes exhibited the highest capacity and capacity retention, lowest charge transfer resistance, and fastest lithium ion diffusion rate. Using a similar functionalization process with PPBT would aid in the understanding of attachment strategies and how non-covalent attachment compares to the Fischer esterification method.

5.2.3.2 Optimizing PPBT-Carbon Interactions

In **Chapter 4**, polymer-carbon interactions were evaluated using 60 wt%, 80 wt%, and 90 wt% carbon with the remaining amount PPBT. It would be useful to find an

optimized carbon loading between 60 wt% and 80 wt% to balance between electrochemical doping enhancements from PPBT and electrode stability. Higher capacity values were demonstrated with a 60 wt% carbon loading, but there was a decline in electrode stability as seen in SEI layer formation, capacity retention, and Li ion diffusion. Whereas, the 80 wt% electrode demonstrated a more stable performance, but lower capacity value. Optimization between these carbon loadings would be helpful in understanding the mechanisms between PPBT and Super P and to allow for enhanced composite electrode fabrication in understanding polymer to carbon loading ratios.

5.2.3.3 Investigating Additional Polymeric Binders

In **Chapter 4**, PPBT was used as both the polymeric binder and coating on the active material surface. To elucidate differences between the active material coating and binder, it would be useful to demonstrate the effects of the PPBT coating using alternative polymeric binders, such as PAA or CMC, which are widely used. Future work will examine the electrochemical performance of the PPBT coating with a PAA binder to further understand practical applications. The use of only a PPBT coating, without a PPBT binder, would also alleviate the cost associated with the conjugated polymer. PAA is commercially available and relatively inexpensive, which would be a more commercially relevant system.

REFERENCES

(1) Zhang, W.-M.; Wu, X.-L.; Hu, J.-S.; Guo, Y.-G.; Wan, L.-J. Carbon Coated Fe 3 O 4 Nanospindles as a Superior Anode Material for Lithium-Ion Batteries. *Adv. Funct. Mater.* **2008**, *18* (24), 3941–3946.

(2) Goriparti, S.; Miele, E.; De Angelis, F.; Di Fabrizio, E.; Proietti Zaccaria, R.; Capiglia, C. Review on Recent Progress of Nanostructured Anode Materials for Li-Ion Batteries. *Journal of Power Sources*. July 2014, pp 421–443.

(3) Goodenough, J. B.; Park, K.-S. The Li-Ion Rechargeable Battery: A Perspective. *J. Am. Chem. Soc.* **2013**, *135* (4), 1167–1176.

(4) Tarascon, J. M.; Armand, M. Issues and Challenges Facing Rechargeable Lithium Batteries. *Nature* **2001**, *414* (6861), 359–367.

(5) Armand, M.; Tarascon, J.-M. Building Better Batteries. *Nature* **2008**, *451* (7179), 652–657.

(6) Balogun, M. S.; Qiu, W.; Luo, Y.; Meng, H.; Mai, W.; Onasanya, A.; Olaniyi, T. K.; Tong, Y. A Review of the Development of Full Cell Lithium-Ion Batteries: The Impact of Nanostructured Anode Materials. *Nano Res.* **2016**, *9* (10), 2823–2851.

(7) Liu, C.; Neale, Z. G.; Cao, G. Understanding Electrochemical Potentials of Cathode Materials in Rechargeable Batteries. *Materials Today*. Elsevier March 1, 2016, pp 109–123.

(8) Tarascon, J. M.; Armand, M. Issues and Challenges Facing Rechargeable Lithium Batteries. *Nature* **2001**, *414* (6861), 359–367.

(9) Balaya, P.; Li, H.; Kienle, L.; Maier, J. Fully Reversible Homogeneous and Heterogeneous Li Storage in RuO2 with High Capacity. *Adv. Funct. Mater.* **2003**, *13* (8), 621–625.

(10) Qi Li, Caihong Xing, Zhaojie Wei, J. M. Enhanced Electrode Composition for Li Ion Battery. US 2011/0171371 A1, 2011.

(11) Kwon, Y. H.; Minnici, K.; Huie, M. M.; Takeuchi, K. J.; Takeuchi, E. S.; Marschilok, A. C.; Reichmanis, E. Electron/Ion Transport Enhancer in High Capacity Li-Ion Battery Anodes. *Chem. Mater.* **2016**, *28* (18), 6689–6697.

(12) Sun, Y.; Liu, N.; Cui, Y. Promises and Challenges of Nanomaterials for Lithium-Based Rechargeable Batteries. *Nat. Energy* **2016**, *1* (7), 16071.

(13) Zhang, W.-M.; Wu, X.-L.; Hu, J.-S.; Guo, Y.-G.; Wan, L.-J. Carbon Coated Fe 3 O 4 Nanospindles as a Superior Anode Material for Lithium-Ion Batteries. *Adv. Funct.*

Mater. **2008**, *18* (24), 3941–3946.

(14) He, C.; Wu, S.; Zhao, N.; Shi, C.; Liu, E.; Li, J. Carbon-Encapsulated Fe3O4 Nanoparticles as a High-Rate Lithium Ion Battery Anode Material. *ACS Nano* **2013**, *7* (5), 4459–4469.

(15) Zhang, W.-M.; Wu, X.-L.; Hu, J.-S.; Guo, Y.-G.; Wan, L.-J. Carbon Coated Fe $_3$ O $_4$ Nanospindles as a Superior Anode Material for Lithium-Ion Batteries. *Adv. Funct. Mater.* **2008**, *18* (24), 3941–3946.

(16) Sun, Y.; Liu, N.; Cui, Y. Promises and Challenges of Nanomaterials for Lithium-Based Rechargeable Batteries. *Nat. Energy* **2016**, *1* (7), 16071.

(17) Nitta, N.; Yushin, G. High-Capacity Anode Materials for Lithium-Ion Batteries: Choice of Elements and Structures for Active Particles. *Part. Part. Syst. Charact.* **2014**, *31* (3), 317–336.

(18) Wu, Y.; Zhan, L.; Huang, K.; Wang, H.; Yu, H.; Wang, S.; Peng, F.; Lai, C. Iron Based Dual-Metal Oxides on Graphene for Lithium-Ion Batteries Anode: Effects of Composition and Morphology. *J. Alloys Compd.* **2016**, *684*, 47–54.

(19) Lian, P.; Zhu, X.; Xiang, H.; Li, Z.; Yang, W.; Wang, H. Enhanced Cycling Performance of Fe3O4–Graphene Nanocomposite as an Anode Material for Lithium-Ion Batteries. *Electrochim. Acta* **2010**, *56* (2), 834–840.

(20) Bruck, A. M.; Cama, C. A.; Gannett, C. N.; Marschilok, A. C.; Takeuchi, E. S.; Takeuchi, K. J. Nanocrystalline Iron Oxide Based Electroactive Materials in Lithium Ion Batteries: The Critical Role of Crystallite Size, Morphology, and Electrode Heterostructure on Battery Relevant Electrochemistry. *Inorg. Chem. Front.* **2016**, *3* (1), 26–40.

(21) Xu, J.; Yang, H.; Fu, W.; Du, K.; Sui, Y.; Chen, J.; Zeng, Y.; Li, M.; Zou, G. Preparation and Magnetic Properties of Magnetite Nanoparticles by Sol–Gel Method. *J. Magn. Magn. Mater.* **2007**, *309* (2), 307–311.

(22) Teo, B. M.; Chen, F.; Hatton, T. A.; Grieser, F.; Ashokkumar, M. Novel One-Pot Synthesis of Magnetite Latex Nanoparticles by Ultrasound Irradiation. *Langmuir* **2009**, *25* (5), 2593–2595.

(23) Lee, Y.; Lee, J.; Bae, C. J.; Park, J.-G.; Noh, H.-J.; Park, J.-H.; Hyeon, T. Large-Scale Synthesis of Uniform and Crystalline Magnetite Nanoparticles Using Reverse Micelles as Nanoreactors under Reflux Conditions. *Adv. Funct. Mater.* **2005**, *15* (3), 503–509.

(24) Mizutani, N.; Iwasaki, T.; Watano, S.; Yanagida, T.; Kawai, T. Size Control of Magnetite Nanoparticles in Hydrothermal Synthesis by Coexistence of Lactate and Sulfate Ions. *Curr. Appl. Phys.* **2010**, *10* (3), 801–806.

(25) Su, M.; He, C.; Shih, K. Facile Synthesis of Morphology and Size-Controlled α-Fe2O3 and Fe3O4 Nano-and Microstructures by Hydrothermal/Solvothermal Process: The Roles of Reaction Medium and Urea Dose. *Ceram. Int.* **2016**, *42* (13), 14793–14804.

(26) Sun, X.; Zheng, C.; Zhang, F.; Yang, Y.; Wu, G.; Yu, A.; Guan, N. Size-Controlled Synthesis of Magnetite (Fe_3O_4) Nanoparticles Coated with Glucose and Gluconic Acid from a Single Fe(III) Precursor by a Sucrose Bifunctional Hydrothermal Method. *J. Phys. Chem. C* **2009**, *113* (36), 16002–16008.

(27) Liu, J.; Wu, Z.; Tian, Q.; Wu, W.; Xiao, X. Shape-Controlled Iron Oxide Nanocrystals: Synthesis, Magnetic Properties and Energy Conversion Applications. **2014**, *18*.

(28) Gnanaprakash, G.; Mahadevan, S.; Jayakumar, T.; Kalyanasundaram, P.; Philip, J.; Raj, B. Effect of Initial PH and Temperature of Iron Salt Solutions on Formation of Magnetite Nanoparticles. *Mater. Chem. Phys.* **2007**, *103* (1), 168–175.

(29) Zhu, S.; Marschilok, A. C.; Takeuchi, E. S.; Yee, G. T.; Wang, G.; Takeuchi, K. J. Nanocrystalline Magnetite: Synthetic Crystallite Size Control and Resulting Magnetic and Electrochemical Properties. *J. Electrochem. Soc.* **2010**, *157* (11), A1158.

(30) Minnici, K.; Kwon, Y. H.; Huie, M. M.; de Simon, M. V.; Zhang, B.; Bock, D. C.; Wang, J.; Wang, J.; Takeuchi, K. J.; Takeuchi, E. S.; Marschilok, A. C.; Reichmanis, E. High Capacity Li-Ion Battery Anodes: Impact of Crystallite Size, Surface Chemistry and PEG-Coating. *Electrochim. Acta* **2018**, *260*.

(31) Huang, X.; Zhou, X.; Qian, K.; Zhao, D.; Liu, Z.; Yu, C. A Magnetite Nanocrystal/Graphene Composite as High Performance Anode for Lithium-Ion Batteries. *J. Alloys Compd.* **2011**, *514*, 76–80.

(32) Zhang, Y.; Li, Y.; Li, H.; Zhao, Y.; Yin, F.; Bakenov, Z. Electrochemical Performance of Carbon-Encapsulated Fe3O4 Nanoparticles in Lithium-Ion Batteries: Morphology and Particle Size Effects. *Electrochim. Acta* **2016**, *216*, 475–483.

(33) Ban, C.; Wu, Z.; Gillaspie, D. T.; Chen, L.; Yan, Y.; Blackburn, J. L.; Dillon, A. C. Nanostructured Fe3O4/SWNT Electrode: Binder-Free and High-Rate Li-Ion Anode. *Adv. Mater.* **2010**, *22* (20), E145–E149.

(34) Yoon, T.; Kim, J.; Kim, J.; Lee, J. K. Electrostatic Self-Assembly of Fe3O4 Nanoparticles on Graphene Oxides for High Capacity Lithium-Ion Battery Anodes. *Energies* **2013**, *6* (9), 4830–4840.

(35) Lian, P.; Zhu, X.; Xiang, H.; Li, Z.; Yang, W.; Wang, H. Enhanced Cycling Performance of Fe3O4–Graphene Nanocomposite as an Anode Material for Lithium-Ion Batteries. *Electrochim. Acta* **2010**, *56* (2), 834–840.

(36) Nithya, V. D.; Arul, N. S. Progress and Development of Fe 3 O 4 Electrodes for Supercapacitors.

(37) Komaba, S.; Mikumo, T.; Ogata, A. Electrochemical Activity of Nanocrystalline Fe3O4 in Aprotic Li and Na Salt Electrolytes. *Electrochem. Commun.* **2008**, *10*, 1276–1279.

(38) Kwon, Y. H.; Huie, M. M.; Choi, D.; Chang, M.; Marschilok, A. C.; Takeuchi, K. J.; Takeuchi, E. S.; Reichmanis, E. Toward Uniformly Dispersed Battery Electrode Composite Materials: Characteristics and Performance. *ACS Appl. Mater. Interfaces* **2016**, *8* (5), 3452–3463.

(39) Si, S.; Kotal, A.; Mandal, T. K.; Giri, S.; Nakamura, H.; Kohara, T. Size-Controlled Synthesis of Magnetite Nanoparticles in the Presence of Polyelectrolytes. *Chem. Mater.* **2004**, *16* (18), 3489–3496.

(40) Zhang, W.-M.; Wu, X.-L.; Hu, J.-S.; Guo, Y.-G.; Wan, L.-J. Carbon Coated Fe 3 O 4 Nanospindles as a Superior Anode Material for Lithium-Ion Batteries**.

(41) Xia, H.; Wan, Y.; Yuan, G.; Fu, Y.; Wang, X. Fe3O4/Carbon Core–Shell Nanotubes as Promising Anode Materials for Lithium-Ion Batteries. *J. Power Sources* **2013**, *241*, 486–493.

(42) Li, D.; Jiang, D.; Chen, M.; Xie, J.; Wu, Y.; Dang, S.; Zhang, J. An Easy Fabrication of Monodisperse Oleic Acid-Coated Fe3O 4 Nanoparticles. *Mater. Lett.* **2010**, *64* (22), 2462–2464.

(43) Tai, M. F.; Lai, C. W.; Hamid, S. B. A. Facile Synthesis Polyethylene Glycol Coated Magnetite Nanoparticles for High Colloidal Stability. *J. Nanomater.* **2016**, *2016*, 1–7.

(44) Liu, J.; Zhao, Z.; Jiang, G. Coating Fe $_3$ O $_4$ Magnetic Nanoparticles with Humic Acid for High Efficient Removal of Heavy Metals in Water. *Environ. Sci. Technol.* **2008**, *42* (18), 6949–6954.

(45) Mukhopadhyay, A.; Joshi, N.; Chattopadhyay, K.; De, G. A Facile Synthesis of PEG-Coated Magnetite (Fe 3O 4) Nanoparticles and Their Prevention of the Reduction of Cytochrome C. *ACS Appl. Mater. Interfaces* **2012**, *4* (1), 142–149.

(46) Ma, X.; Zou, S.; Tang, A.; Chen, L.; Deng, Z.; Pollet, B. G.; Ji, S. Three-Dimensional Hierarchical Walnut Kernel Shape Conducting Polymer as Water Soluble Binder for Lithium-Ion Battery. *Electrochim. Acta* **2018**, *269*, 571–579.

(47) Li, D.; Wang, Y.; Hu, J.; Lu, B.; Dang, D.; Zhang, J.; Cheng, Y.-T. Role of Polymeric Binders on Mechanical Behavior and Cracking Resistance of Silicon Composite Electrodes during Electrochemical Cycling. *J. Power Sources* **2018**, *387*, 9–15.

(48) Mazouzi, D.; Lestriez, B.; Roué, L.; Guyomard, D. Silicon Composite Electrode with High Capacity and Long Cycle Life. *Electrochem. Solid-State Lett.* **2009**, *12* (11), A215.

(49) Courtel, F. M.; Niketic, S.; Duguay, D.; Abu-Lebdeh, Y.; Davidson, I. J. Water-Soluble Binders for MCMB Carbon Anodes for Lithium-Ion Batteries. *J. Power Sources* **2011**, *196* (4), 2128–2134.

(50) Magasinski, A.; Zdyrko, B.; Kovalenko, I.; Hertzberg, B.; Burtovyy, R.; Huebner, C. F.; Fuller, T. F.; Luzinov, I.; Yushin, G. Toward Efficient Binders for Li-Ion Battery Si-Based Anodes: Polyacrylic Acid. *ACS Appl. Mater. Interfaces* **2010**, *2* (11), 3004–3010.

(51) Bridel, J. S.; Azaïs, T.; Morcrette, M.; Tarascon, J. M.; Larcher, D. Key Parameters Governing the Reversibility of Si/Carbon/CMC Electrodes for Li-Ion Batteries. *Chem. Mater.* **2010**, *22* (3), 1229–1241.

(52) Lestriez, B.; Bahri, S.; Sandu, I.; Roué, L.; Guyomard, D. On the Binding Mechanism of CMC in Si Negative Electrodes for Li-Ion Batteries. *Electrochem. commun.* **2007**, *9* (12), 2801–2806.

(53) Koo, B.; Kim, H.; Cho, Y.; Lee, K. T.; Choi, N.-S.; Cho, J. A Highly Cross-Linked Polymeric Binder for High-Performance Silicon Negative Electrodes in Lithium Ion Batteries. *Angew. Chemie* **2012**, *124* (35), 8892–8897.

(54) Ryou, M. H.; Kim, J.; Lee, I.; Kim, S.; Jeong, Y. K.; Hong, S.; Ryu, J. H.; Kim, T. S.; Park, J. K.; Lee, H.; Choi, J. W. Mussel-Inspired Adhesive Binders for High-Performance Silicon Nanoparticle Anodes in Lithium-Ion Batteries. *Adv. Mater.* **2013**, *25* (11), 1571–1576.

(55) Shao, D.; Zhong, H.; Zhang, L. Water-Soluble Conductive Composite Binder Containing PEDOT: PSS as Conduction Promoting Agent for Si Anode of Lithium-Ion Batteries. *ChemElectroChem* **2014**, *1* (10), 1679–1687.

(56) Karkar, Z.; Guyomard, D.; Roué, L.; Lestriez, B. A Comparative Study of Polyacrylic Acid (PAA) and Carboxymethyl Cellulose (CMC) Binders for Si-Based Electrodes. *Electrochim. Acta* **2017**, *258*, 453–466.

(57) Hu, B.; Shkrob, I. A.; Zhang, S.; Zhang, L.; Zhang, J.; Li, Y.; Liao, C.; Zhang, Z.; Lu, W.; Zhang, L. The Existence of Optimal Molecular Weight for Poly(Acrylic Acid) Binders in Silicon/Graphite Composite Anode for Lithium-Ion Batteries. *J. Power Sources* **2018**, *378*, 671–676.

(58) Hochgatterer, N. S.; Schweiger, M. R.; Koller, S.; Raimann, P. R.; Wöhrle, T.; Wurm, C.; Winter, M. Silicon/Graphite Composite Electrodes for High-Capacity Anodes: Influence of Binder Chemistry on Cycling Stability. *Electrochem. Solid-State Lett.* **2008**, *11* (5), A76–A80.

(59) Kasinathan, R.; Marinaro, M.; Axmann, P.; Wohlfahrt-Mehrens, M. Influence of the Molecular Weight of Poly-Acrylic Acid Binder on Performance of Si-Alloy/Graphite Composite Anodes for Lithium-Ion Batteries. *Energy Technol.* **2018**, *6* (11), 2256–2263.

(60) Salem, N.; Lavrisa, M.; Abu-Lebdeh, Y. Ionically-Functionalized Poly(Thiophene) Conductive Polymers as Binders for Silicon and Graphite Anodes for Li-Ion Batteries. *Energy Technol.* **2016**, *4* (2), 331–340.

(61) Wu, M.; Xiao, X.; Vukmirovic, N.; Xun, S.; Das, P. K.; Song, X.; Olalde-Velasco, P.; Wang, D.; Weber, A. Z.; Wang, L. W.; Battaglia, V. S.; Yang, W.; Liu, G. Toward an Ideal Polymer Binder Design for High-Capacity Battery Anodes. *J. Am. Chem. Soc.* **2013**, *135* (32), 12048–12056.

(62) Zhao, H.; Du, A.; Ling, M.; Battaglia, V.; Liu, G. Conductive Polymer Binder for Nano-Silicon/Graphite Composite Electrode in Lithium-Ion Batteries towards a Practical Application. *Electrochim. Acta* **2016**, *209*, 159–162.

(63) Zhao, H.; Yuca, N.; Zheng, Z.; Fu, Y.; Battaglia, V. S.; Abdelbast, G.; Zaghib, K.; Liu, G. High Capacity and High Density Functional Conductive Polymer and SiO Anode for High-Energy Lithium-Ion Batteries. *ACS Appl. Mater. Interfaces* **2015**, *7* (1), 862–866.

(64) Zhao, H.; Wang, Z.; Lu, P.; Jiang, M.; Shi, F.; Song, X.; Zheng, Z.; Zhou, X.; Fu, Y.; Abdelbast, G.; Xiao, X.; Liu, Z.; Battaglia, V. S.; Zaghib, K.; Liu, G. Toward Practical Application of Functional Conductive Polymer Binder for a High-Energy Lithium-Ion Battery Design. *Nano Lett.* **2014**, *14* (11), 6704–6710.

(65) Wu, M.; Song, X.; Liu, X.; Battaglia, V.; Yang, W.; Liu, G. Manipulating the Polarity of Conductive Polymer Binders for Si-Based Anodes in Lithium-Ion Batteries. *J. Mater. Chem. A* **2015**, *3* (7), 3651–3658.

(66) Liu, G.; Xun, S.; Vukmirovic, N.; Song, X.; Olalde-Velasco, P.; Zheng, H.; Battaglia, V. S.; Wang, L.; Yang, W. Polymers with Tailored Electronic Structure for High Capacity Lithium Battery Electrodes. *Adv. Mater.* **2011**, *23* (40), 4679–4683.

(67) Ouyang, J.; Chu, C.-W.; Chen, F.-C.; Xu, Q.; Yang, Y. High-Conductivity Poly(3,4-Ethylenedioxythiophene):Poly(Styrene Sulfonate) Film and Its Application in Polymer Optoelectronic Devices. *Adv. Funct. Mater.* **2005**, *15* (2), 203–208.

(68) Groenendaal, L.; Jonas, F.; Freitag, D.; Pielartzik, H.; Reynolds, J. R. Poly(3,4-Ethylenedioxythiophene) and Its Derivatives: Past, Present, and Future. *Adv. Mater.* **2000**, *12* (7), 481–494.

(69) Bridel, J.-S.; Azaïs, T.; Morcrette, M.; Tarascon, J.-M.; Larcher, D. Key Parameters Governing the Reversibility of Si/Carbon/CMC Electrodes for Li-Ion Batteries. *Chem. Mater.* **2010**, *22* (3), 1229–1241.

(70) Magasinski, A.; Zdyrko, B.; Kovalenko, I.; Hertzberg, B.; Burtovyy, R.; Huebner, C. F.; Fuller, T. F.; Luzinov, I.; Yushin, G. Toward Efficient Binders for Li-Ion Battery Si-Based Anodes: Polyacrylic Acid. *ACS Appl. Mater. Interfaces* **2010**, *2* (11), 3004–3010.

(71) Kovalenko, I.; Zdyrko, B.; Magasinski, a.; Hertzberg, B.; Milicev, Z.; Burtovyy, R.; Luzinov, I.; Yushin, G. A Major Constituent of Brown Algae for Use in High-Capacity Li-Ion Batteries. *Science (80-.).* **2011**, *334* (6052), 75–79.

(72) Goodenough, J. B.; Park, K.-S. The Li-Ion Rechargeable Battery: A Perspective. *J. Am. Chem. Soc.* **2013**, *135* (4), 1167–1176.

(73) Smith, P. F.; Takeuchi, K. J.; Marschilok, A. C.; Takeuchi, E. S. Holy Grails in Chemistry: Investigating and Understanding Fast Electron/Cation Coupled Transport within Inorganic Ionic Matrices. *Accounts of Chemical Research*. American Chemical Society March 21, 2017, pp 544–548.

(74) Chen, J.; Xu, L.; Li, W.; Gou, X. Alpha-Fe2O3 Nanotubes in Gas Sensor and Lithium-Ion Battery Applications. *Adv. Mater.* **2005**, *17* (5), 582–586.

(75) Poizot, P.; Laruelle, S.; Grugeon, S.; Dupont, L.; Tarascon, J.-M. Searching for New Anode Materials for the Li-Ion Technology: Time to Deviate from the Usual Path. *J. Power Sources* **2001**, *97–98*, 235–239.

(76) Tarascon, J.-M.; Poizot, P.; Laruelle, S.; Grugeon, S.; Dupont, L. Nano-Sized Transition-Metal Oxides as Negative-Electrode Materials forlithium-Ion Batteries. *Nature* **2000**, *407* (6803), 496–499.

(77) Ito, S.; Nakaoka, K.; Kawamura, M.; Ui, K.; Fujimoto, K.; Koura, N. Lithium Battery Having a Large Capacity Using Fe3O4 as a Cathode Material. *J. Power Sources* **2005**, *146* (1–2), 319–322.

(78) Taberna, P. L.; Mitra, S.; Poizot, P.; Simon, P.; Tarascon, J.-M. High Rate Capabilities Fe3O4-Based Cu Nano-Architectured Electrodes for Lithium-Ion Battery Applications. *Nat. Mater.* **2006**, *5* (7), 567–573.

(79) Mitra, S.; Poizot, P.; Finke, A.; Tarascon, J.-M. Growth and Electrochemical Characterization versus Lithium of Fe3O4 Electrodes Made by Electrodeposition. *Adv. Funct. Mater.* **2006**, *16* (17), 2281–2287.

(80) Yu, Y.; Chen, C.-H.; Shi, Y. A Tin-Based Amorphous Oxide Composite with a Porous, Spherical, Multideck-Cage Morphology as a Highly Reversible Anode Material for Lithium-Ion Batteries. *Adv. Mater.* **2007**, *19* (7), 993–997.

(81) Zhang, W.; Bock, D. C.; Pelliccione, C. J.; Li, Y.; Wu, L.; Zhu, Y.; Marschilok, A. C.; Takeuchi, E. S.; Takeuchi, K. J.; Wang, F. Insights into Ionic Transport and Structural Changes in Magnetite during Multiple-Electron Transfer Reactions. *Adv. Energy Mater.* **2016**, 1–11.

(82) Abraham, A.; Housel, L. M.; Lininger, C. N.; Bock, D. C.; Jou, J.; Wang, F.; West, A. C.; Marschilok, A. C.; Takeuchi, K. J.; Takeuchi, E. S. Investigating the Complex Chemistry of Functional Energy Storage Systems: The Need for an Integrative, Multiscale (Molecular to Mesoscale) Perspective. *ACS Cent. Sci.* **2016**, *2* (6), acscentsci.6b00100.

(83) Shi, Y.; Zhang, J.; Bruck, A. M.; Zhang, Y.; Li, J.; Stach, E. A.; Takeuchi, K. J.; Marschilok, A. C.; Takeuchi, E. S.; Yu, G. A Tunable 3D Nanostructured Conductive Gel Framework Electrode for High-Performance Lithium Ion Batteries. *Adv. Mater.* **2017**, *29* (22), 1603922.

(84) Mukhopadhyay, A.; Joshi, N.; Chattopadhyay, K.; De, G. A Facile Synthesis of PEG-Coated Magnetite (Fe3O4) Nanoparticles and Their Prevention of the Reduction of Cytochrome C. *ACS Appl. Mater. Interfaces* **2012**, *4* (1), 142–149.

(85) Zhang, L.; He, R.; Gu, H.-C. Oleic Acid Coating on the Monodisperse Magnetite Nanoparticles. *Appl. Surf. Sci.* **2006**, *253* (5), 2611–2617.

(86) Kwon, Y. H.; Minnici, K.; Park, J. J.; Lee, S. R.; Zhang, G.; Takeuchi, E. S.; Takeuchi, K. J.; Marschilok, A. C.; Reichmanis, E. SWNT Anchored with Carboxylated Polythiophene "Links" on High-Capacity Li-Ion Battery Anode Materials. *J. Am. Chem. Soc.* **2018**, *140* (17).

(87) Salem, N.; Lavrisa, M.; Abu-Lebdeh, Y. Ionically-Functionalized Poly(Thiophene) Conductive Polymers as Binders for Silicon and Graphite Anodes for Li-Ion Batteries. *Energy Technol.* **2016**, *4* (2), 331–340.

(88) Zhu, S.; Marschilok, A. C.; Takeuchi, E. S.; Takeuchi, K. J. Crystallite Size Control and Resulting Electrochemistry of Magnetite, Fe 3 O 4. *Electrochem. Solid-State Lett.* **2009**, *12* (4), A91–A94.

(89) Thermo Scientific. XPS Interpretation of Carbon http://xpssimplified.com/elements/oxygen.php (accessed Aug 12, 2017).

(90) Everett, D. H. *Basic Principles of Colloid Science*; Royal Society of Chemistry, 1988.

(91) Maltesh, C.; Somasundaran, P. Size of the Sodium Dodecylsulfate Aggregate Bound to Polyethylene Glycol: Effect of Different Cations. *J. Colloid Interface Sci.* **1993**, *157* (1), 14–18.

(92) Chen, H.; Choi, J.-H.; Salas-de la Cruz, D.; Winey, K. I.; Elabd, Y. A. Polymerized Ionic Liquids: The Effect of Random Copolymer Composition on Ion Conduction. *Macromolecules* **2009**, *42* (13), 4809–4816.

(93) Green, M. D.; Salas-de la Cruz, D.; Ye, Y.; Layman, J. M.; Elabd, Y. A.; Winey, K. I.; Long, T. E. Alkyl-Substituted N-Vinylimidazolium Polymerized Ionic Liquids: Thermal Properties and Ionic Conductivities. *Macromol. Chem. Phys.* **2011**, *212*

(23), 2522–2528.

(94) Hugger, S.; Thomann, R.; Heinzel, T.; Thurn-Albrecht, T. Semicrystalline Morphology in Thin Films of Poly(3-Hexylthiophene). *Colloid Polym. Sci.* **2004**, *282* (8), 932–938.

(95) Kwon, Y. H.; Minnici, K.; Lee, S. R.; Zhang, G.; Takeuchi, E. S.; Takeuchi, K. J.; Marschilok, A. C.; Reichmanis, E. SWNT Networks with Polythiophene Carboxylate Links for High-Performance Silicon Monoxide Electrodes. *ACS Appl. Energy Mater.* **2018**, *1* (6), 2417–2423.

(96) Lindstro, H.; So, S.; Solbrand, A.; Rensmo, H.; Hjelm, J.; Hagfeldt, A.; Lindquist, S.-E. Li + Ion Insertion in TiO 2 (Anatase). 2. Voltammetry on Nanoporous Films. *J. Phys. Chem. B* **1997**, *101*, 7717–7722.

(97) Dong, X.; Chen, L.; Liu, J.; Haller, S.; Wang, Y.; Xia, Y. Environmentally-Friendly Aqueous Li (or Na)-Ion Battery with Fast Electrode Kinetics and Super-Long Life. *Sci. Adv.* **2016**, *2* (1), e1501038.

(98) Tao, Y.; Wei, Y.; Liu, Y.; Wang, J.; Qiao, W.; Ling, L.; Long, D. Kinetically-Enhanced Polysulfide Redox Reactions by Nb_2O_5 Nanocrystals for High-Rate Lithium–Sulfur Battery. *Energy Environ. Sci.* **2016**, *9* (10), 3230–3239.

(99) Simon, P.; Gogotsi, Y.; Dunn, B. Where Do Batteries End and Supercapacitors Begin? *Science (80-.).* **2014**, *343* (6176), 1210–1211.

(100) Jow, T. R.; Shacklette, L. W. Electrochemical Characteristics of Alkali-Metal Doped Polyacetylene Electrodes. *J. Electrochem. Soc.* **1988**, *135* (3), 541.

(101) Jaumann, T.; Balach, J.; Klose, M.; Oswald, S.; Langklotz, U.; Michaelis, A.; Eckert, J.; Giebeler, L. SEI-Component Formation on Sub 5 Nm Sized Silicon Nanoparticles in Li-Ion Batteries: The Role of Electrode Preparation, FEC Addition and Binders. *Phys. Chem. Chem. Phys.* **2015**, *17* (38), 24956–24967.

(102) Yang, J.; Zou, P.; Yang, L.; Cao, J.; Sun, Y.; Han, D.; Yang, S.; Wang, Z.; Chen, G.; Wang, B.; Kong, X. A Comprehensive Study on the Synthesis and Paramagnetic Properties of PEG-Coated Fe3O4 Nanoparticles. *Appl. Surf. Sci.* **2014**, *303*, 425–432.

(103) Zhang, W.; Bock, D. C.; Pelliccione, C. J.; Li, Y.; Wu, L.; Zhu, Y.; Marschilok, A. C.; Takeuchi, E. S.; Takeuchi, K. J.; Wang, F. Insights into Ionic Transport and Structural Changes in Magnetite during Multiple-Electron Transfer Reactions. *Adv. Energy Mater.* **2016**, *6* (10), 1502471.

(104) Zhao, H.; Wang, Z.; Lu, P.; Jiang, M.; Shi, F.; Song, X.; Zheng, Z.; Zhou, X.; Fu, Y.; Abdelbast, G.; Xiao, X.; Liu, Z.; Battaglia, V. S.; Zaghib, K.; Liu, G. Toward Practical Application of Functional Conductive Polymer Binder for a High-Energy Lithium-Ion Battery Design. *Nano Lett.* **2014**, *14* (11), 6704–6710.

(105) Liu, G.; Xun, S.; Vukmirovic, N.; Song, X.; Olalde-Velasco, P.; Zheng, H.; Battaglia, V. S.; Wang, L.; Yang, W. Polymers with Tailored Electronic Structure for High Capacity Lithium Battery Electrodes. *Adv. Mater.* **2011**, *23* (40), 4679–4683.

(106) Kwon, Y. H.; Minnici, K.; Huie, M. M.; Takeuchi, K. J.; Takeuchi, E. S.; Marschilok, A. C.; Reichmanis, E. Electron/Ion Transport Enhancer in High Capacity Li-Ion Battery Anodes. *Chem. Mater.* **2016**, *28* (18).

(107) Lang, A. W.; Ponder, J. F.; Österholm, A. M.; Kennard, N. J.; Bulloch, R. H.; Reynolds, J. R. Flexible, Aqueous-Electrolyte Supercapacitors Based on Water-Processable Dioxythiophene Polymer/Carbon Nanotube Textile Electrodes. *J. Mater. Chem. A* **2017**, *5* (45), 23887–23897.

(108) Kwon, Y. H.; Park, J. J.; Housel, L. M.; Minnici, K.; Zhang, G.; Lee, S. R.; Lee, S. W.; Chen, Z.; Noda, S.; Takeuchi, E. S.; Takeuchi, K. J.; Marschilok, A. C.; Reichmanis, E. Carbon Nanotube Web with Carboxylated Polythiophene "Assist" for High-Performance Battery Electrodes. *ACS Nano* **2018**, acsnano.7b08918.

(109) Chang, M.; Lee, J.; Kleinhenz, N.; Fu, B.; Reichmanis, E. Photoinduced Anisotropic Supramolecular Assembly and Enhanced Charge Transport of Poly(3-Hexylthiophene) Thin Films. *Adv. Funct. Mater.* **2014**, *24* (28), 4457–4465.

(110) Chang, M.; Choi, D.; Fu, B.; Reichmanis, E. Solvent Based Hydrogen Bonding: Impact on Poly(3-Hexylthiophene) Nanoscale Morphology and Charge Transport Characteristics. *ACS Nano* **2013**, *7* (6), 5402–5413.

(111) Lininger, C. N.; Brady, N. W.; West, A. C. Equilibria and Rate Phenomena from Atomistic to Mesoscale: Simulation Studies of Magnetite. *Acc. Chem. Res.* **2018**, *51* (3), 583–590.

(112) Abott; Hansen. Hansen Solubility Parameters in Practice.

(113) Hansen, C. *Hansen Solubility Parameters*; CRC Press, 1999.

(114) Bergin, S. D.; Sun, Z.; Rickard, D.; Streich, P. V.; Hamilton, J. P.; Coleman, J. N. Multicomponent Solubility Parameters for Single-Walled Carbon Nanotube−Solvent Mixtures. *ACS Nano* **2009**, *3* (8), 2340–2350.

(115) Launay, H.; Hansen, C. M.; Almdal, K. Hansen Solubility Parameters for a Carbon Fiber/Epoxy Composite. *Carbon N. Y.* **2007**, *45* (15), 2859–2865.

(116) Turcheniuk, K.; Bondarev, D.; Singhal, V.; Yushin, G. Ten Years Left to Redesign Lithium-Ion Batteries. *Nature* **2018**, *559* (7715), 467–470.

(117) Bock, D. C.; Waller, G. H.; Mansour, A. N.; Marschilok, A. C.; Takeuchi, K. J.; Takeuchi, E. S. Investigation of Solid Electrolyte Interphase Layer Formation and Electrochemical Reversibility of Magnetite, Fe_3O_4, Electrodes: A Combined X-

Ray Absorption Spectroscopy and X-Ray Photoelectron Spectroscopy Study. *J. Phys. Chem. C* **2018**, *122* (26), 14257–14271.

(118) Wang, L.; Li, Y. R.; Li, J.; Zou, S.; Stach, E. A.; Takeuchi, K. J.; Takeuchi, E. S.; Marschilok, A. C.; Wong, S. S. Correlating Preparative Approaches with Electrochemical Performance of Fe_3O_4-MWNT Composites Used as Anodes in Li-Ion Batteries. *ECS J. Solid State Sci. Technol.* **2017**, *6* (6), M3122–M3131.

(119) Wang, L.; Zhang, Y.; McBean, C. L.; Scofield, M. E.; Yin, J.; Marschilok, A. C.; Takeuchi, K. J.; Takeuchi, E. S.; Wong, S. S. Understanding the Effect of Preparative Approaches in the Formation of "Flower-like" $Li_4Ti_5O_{12}$ — Multiwalled Carbon Nanotube Composite Motifs with Performance as High-Rate Anode Materials for Li-Ion Battery Application. *J. Electrochem. Soc.* **2017**, *164* (2), A524–A534.

(120) Yin, H.; Zhou, Y.; Liu, T.; Tang, T.; Ai, S.; Zhu, L. Determination Aminopyrine in Pharmaceutical Formulations Based on APTS-Fe3O4 Nanoparticles Modified Glassy Carbon Electrode. *J. Solid State Electrochem.* **2012**, *16* (2), 731–738.

(121) Wei, W.; Yang, S.; Zhou, H.; Lieberwirth, I.; Feng, X.; Müllen, K. 3D Graphene Foams Cross-Linked with Pre-Encapsulated Fe_3O_4 Nanospheres for Enhanced Lithium Storage. *Adv. Mater.* **2013**, *25* (21), 2909–2914.

(122) Kovalenko, I.; Zdyrko, B.; Magasinski, A.; Hertzberg, B.; Milicev, Z.; Burtovyy, R.; Luzinov, I.; Yushin, G. A Major Constituent of Brown Algae for Use in High-Capacity Li-Ion Batteries. *Science* **2011**, *334* (6052), 75–79.

(123) Zhou, G.; Wang, D.-W.; Li, F.; Zhang, L.; Li, N.; Wu, Z.-S.; Wen, L.; Lu, G. Q. (Max); Cheng, H.-M. Graphene-Wrapped Fe_3O_4 Anode Material with Improved Reversible Capacity and Cyclic Stability for Lithium Ion Batteries. *Chem. Mater.* **2010**, *22* (18), 5306–5313.

(124) Do, J.-S.; Weng, C.-H. Preparation and Characterization of CoO Used as Anodic Material of Lithium Battery. *J. Power Sources* **2005**, *146* (1–2), 482–486.

(125) Grugeon, S.; Laruelle, S.; Dupont, L.; Tarascon, J.-M. An Update on the Reactivity of Nanoparticles Co-Based Compounds towards Li. *Solid State Sci.* **2003**, *5* (6), 895–904.

(126) Qie, L.; Chen, W.-M.; Wang, Z.-H.; Shao, Q.-G.; Li, X.; Yuan, L.-X.; Hu, X.-L.; Zhang, W.-X.; Huang, Y.-H. Nitrogen-Doped Porous Carbon Nanofiber Webs as Anodes for Lithium Ion Batteries with a Superhigh Capacity and Rate Capability. *Adv. Mater.* **2012**, *24* (15), 2047–2050.

(127) Song, H.; Li, N.; Cui, H.; Wang, C. Enhanced Storage Capability and Kinetic Processes by Pores- and Hetero-Atoms- Riched Carbon Nanobubbles for Lithium-Ion and Sodium-Ion Batteries Anodes. *Nano Energy* **2014**, *4*, 81–87.

(128) McBride, M.; Persson, N.; Keane, D.; Bacardi, G.; Reichmanis, E.; Grover, M. A. A Polymer Blend Approach for Creation of Effective Conjugated Polymer Charge Transport Pathways. *ACS Appl. Mater. Interfaces* **2018**, *10* (42), 36464–36474.

(129) Lestriez, B.; Bahri, S.; Sandu, I.; Roué, L.; Guyomard, D. On the Binding Mechanism of CMC in Si Negative Electrodes for Li-Ion Batteries. *Electrochem. commun.* **2007**, *9* (12), 2801–2806.